Master thesis

The influence of different mechanisms on the self-organized consolidation of memory representations in spiking neuronal networks

Moritz Becker

Third Institute of Physics
University of Göttingen

This dissertation is submitted for the degree of
Master of Physics

Georg-August-Universität Göttingen

Master Thesis

The influence of different mechanisms on the self-organized consolidation of memory representations in spiking neural networks

Moritz Becker

Third institute of physics

supervised by
Dr. Christian Tetzlaff
primary reviewer:
Dr. Christian Tetzlaff
secondary reviewer:
Prof. Dr. Stefan Klumpp

Wednesday 19th April, 2023

Declaration

Abstract

Several experimental studies indicate that during sleep induced ripple-like activity in the hippocampus [21], some synapses are strengthened while others are weakened [71, 89]. Further, during slow wave sleep, memories become consolidated, i.e. are stabilized and enhanced [87, 26]. However, the underlying processes of synaptic changes during sleep are mainly unknown. This study investigates the role of Spike-Timing-Dependent Plasticity (STDP) and Synaptic Scaling (SS) on the time evolution of memory representations in the presence of spontaneous, ripple-like activity. Based on our previous work [98], in this study we show that STDP in combination with SS [105], enables a spiking neural network to selectively scale up or down synapses depending on their strength. During this process, synapses are reorganized/consolidated from a long-tailed unimodal into a stable, bimodal distribution. While this leads to a down-regulation of the network strength on average, a subset of strong connections associated with the memory are retained while the temporal order of memory replay is even enhanced on a single neuron pair basis. In our theoretical model, we use a network of leaky integrate and fire neurons with STDP, and activity-dependent homeostatic synaptic scaling. Memories are represented in the form of a FeedForward (FF) - structure [49]. Spontaneous, ripple-like network activity is caused by fast dendritic spikes [49] which triggers synaptic changes. In addition, we study STDP and SS over a wide range of synaptic strengths and stimulus amplitudes. We show that there is a high dependence between synaptic potentiation and depression and the exact form of the STDP rule. Further, analytical methods for the estimation of STDP induced synaptic change are studied and compared with simulations.

Table of contents

List of figures

List of tables

Nomenclature

Acronyms / Abbreviations

AP   Action Potential

EIF   Exponential Integrate and Fire model

EPSP   Excitatory Postsynaptic Potential

FF   FeedForward

LIF   Leaky Integrate and Fire model

LTD   Long Term Depression

LTP   Long Term Potentiation

PSC   Postsynaptic Current

PSD   PostSynaptic Density

PSP   PostSynaptic Potential

PSP   Postsynaptic Potential

SHY   Synaptic Homeostasis Hypothesis

SS   Synaptic Scaling

STDP   Spike-Timing-Dependent Plasticity

SWR   Sharp Wave and Ripples

SWS   Slow Wave Sleep

Chapter 1

Background

In this chapter we give an overview over the properties of neurons and neural networks as well as outline current findings and hypothesis about memory, learning and sleep. We start by delivering a short background on neurons, synapses and dendrites. Then neural networks and synaptic plasticity mechanisms are introduced. Subsequent we review current findings and hypothesis regarding learning spatial tasks with place cells, the role of memory consolidation and sleep. This will form the basis from which our model is constructed. With this model we try to answer the question how synapses may get regulated during sleep, while representations of memory in a neural network get consolidated.

1.1 Neurons, synapses and dendrites

1.1.1 Neurons

The neuron (Fig. 1.1) is the central processing unit of the brain. It transmits and modifies the information that it receives from other neurons in a network. Information is transmitted to other cells in the form of electrical or chemical signals. The neuron can be divided into three main parts [1]. The **dendrite (1)**, receiving inputs from other units and transmitting it to the **soma (2)**, which is the processing kernel of the neuron. The soma generates an electrical output signal, also called action potential (AP) or spike, whenever the input it receives crosses a certain threshold. This nonlinear process is the basic principle of neural computation [1]. The signal is then send to neighboring neurons along the **axon (3)**, a single long fiber. However, recent experimental observation have shown that not only the soma but also the dendrite

itself is able to generate electrical signals. Details will be given in section 1.1.3.

Processing of incoming signals

How does the neuron process incoming electrical signals? The neuron is surrounded by a membrane that is build from lipids that form a bilayer. The extra- and intracellular space, which is divided by the membrane, inhabit several ion-types of different concentrations. The lipid bilayer is in general a very good insulator, thereby prohibiting the flow of electrical charges from the inside of the cell to the outside or vice versa. However, embedded in the membrane are different proteins that allow for ion currents to flow through in an organized manner. At the arrival of an electrical signal, these proteins, also called ion channels, get activated and thereby change the electrical potential between the inside and outside of the cell. If the membrane potential crosses a certain threshold (the spiking threshold), a signal is generated by the soma. Thereby, the ion flow through these ion channels is, what enables neurons to communicate with each other. There are many different types of ions involved in the machinery of the neuronal cell. Fortunately however the basic dynamics of the neuronal membrane potential can be described by models which only take into account very view ion types.

The reversal and the resting potential

The difference in the membrane potential between interior and exterior of the cell depends on the difference in ion concentration, which is generated by active ion transport through the protein channels. At equilibrium, the voltage across the membrane generated by the ion concentration differences can be described by the Nernst equation:

$$E_{ion} = \frac{k_B T}{q} ln\left(\frac{[ion]_{out}}{[ion]_{in}}\right) \tag{1.1}$$

Where q is the ion charge, k_B the Boltzman constant and T the temperature. $[ion]_{out}$ and $[ion]_{out}$ are the different concentration outside and inside the membrane. The concentration of e.g. sodium (Na^+) is lower inside the membrane than outside, generating a positive Nernst potential that lies around $67mV$. In Neuroscience the Nernst potential of an ion type is also called reversal potential since its value determines at what voltage differences across the membrane some ion type would flow in or out of the cell. While the membrane potential that fluctuates due to incoming signals lies below the reversal potential, sodium ions would flow into the cell, lowering the potential
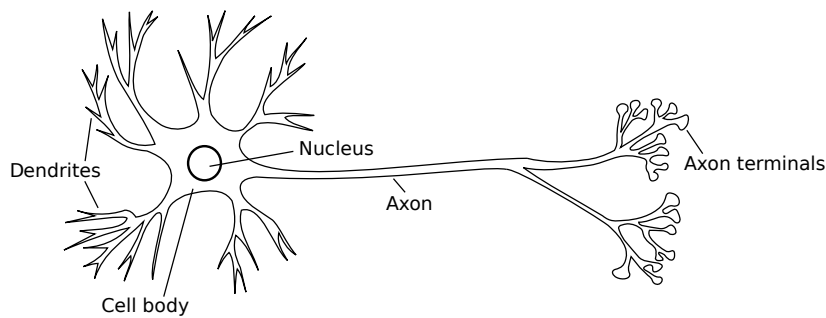
Fig. 1.1: The neuron is the primary processing unit of the brain. Here a sketch is shown. Apart from the nucleus, which contains most of the cell's genetic material, the neuronal cell also inhabits the ribosome for protein synthesis and other biological machineries which are not shown. Within the Cell body or 'soma' the action potential is generated and send down the axon. At the axon terminals, the neuron is connected to other neurons via their dendrites. The dendrites are the part of the neuron where incoming signals are summed up and transmitted to the soma, which in case of excitatory input might lead to the emission of a somatic spike. Sketched after [Karpathy]

difference. If the membrane potential would rise above the reversal potential, the direction of ion flow would reverse. In the absence of any stimuli, the reversal potentials of all the different ion types together determine the resting membrane potential. The resting potential usually is about -70 mV [26]. The potential is always measured from inside the cell relative to the outside.

The generation of a spike

Positively charged ions leaving the cell result in a hyperpolarization of the membrane potential, i.e. the electric potential becomes more negative. Positive ion flow into the cell results in the depolarization of the membrane potential. If the depolarization reaches a certain threshold (spiking threshold), sodium ion channels become highly active for a short period, resulting in an influx of sodium ions. This results in a peak in the membrane potential. This peak is shortly after counterbalanced by a potassium efflux. The action-potential has a strength of several mV and can be transmitted over large distances along the neurons axon. After a spike, the neuron is reset to a potential of about -60 mV. Table 2.2 shows some of the typical parameter values of a pyramidal neuron.

a
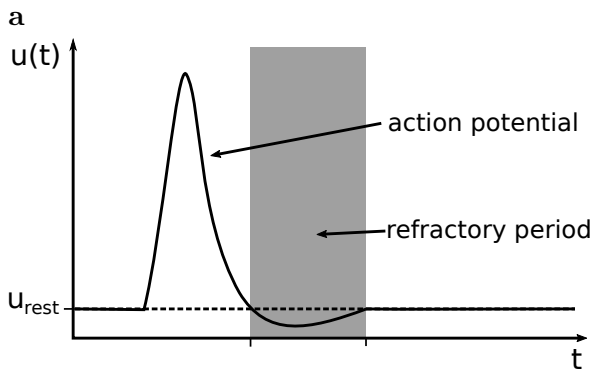
Fig. 1.2: The figure shows a sketch of a typical action potential. When the spiking threshold is reached, the depolarization through sodium influx into the cell takes place. Subsequent, potassium efflux re-polarizes the cell membrane and eventually hyper-polarizes it. During the phase of hyper-polarization (refractory period), incoming stimuli have to overcome a larger potential difference to reach the spiking threshold. Also sodium channels are inactivated after the initial spike and therefore unable to exhibit another one.

Refractoriness

The refractory period (Fig. 1.2) is a time window after the initialization of a spike, during which no spike can be generated. The sodium ion channels that get activated to produce the action potential get inactivated subsequent and remain this way until the membrane is hyper-polarized. The hyper-polarization is generated by voltage gated potassium channels. Potassium ions flow out of the cell bringing the membrane potential below the resting potential. The refractory period ends when the membrane potential returned to its resting value and sodium channels got activated again. The refractory period usually lasts for about 2-3 ms.

1.1.2 Synapses

The action potential generated by the neuron travels along the axon and ends at the axonal terminal of the synapse, which is the connection between two neurons (Fig. 1.3). The neuron that transmits a signal is called the presynaptic neuron while the receiving neuron is called postsynaptic. The synapse itself can be divided into three parts.

1. The axon terminal, which is at the presynaptic site,

2. the dendritic spine, which belongs to the postsynaptic neuron

3. and the synaptic cleft, separating the two sites.

At the arrival of a spike, ion channels at the axonal terminal open, resulting in an influx of calcium ions. Embedded in the axon terminal are vesicles, structures formed by a lipid bilayer that encloses neurotransmitter molecules. These vesicles release neurotransmitters into the synaptic cleft in response to the calcium ion influx. At the head of the dendritic spine sits a structure called the postsynaptic density (PSD). The PSD contains neural receptors that are associated with specific ion channels that get activated at the conjunction with the neurotransmitters.

inhibitory and excitatory synapses

Whether the binding of neurotransmitter molecules to the receptors triggers ion in- or efflux depends on the receptor type and its associated ion channels. Lowering (hyperpolarizing) the membrane potential, i.e. efflux of positively charged ions (K^+) or influx of negatively charged ions (Cl^-), results in a so called inhibitory postsynaptic potential (IPSP). Inhibitory synapses mostly contain receptors that respond to GABA (Gamma-aminobutyric acid). The influx of positively charged ions (Na^+) results in an excitatory postsynaptic potential (EPSP). Excitatory synapses mostly contain receptors that get activated by glutamate ($\alpha - amino$ acid). This process of synaptic transmission filters the original action potential, resulting in the postsynaptic current (PSC). Neurons either create inhibitory or excitatory connections with postsynaptic neurons, which is also known as Dale's law [94]. Whether a synapse is inhibitory or excitatory depends on the reversal potential E_{ion}, which depends on the type of ions and therefore the type of ion-channels that get activated by the receptors. For example, the reversal potential for inhibitory synapses that activate Cl^--channels is $E_{inh} \approx -70mV$. Excitatory synapses that activate Na^+- and K^+-channels have a reversal potential of $E_{exc} \approx 0mV$ ($E_{Na^+} \approx 70mV$, $E_{K^+} \approx -70mV$) [84]. The concentration of receptors in the PSD alongside the likelihood of synaptic vesicles to undergo exocytosis at the arrival of a spike, determines the strength and timing of PSC which is then fed through the dendritic spine to the soma of the corresponding neuron. It is thought that action potentials, that propagate back through the dendritic tree, are responsible for signaling the synapse that the postsynaptic neuron has generated an output spike, which is important for synaptic plasticity (see section 1.3).
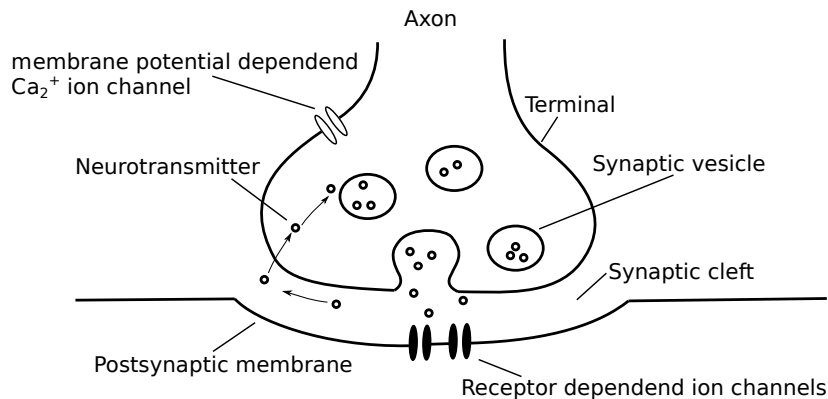
Fig. 1.3: The synapse enables a neuron to transmit electrical signals from one neuron to the other by translating that electrical signal into a chemical signal and back. An action potential that arrives at the axonal site of the synapse triggers a calcium ion influx, which in turn triggers the release of neurotransmitters into the synaptic cleft. The neurotransmitters bind with receptors (AMPA, NMDA) at the dendritic site, which again triggers ion flux. The electrical signal evolving from the ion influx is then fed forward to the soma.

1.1.3 Dendrites

The synaptic input, a neuron receives, is combined within the dendritic tree, which is a structure emerging from the soma of the neuron. The summation of all the incoming signals in the dendritic tree results in a new, filtered version of the original signals, the dendritic signal. The size and shape of the membrane potential transient at the soma in response to the incoming spikes therefore depends on the dendritic structure and its electrical properties. This results extremely diverse and complex dendritic signaling properties [45]. Morover, neuronal recordings have shown that dendrites are not only passive cables, that transmit electrical signals, but that they actively modulate the signal by voltage gated ion channels, generating so called dendritic spikes[39, 61]. It is found experimentally that these dendritic spikes are faster and stronger than somatic spikes, enabling sub-millisecond precision of input-output transformation [6]. The voltage threshold for the generation of these dendritic spikes is higher than for the generation of action potentials in the soma, therefore requiring strong synchronous synaptic inputs. In this regard the dendritic spike generation process can be interpreted as a detector for strong and synchronous events, which might be an important feature in neuronal communication and synaptic plasticity [45, 51]. A model that describes the form and generation process of these dendritic spikes has been introduced in [66]. The same model has been used to identify dendritic spikes as a possible mechanism for

sharp wave ripples and replay generation, observed in the hippocampus during slow wave sleep (see section 1.6).

1.2   Neural Networks

In the brain, neurons are densely packed with about 10^4 cells within a cubic millimeter [42]. Each neuron has up to 10^4 connections to postsynaptic neurons. Therefore, the main source of noise that a neuron is exposed to comes from the high amount of synaptic input it receives [82]. To detangle the connectivity of the brain is of great interest and researchers have tried to figure out the underlying principles for many decades[22, 15, 96]. One approach is to look for anomalies in synaptic probability distributions that differ from what one would expect from a completely random network. For instance, synaptic weight distributions differ from neuron type to neuron type and from brain region to brain region [90]. Experimental distributions of synaptic weights show that the range of synaptic weights in the cortex is much higher than in the hippocampus or the cerebellum. The mean synaptic weight in form of the EPSP amplitude is approximately 0.1 mV in the hippocampus and cerebellum, while in the cortex EPSPs are much stronger on average with $\approx 1\ mV$ [9]. Further, neuroscientists have been debating about weather synaptic weight distributions are unimodal or bimodal [9]. Experimental synaptic weight distributions often seem to be unimodal, while they are also extremely skewed [29]. However, it has been observed in experiments that EPSPs can take values up to $8 - 10mV$, which is much higher than the average, supporting the hypothesis of at least weakly bimodal synaptic distributions [100, 59, 62, 92].

1.3   Synaptic plasticity

Biological neural networks are not static but plastic. Their connections underly constant changes due to mechanisms of synaptic plasticity. These are distinguished between homeostatic mechanisms, depending on the postsynaptic activity and Hebbian mechanisms, which rely also on the correlated firing of the post- and presynaptic. There exist two main types of theoretical neuron models: spiking neuron models and rate models. Rate models neglects the single spikes and only model the neuronal activity, i.e. the firing rate in spikes per second. Whereas spiking models, which are more biologically accurate, model the single spikes. Hebbian plasticity models differ, depending on whether a spiking or rate model is used. In the current work we focus on spiking neural networks.

Spike-timing-dependent plasticity

A well established form of a Hebbian plasticity is spike-timing-dependent plasticity (STDP). The key idea of STDP is that only those connections between neurons should experience potentiation that have the "right" timing. "The timing must be such that synapses that contribute to firing the postsynaptic neuron are maximally strengthened. Hence long-term potentiation (LTP) must be maximal if the spike arrives at the synapse 1 or 2 ms before the postsynaptic spike so as to compensate for the rise time of the excitatory postsynaptic potential" (cited from [40]). In addition, if a presynaptic spike arrives shortly after the emission of a postsynaptic spike, the synapse experiences long term depression (LTD).

LTP vs. LTD: The function describing the synaptic change depending on the spike-timing can take different forms but is in general described by a LTP domain, describing the synaptic change for positive spike-timing ($t_{post} - t_{pre} > 0$) and a LTD domain ($t_{post} - t_{pre} < 0$). Whether the STDP function is dominated[1] by the LTP domain or the LTD domain seems to be different from brain region to brain region [1]. Different results in this regard are however also known for same brain regions depending on stimulus protocols and other factors [1]. In layer 2/3 pyramidal neurons and also in the hippocampus, LTD is found in some scenarios to dominate over LTP, i.e. when pre- and postsynaptic spiking occur completely random, LTD will be induced. "This makes functional sense, because it weakens input that "accidentily" fire in approximate coincidence with postsynaptic action potentials, but that do not consistently contribute to evoking them" (cited from [1], p. 1180). As it is still not clear what exact functional purposes these different forms of STDP have, we do not restrict the study of our model to one form of STDP but investigate the impact from changing STDP from LTD- to LTP-dominant.

While the mechanism of STDP is powerful, it comes with the downside of being unstable. As those synapses that get strengthened receive as a result more correlated signals from the corresponding post- and presynaptic neuron, such that they eventually grow unbounded. Therefore the excitatory drive to a neuron needs to be regulated in such a way that the network can operate stable. This issue can be solved by either

---

[1]The term dominance is not strictly defined but can be viewed as to whether the integral over the negative part of the function is greater than the integral over the positive part or vice versa. Another way to define dominance would be, to demand that, if both neurons are uncorrelated, the ensemble averaged synaptic change induced by STDP should be zero if STDP is balanced, positive if it is LTP-dominated and negative if it is LTD-dominated

introducing weight depended STDP [108] or homeostatic plasticity mechanisms that scale down excitatory synapses if the postsynaptic activity or the excitatory synaptic strength exceeds a certain level [1].

Synaptic scaling

Synaptic scaling is a proposed homeostatic plasticity mechanism that counteracts the changes introduced by STDP induced potentiation [106]. In contrast to Hebbian plasticity such a mechanism is not necessarily synapse specific but acts global on all synapses of a postsynaptic neuron. While Hebbian plasticity is considered to be a relatively fast process, homeostatic plasticity has been generally considered to be slow. However there has been recent evidence that homeostatic plasticity might also act rapid and local [104] (See also SHY in section 1.6). In [97] it has been demonstrated that weight dependent synaptic scaling in a rate model is able to stabilize synaptic change, where synaptic scaling with a convex non-linear weight dependence generically stabilizes excitatory and inhibitory synapses, whereas linear weight dependence only stabilizes under certain conditions. For more details see Methods.

1.4   Spatial learning and place cells

Learning is closely related to synaptic plasticity. How we learn and therefore how the brain encodes information is however to a large degree still unknown. One way to get an idea of how information is processed and stored in the brain is to look for reliable links between neural activity and behavior. O'Keefe et al.[74] found that hippocampal cells recorded in free moving rats respond specifically to the animals location. Different cells responded to different locations, therefore, they are known as place cells. The associated locations in which a place cell is active define the place field of that cell. Besides that, studies showed that place cell also encode a memory of locations the animal has visited in the past, supporting the hypothesis that the hippocampus has a role in the memory and learning of spatial tasks [76]. Further it was shown that firing patterns during exploration were replayed during sleep subsequent to the exploration phase [80] and that this replay of place selective firing appears during sharp wave/ripples (see below) [77]. The hippocampus is usually subdivided into the regions CA1-CA4, where the CA1- and CA3-pyramidal neurons are most involved in spatial learning and replay. The CA1 region is largely parallel organized and displays the larger amount of place field related cells, whereas CA3 is highly recurrent. How

exactly spatial memories are represented in the CA1 and CA3 neural network is not entirely clear. In [49] , Jahnke et al. introduced a phenomenological model where representations of spatial memories are encoded in form of feedforward structures that shows parallels to what can be observed during spatial learning in experiments [49].

1.5   Memory and consolidation

Memory Consolidation describes the process of the formation of long lasting memories subsequent to learning. It has been argued and experimental observations support this view, that memory consolidation mainly occurs during sleep [101, 32, 31]. Consolidation is commonly divided into three levels of description. The synaptic consolidation, the system consolidation and the network consolidation level [32, 31, 106, 98].

Synaptic consolidation

Synaptic consolidation describes the process of transferring information into long-term memory at the local synaptic level. The information is usually assumed to be encoded in form of a sequence of potentiated synaptic connections. The general hypothesis assumes that for synaptic consolidation a directed stimulus is needed that triggers the activation of a memory trace, resulting in a signaling cascade. This will in turn lead to a modification of gene expression and the synthesis of gene products that change the synaptic efficacy and protect the synapse from "amnesic agents" that would prevent the transformation of the memory to a long term state [52]. The process of synaptic consolidation is assumed to be fast compared to system consolidation, meaning that it will act on a timescale of hours.

System consolidation

System consolidation is a slow process, taking hours to days. When completed it is thought to be long lasting, ranging time scales from days to even years. The idea behind system consolidation is the reorganization of a memory from a temporal device, which accounts for our short-term memory, to a long lasting representation in a different region of the brain. Short-term storage is thought to be connected to the hippocampus and long term-storage to the neocortex [20], [14].

Network consolidation

The synaptic homeostasis hypothesis (See section 1.6) states that during sleep the brain has to get back into a homeostatic state [101]. The homeostatic state is defined
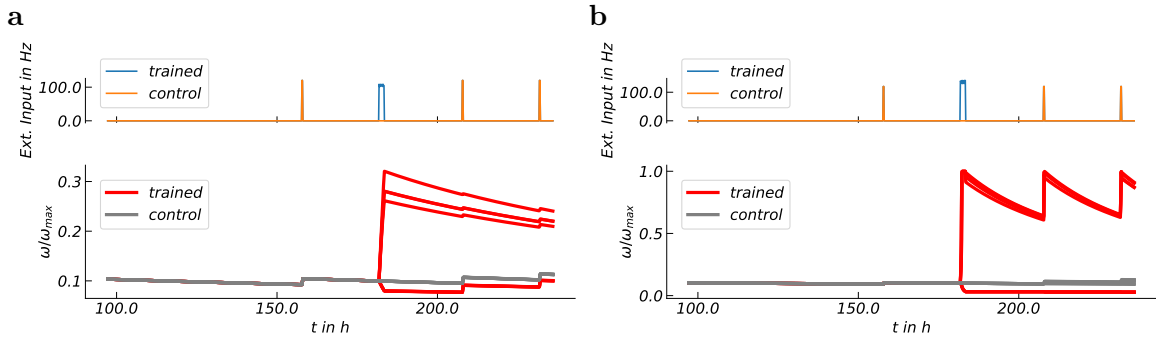
Fig. 1.4: In a network of rate coded neurons an external stimulus of a certain rate is fed into the network (**a**, **b**, top). For low stimuli rates, the synaptic weights stay at a control level (figure a,b bottom, 100-160 h). At certain points in time, a high rate stimulus of 120 Hz is introduced for 15 min. (figure a, b top, yellow peaks). For the control group, the weight change due to these stimuli is small (figure a,b, bottom). At time 180 h a training stimulus is introduced which leads to a significant growth in the synaptic weights (figure a,b top: blue peak, bottom: red lines). In panel **a** the training stimulus has been slightly weaker then in panel **b**, resulting in a smaller synaptic growth in **a** compared to **b**. Subsequent to the training stimulus, further short (15 min.) consolidation stimuli are introduced, resulting in strong consolidation of synapses in panel **b**, whereas in panel **a** the synaptic weights are basically unaffected. The results shown have been reproduced from [98].

as a state in which neural activity and synaptic connections are stable and optimized for task performance, memory retrieval and learning. During wake however, synaptic connections get potentiated due to external stimuli, driving the brain out of the homeostatic state. In order to get back into the homeostatic state, some synapses need to get scaled up while others get scaled down, supporting forgetting as well as consolidation [102]. In [98] a model of Hebbian learning combined with homeostatic synaptic scaling [99] was used that enabled a network of rate neurons to distinguish between synapses relevant for long-term storage and those not by distinct up and down scaling of connections depending on their synaptic weight (see fig. 1.4). In the current work a similar approach is used for a spiking neural network.

1.6   Sleep

Sleep in mammals consists of two main sleep stages: slow-wave sleep (SWS) and rapid-eye-movement (REM) sleep. These stages are accompanied by electrical field potential oscillations originating from the spiking activity of the neurons in the brain. During SWS oscillations of about 0.8 Hz are observed in the neocortex, while the

hippocampus exhibits sharp waves and ripples in the range of 100-300 Hz and the thalamus displays so called spindles (10-15 Hz) [87]. The hippocampal ripples are tightly linked to the slow waves observed in the neocortex [69], leading to the assumption that neocortical slow waves group the activity in the brain during sleep. Sharp-wave/ripples occur together with the replay of sequences that where encoded during wake [70], supporting the hypothesis that the hippocampus is involved in the consolidation of previously encoded memories (see section 1.5). That sleep plays a crucial role in this overall process has long been known. Studies show that sleep deprivation results in cognitive problems and memory loss [56]. However details about the mechanisms behind memory consolidation during sleep are still not entirely clear. In recent years it has become evident, that, while during wake the neural excitability increases, sleep is associated to synaptic downscaling [48], [109], [27]. Down regulation of synapses has recently also been connected to hippocampal ripples during Slow wave sleep, [71]. This supports the hypothesis that sleep not only plays an important role in memory consolidation but also in forgetting .

Synaptic homeostasis hypothesis (SHY)
The synaptic homeostasis hypothesis (SHY) [101] suggests that during sleep the synaptic connections formed during wake get back into a homeostatic state. While encoding new information, synaptic connections get scaled up and the brain will eventually end up in an overly excited state with many strong connections. These prohibit the brain to operate in a balanced, stable state and also aggravates the integration/encoding of new information. To get back into a homeostatic state, the SHY states that during SWS overly strong connections get pruned, non relevant structures get scaled down while relevant memory representations get scaled up and eventually consolidated. This renormalization of connectivity is driven by spontaneous activity, which depends on the connection strength. This activity dependent down-selection should occur mainly during sleep, when the brain is off-line. This enables the brain to get a less biased sample of the memory environment that is represented in the spontaneous activity that would be altered by external sensory input [102].

Chapter 2

Models and Methods

In this chapter we introduce the models and methods for constructing a neural network that has many of the properties that have been described in the Background section. We start with a model for neurons and synaptic signals. Next the properties of our network topology are specified. Then two models for spike-timing dependent plasticity and synaptic scaling are introduced as well as a method for learning spatial tasks. At last, measures for describing and quantifying network dynamics as well as analytical methods are discussed.

2.1 Network model

2.1.1 The leaky integrate and fire (LIF) model

The integrate and fire model has since its introduction in 1907 by Lapicque become the most used canonical model for the description of spiking neurons. Its benefit compared to other models like the Hodgkin Huxley model [47] lies in its simplicity, which makes it analytically tractable, but it is at the same time sufficiently complex to reproduce many of the essential features of real neurons observed in vitro and in vivo [42]. There are some variations to the original approach, such as the leaky integrate and fire model (LIF), or the exponential integrate and fire model (EIF) [42]. In this work, we consider the LIF. The LIF model approximates the conductances of all ion channels in the neuron by one resistor, which accounts for the leakage through these ion channels. The resistance is not variable but constant, since the variability of the ion channels resistance is only important in the regime where the action potential is generated. Action potentials however last less than one millisecond and their exact form is believed to not carry any valuable information in terms of neuronal computation. The action

potential is therefore not modeled but only the PSC at the postsynaptic neuron in response to a presynaptic neuron crossing u^{th}. The PSC that is generated by an action potential at the postsynaptic site of a connection is described by a different model (see section 2.1.2).

model

The idea behind the LIF model is, to model the real neuron by a resistor-capacitor (RC) circuit. The membrane is apart from its ion channels a very good insulator that separates the extracellular and intracellular space.Since the inside of the cell inabits different concentrations of ions than the outside, the membrane can be described by a capacitance C_m in parallel with a resistor R_m that accounts for the leakage of ions through the several ion channels (Fig. 2.1). The consistent transport of ions through active ion channels however always keeps the membrane potential at some minimum value u_{rest}. This can simply be modeled by a battery in series to the leakage resistance. Deviations from this resting potential are induced by synaptic or other external currents that are fed into the neuron or, in the model case, the RC-circuit. Due to the leakage term, these deviations decay with a characteristic time constant $\tau_m = R_m \, C_m$ back to the resting potential u^{rest} if the stimulus stops. If the input current is strong enough to drive the membrane potential over the spiking threshold u_{th}, an output signal is generated and the membrane is set to a reset potential u_{reset} for a time interval of $3ms$. During this time, the ion channels that usually respond to incoming signals are deactivated, i.e. the neuron does not respond to any incoming currents. This is modeled by a simple switch that cuts of the capacitance from the rest of the circuit and instead connects it to a battery with voltage u_{reset}.

Table 2.2 gives some common parameter values for the LIF model that are a good fit to biological pyramidal neurons. The equation describing the time evolution of the membrane potential in the LIF model is (Fig. 2.1):

$$\tau_m \frac{du_i(t)}{dt} = u_{rest} - u_i(t) + R_m \, I_i(t) \tag{2.1}$$

Here $I_i(t)$ describes the current input from other neurons as well as sensory input. The spiking and subsequent reset of the membrane potential is not directly described in the mathematical formulation and needs to be implemented in addition to solving the differential equation then doing simulations on the computer.
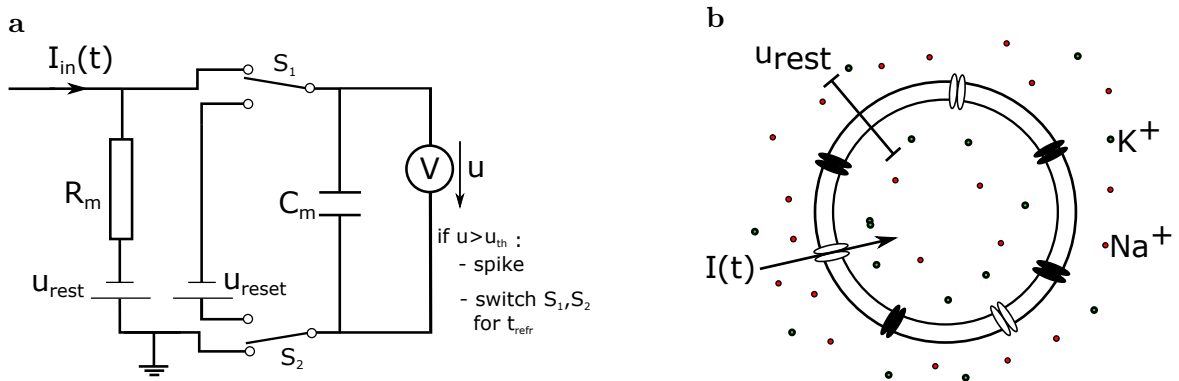
Fig. 2.1: The circuit shown in panel **a** is a slightly improved version of the classical model as it considers the resetting of the membrane potential. The idea behind the LIF model is that the dynamics of the membrane potential can be described independent of the different ion types and channels by reducing them to one parameter, the leakage through the resistor R_m. The capacitance of the cell membrane is described by the capacitor C_m. The battery with the voltage u_{rest} accounts for the Nernst potential (or reversal potential) at equilibrium, i.e. if no driving current $I(t)$ is present. The Action potential is not modeled by ion channels in form of variable resistors but is generated simply when the voltage across the capacitor reaches a threshold value. At the same time a voltage driven switch cuts of the circuit from the driving current and resets the voltage across the membrane to u_{reset}. This accounts for the refractory period after the emission of a spike.

2.1.2   Synaptic currents

We use a simple approximation to model the real process of synaptic transmission (background section 1.1.2). Instead of modeling the PSC directly, the change in the synaptic conductance is modeled. The resulting current flow is then determined by the synaptic conductivity and the membrane potential $u(t)$ (which is assumed to be the same at the synapse as at the soma of the corresponding postsynaptic neuron) and the reversal potential E_{syn}. The maximum amplitude of the synaptic conductance g_0 is referred to as synaptic weight, strength or efficacy.

The model

The transient conductance change is modeled by a simple jump and an exponential
decay:

$$g_{i,j}(t) = \begin{cases} 0 & \text{if } t - t_j < \Delta\tau \text{ ,} \\ g_{0;i,j} \, exp(-((t - t_j) - \Delta\tau)/\tau_s) & \text{if } t - t_j > \Delta\tau \text{ .} \end{cases} \qquad (2.2)$$

Where t_j is the spike time of the presynaptic neuron and $g_{0;i,j}$ the peak conductance
of the synapse between presynaptic neuron j and postsynaptic neuron i. The peak
conductance is a measure for the synaptic strength (that is altered by synaptic plasticity,
see section 2.2.1). The jump occurs at the income of a synaptic spike, delayed by the
dendritic latency time constant $\Delta\tau$ that accounts for the fluctuations observed between
the peak AP and the beginning of the PSP measured in rat pyramidal neurons [65].
The resulting synaptic current (PSC), the soma of the postsynaptic neuron receives,
depends on the difference between membrane potential and reversal potential E_{syn},
where it is assumed that the membrane potential is constant along the synapse and
the soma:

$$I_{syn;i,j} = g_{i,j}(t)(E_{syn} - u_i(t)) \qquad (2.3)$$

Here E_{syn} is the reversal potential of the ion type at the synapse, which in the current
work is set to $0mV$ for excitatory synapses and $-70mV$ for inhibitory synapses. Realistic
excitatory postsynaptic potentials (EPSPs) lie in the range of $0-10mV$ [100, 59, 62, 92].
This corresponds to PSC amplitudes around $0 - 1.45nA$ and conductances $g_{0;i,j}$ in the
range of $0 \, nS - 26.5nS$. Note however, that these values for the synaptic conductivity
are based on the parameter we chose in the current work and depend explicitly on
what value the reversal potential E_{syn} takes!

The value of E_{syn} is the only factor in the model that distinguishes postsynaptic
excitation from inhibition [83]. Although mathematically it could simply be incor-
porated in the sign and magnitude of $g_{0;i,j}$. However negative conductivity lags a
proper physical interpretation. If E_{syn} is smaller than the spiking threshold u_{th}, the
postsynaptic potential (PSP) generated by the synapse will be negative and therefore
inhibitory (IPSP) as it lowers the probability of the postsynaptic neuron to exhibit
a spike. For E_{syn} higher than the spiking threshold u_{th} the synapse will generate an

excitatory PSP (EPSP). If $|(\mu_i - E_{syn})|$ is small, where μ is the mean or effective membrane potential, fluctuations in the membrane potential due to input from other synapses have a large impact on the form of the PSP. For excitatory synapses with glutamate receptors that activate Na^+ and K^+ ion flow, the reversal potential is approximately $0\ mV$. With the mean effective membrane potential being about $-55\ mV$, fluctuations in the membrane potential that lie in the range of $\sigma = 1 - 6\ mV$ will have a relatively small impact on the PSP. inhibitory synapses with GABA receptors usually activate Cl^- current flow across the membrane. In this case the reversal potential is about $-70mV$, here the impact of fluctuations is slightly higher [83]. In the following course of this work we will only consider such cases in which $|(\mu_i - E_{syn})| >> \sigma$.

The diffusion approximation

As each neuron receives thousands of presynaptic input spikes it would be very difficult to simulate such a system with the method described above. However, if it is assumed that each postsynaptic current is small and the number of events is large, the fluctuations of the membrane potential can be described as a Gaussian random process. This is called the diffusion approximation [103]. In detail, the total synaptic input current at a given time point t can be written as:

$$I_{tot;i}^{ex,in}(t) = (u_i(t) - E_{syn}^{ex}) \sum_j^{N_{ex}} g_{i,j}^{ex}(t) + (u_i(t) - E_{syn}^{in}) \sum_k^{N_{in}} g_{i,k}^{in}(t) \qquad (2.4)$$

This total current can now be decomposed into a voltage dependent and a voltage independent part. The voltage independent part can be described by a constant current $I_{0;i}$ that originates from averaging over all excitatory and inhibitory conductances $\overline{g^{ex,in}} = (\sum_j^{N_{ex}} g_{i,j}^{ex}(t) + \sum_k^{N_{in}} g_{i,k}^{in}(t))/(N_{ex} + N_{in})$ and a fluctuating part that can be described by the standard deviation of the synaptic background current σ and a Gaussian stochastic process $\eta(t)$ of zero mean and unit standard deviation. For more details see [88]. The voltage dependent part is given by $\overline{g^{ex,in}}\ u_i(t)$ and has no fluctuating part within the diffusion approximation. It can however be included in the model by simply setting R_m to a lower value [78]. The approximation of the input a neuron in a large network receives can therefore be formulated as:

$$I_i(t) = I_{0;i} + I_{Noise;i}(t) \ , \qquad (2.5)$$

Table 2.1: Typically measured values for layer 5 neocortical pyramidal neurons. The values are taken from [78] and [7], where the value for R_m has been reduced by a factor of 2-3 compared to the in vitro values to account for the increased synaptic background input in vivo.

u_{th}	u_{reset}	u_{rest}	R_m	C_m	τ_m	I_{syn}	E_{syn}^{ex}	E_{syn}^{in}	σ
-50 mV	-60 mV	-70 mV	40 MΩ	250 pF	10 ms	10-300 pA	0 mV	-70 mV	1-6 mV

with

$$I_{Noise;i}(t) = \frac{\sigma_i}{\sqrt{\tau}}\eta(t) \tag{2.6}$$

If apart from this background input, the neuron receives any additional input such as specific sensory stimuli $I_{sens;i}(t)$ or synaptic input $I_{syn;i}(t)$ from other neurons that are explicitly modeled, the total input current reads

$$I_i(t) = I_{0;i} + I_{Noise;i}(t) + I_{syn;i}(t) + I_{sens;i}(t) \tag{2.7}$$

2.1.3   Dendritic Spikes

As has been discussed in the background section, dendrites not only sum up and filter the input to the postsynaptic neuron, but also evoke strong and fast spikes. These spikes are found to be triggered by strong synchronous inputs. Jahnke, Timme and Memmesheimer introduced a model that fits the experimentally observed form of a dendritic spike in [49]. The dendritic spike current is described by a sum of exponential functions:

$$I_{dendr} = \theta(t - \tau_{dendr})\left[-A\,exp(-\frac{t - \tau_{dendr}}{\tau_{ds,1}}) + B\,exp(-\frac{t - \tau_{dendr}}{\tau_{ds,2}}) - C\,exp(-\frac{t - \tau_{dendr}}{\tau_{ds,3}})\right] \tag{2.8}$$

With $A = 55nA$, $B = 64nA$ and $C = 9nA$. The dendritic time constants are $\tau_{ds,1} = 0.2ms$, $\tau_{ds,2} = 0.3ms$, $\tau_{ds,3} = 0.7ms$. and the dendritic delay $\tau_{Dendr} = 3ms$ (These parameter values are oriented on the values from the original paper by Jahnke et al. [49]).
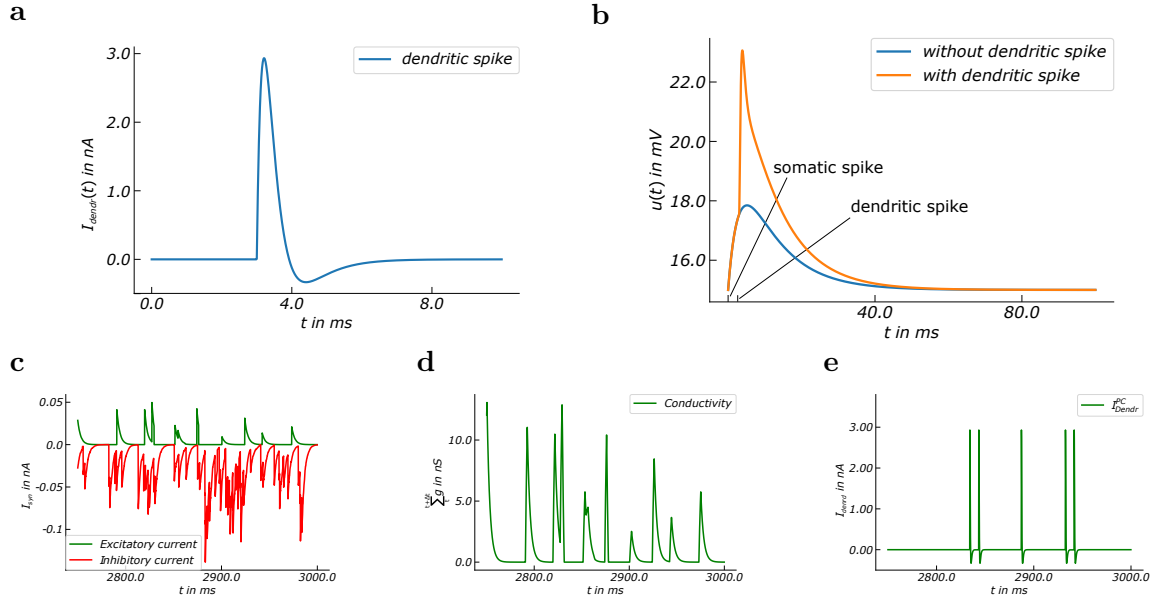
Fig. 2.2: Panel **a** shows the transient of a dendritic spike which evokes a fast and strong depolarization response in the membrane potential (Fig. **b**). The PSCs evoked by by incoming spikes $I_i(t)$ are shown in panel **c** (excitatory currents are shown in green and inhibitory currents in red). The PSCs are modeled via synaptic conductance changes. If the sum of these conductance changes over a time period of $\Delta\tau = 2ms$ (**d**) crosses the dendritic spiking threshold Θ, dendritic spikes are generated (**e**).

The dendritic spikes are evoked if the sum over the total synaptic conductivity transient in a time window $\Delta t = 2ms$ crosses a threshold Θ. While somatic spikes alter the conductivity and thereby determine the PSC amplitude, the dendritic current is approximated to be of constant shape and not dependent on $u_i(t)$.

2.1.4 Network-topology

The goal of the current work is to investigate the dynamics of a network that has properties of those found in the hippocampus. Since it is not known how exactly the hippocampus is wired, some approximations based on current knowledge about the hippocampus have to be made.

connectivity experimental: Most biological neural networks are sparse with a connectivity of roughly 10 %. However this number is an estimate based on EPSP recordings and it is unclear how many connections are not detected because they are too weak [9]. Recent findings also show that the connection probability in some brain

areas depends on different properties such as inter-somatic distance [81],[34].

weights experimental: Measurements of EPSP amplitudes in slices of hippocampal CA1 and CA3 neurons are available [90], from which the weight disribution can be estimated. It is found that the hippocampal weight distribution for excitatory connections peaks around $0.1mV$ (Fig. 2.3, **b**).

connectivity model: The current work will not focus on the details of neuronal connectivity and initiate connections randomly. Non random features will, for reasons of simplicity and scope of this work, be ignored. The network used in this work is constructed of N_{ex} excitatory and N_{in} inhibitory neurons., with a ratio of $4 : 1$. This ratio is often used in theoretical frameworks and found to be a good balance between excitation and inhibition, where the firing statistics match those observed experimentally (firing is irregular and asynchronous) [8],[16]. The initial connectivity is drawn randomly with connection probabilities $p_{ex,ex} = 0.1$, $p_{ex,in} = 0.1$, $p_{in,ex} = 0.1$, $p_{in,in} = 0.02$ that account for the observation that connectivity is sparse ($\approx 10\%$).

synaptic weight-distribution model: Based on known weight distributions, the connection strengths are drawn from a Gaussian distribution, truncated at 0 to ensure only positive connection strengths. Mean and standard deviation are chosen to approximately fit experimental observations [90] with $\mu_{ex,ex} = 0.35nS$ and $\sigma_{ex,ex} = 0.08nS$ (see fig. 2.3). The weights for the other connection types are also drawn from Gaussian distributions, where the values for mean and STD are oriented on [49], with $\mu_{ex,in} = 1.2nS$ and $\sigma_{ex,in} = 0.12nS$, $\mu_{in,ex} = 0.5nS$ and $\sigma_{in,ex} = 0.05nS$, $\mu_{in,in} = 1nS$ and $\sigma_{ex,ex} = 0.1nS$. Note again that the estimation of these conductivities is based on the reversal potential we chose in the current work (see equation 2.3).

Axonal and dendritic delays

Signal transmission in the brain does not happen instantaneously but is delayed by the time a signal needs to travel through the axon and the dendrites. The time, the signal travels from the synapse, along the dendrite to the soma, has an direct impact on STDP, since a large dendritic delay time means that the back propagating signal from the soma that tells the synapse that a postsynaptic spike occurred is delayed. The axonal delay might underly large fluctuations from neuron pair to neuron pair, since neuron pairs can be spatially spread. Dendrites are however a rather local structure,
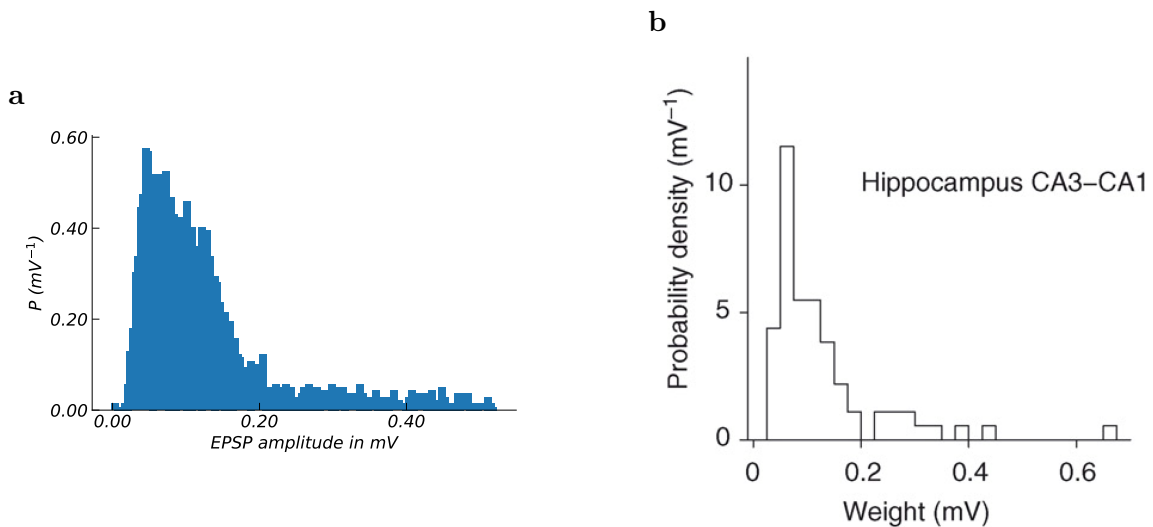
Fig. 2.3: Weight distribution in terms of the EPSP amplitudes. Panel **a** shows the weight distribution drawn from a Gaussian distribution that is truncated at 0 (see text). Panel **b** shows the weight distribution determined from experimental data of hippocampal CA1-CA3 excitatory neuron connections. Panel **b** is taken from [9], where Barbour et al. estimated the weight distribution with data from [90]

therefore fluctuations are comparably small.In the current work it is assume that the dendritic delay is constant for all synaptic connection. Further we assume that the here studied neuron ensemble is spatially close, such that differences in axonal delays between the neurons are small. We therefore ignore axonal delays. The value of the dendritic delay is set to equal the time interval, at which the LTP-domain of the STDP rule has its maximum (see section 2.2.1). We motivate this choice by the argument that a strong PSC that evokes a direct postsynaptic spike response should result in maximal potentiation.

a
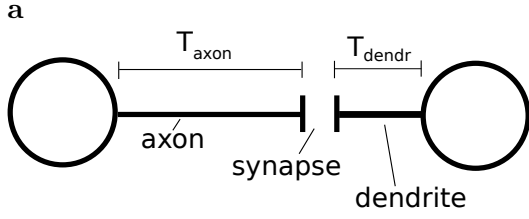
Fig. 2.4: Conduction delay has to be differentiated into axonal delay τ_{axon} and dendritic delay $\tau_{dendr.}$. Axonal delay describes the time, an action potential travels from the presynaptic neuron to the synapse that connects it to a postsynaptic neuron. The dendritic delay accounts for the time, the synaptic current signal travels from the synapse to the soma of the postsynaptic neuron

2.2 Synaptic plasticity

2.2.1 Spike time depended plasticity and synaptic scaling

In this section the form of the function describing the STDP learning window as well as a mechanism for homeostatic scaling are presented.

Different forms of STDP rules have been observed [52]. It is therefore important to first specify which properties of STDP to include in the model and to make clear that synaptic plasticity can be much more diverse. STDP rules have been fitted to several experimental data, most commonly [64] and [85]. Experimental data is usually fitted by two exponential functions [85], [55]. Here the results from [55] are taken as the basis for the analysis and model.

$$\Delta g_0 = W(\Delta t) = \eta \begin{cases} e^{-\frac{\Delta t}{\tau_s}} \left[A_+ \left(1 + \frac{\Delta t}{\tau_{+,1}} \right) + A_- \left(1 + \frac{\Delta t}{\tau_{-,1}} \right) \right] & \text{if } \Delta t \geq 0 \\ \\ A_+ \ e^{\frac{\Delta t}{\tau_{+,0}}} + A_- \ e^{\frac{\Delta t}{\tau_{-,0}}} & \text{if } \Delta t < 0 \ , \end{cases} \tag{2.9}$$

with

$$\begin{aligned} \tau_{+,1} &= \tau_s \ \frac{\tau_{+,0}}{\tau_s + \tau_{+,0}} \\ \tau_{-,1} &= \tau_s \ \frac{\tau_{-,0}}{\tau_s + \tau_{-,0}} \ . \end{aligned} \tag{2.10}$$

η is the so called STDP learning rate, which defines how fast (by what amount per spike pair) the synapse is changed. Values for the several parameter are given in table

a

$$
\begin{array}{l}
\tau_s = 3.0\ ms \\
\tau_s = 4.0\ ms \\
\tau_s = 5.0\ ms
\end{array}
$$
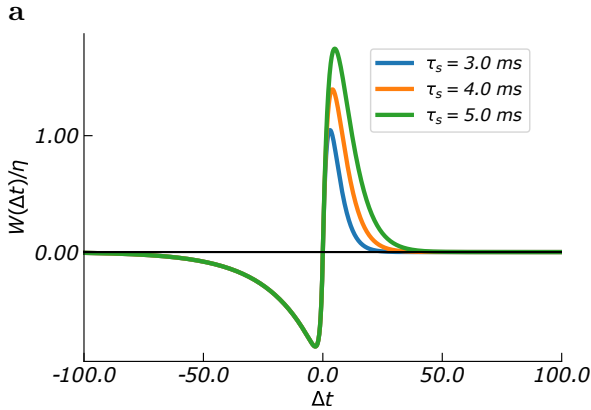
Fig. 2.5: STDP learning window taken from [55] that has been fitted to experimental data. The learning window is described by two regions. For negative spike timing differences between pre- and postsynaptic neuron (i.e. postsynaptic firing occurs before the presynaptic firing), STDP is characterized by a negative synaptic change, also referred to as long term depression (LTD). For positive spike timing difference, synaptic connection are strengthened, referred to as Long term potentiation (LTP). The exact form of the STDP window varies depending on neuron type, brain region and stimulus.Therefore we here shown STDP rule, although fitted to experimental data (for $\tau_s = 5ms$), is only a rough approximation. An important property of STDP is however, whether it is LTD-dominated, balanced or LTP-dominated. These three cases can be established with the original fit as a basis by altering τ_s. $\tau_s = 3ms$ corresponds to LTD-dominated, $\tau_s = 4ms$ to balanced and $\tau_s = 5ms$ to LTP-dominated.

2.2. The values of the exponential decay constants determine weather LTP dominates over LTD or vice versa. In the current work we change the dominance of STDP by changing the size of the LTP domain via τ_s. $\tau_s = 3$ generates a LTD-dominated, $\tau_s = 5$ a LTP dominated STDP rule (Fig. 2.5).

Table 2.2

η	τ_s	$\tau_{+,0}$	$\tau_{-,0}$	A_+	A_-
12 pS	3,4,5 ms	1 ms	20 ms	1	-1

While this form of STDP learning rule is most established, STDP rules can also have very different shapes depending on the brain region, firing rate, bursting and synaptic strength [19], e.g. where LTP only depends on the absolute value of of the time difference but not on its sign as described above [19], [1]. However the analysis of all these different types is not the focus and would go beyond the scope of this work.

Synaptic scaling

Hebbian plasticity needs to be regulated, since the positive feedback, that originates from the fact that synapses that got potentiated, increase the probability that a presynaptic evokes a postsynaptic spike, which leads to even more potentiation. Weight independent STDP, also referred to as additive STDP, leads to unrealistic weight distributions, where synapses grow unbounded or shrink down to zero. One way to stabilize synaptic growth is via weight dependent STDP (multiplicative STDP), where strong synapses grow slower than weak synapses. This leads to stable hebbian learning [108]. Another proposed regulatory mechanism is Synaptic Scaling (SS), which globally adjusts all synapses onto a postsynaptic neuron depending on the postsynaptic firing rate. As for STDP, this mechanism can be either weight dependent (multiplicative) or weight independent (subtractive). Both cases introduce further competition between synapses, since all connections get scaled down if some subset triggers a high postsynaptic activity. Therefore only those connections which are highly correlated with the postsynaptic neuron are likely to survive due to STDP induced LTP. Such a mechanism that globally alters synaptic strength based on neuronal activity has been observed in cultured networks, where inhibition of activity let to synaptic strengthening and increasing the activity let to downscaling [105], [60] (hippocampus), [72].

Synaptic scaling can be described by a mechanism similar to Oja's rule who introduced a regulating term to hebbian learning that depends on the square of the output response of a neuron and the synaptic weight [73].

A slightly altered function for the synaptic scaling mechanism has been introduced in [97], where it has been shown that a convex non-linear weight dependence generically stabilizes excitatory and inhibitory synapses, whereas linear weight dependence only stabilizes under certain conditions. In the current work the following rule will therefore be used as a basis:

$$\frac{dg_{0;i,j}}{dt} = \eta_{SS} \left(\frac{g_{0;i,j}}{g^*} \right)^\lambda [r_T - r_i(t)] \; , \tag{2.11}$$

where η_{SS} is the SS learning rate of the synaptic scaling mechanism that defines the timescale on which the mechanism acts and g^* a normalization factor in nS. r_T is the target firing rate. In the current work we study SS for $\lambda = 1$, which will be referred to as the linear SS rule and $\lambda = 2$, referred to as the convex SS. r_T is set to 0. η_{SS} is

adjusted depending on the STDP parameter τ_s, i.e. depending on whether STDP is LTD-dominated, balanced or LTP-dominated.

Estimating the instantaneous firing rate

Because in the current work, a spiking neural network model is used, the firing rate $r(t)$ needs to be estimated from the spike train a neuron exhibits. Alternatively, the synaptic scaling rule 2.11 could be implemented in such a model by reformulating it to an event driven rule, where scaling is introduced each time the postsynaptic neuron spikes. Here we use the first approach. The instantaneous firing rate is in practice often estimated by binning a recorded spike train. A biological neuron however probably has no mechanism that determines the firing rate of the neuron by binning its past spikes. Rather the firing rate of a neuron is saved in some concentration transient. The instantaneous firing rate is indeed well approximated by a function describing an instantaneous jump with a subsequent exponential decay. Biologically this could be interpreted as a model for the calcium concentration in the soma which would reflect the neurons activity. The time constant with which the concentration decays can be interpreted as the size of the binning window. Figure 2.6 show a comparison between the estimated spontaneous firing rate using the binning method and the exponential function method, which is described by eq. 2.12, which is in analogy to the model for calcium-based plasticity in [44]:

$$\frac{dc}{dt} = -\frac{c}{\tau_c} + C_{post} \sum_i \delta(t - ti) \ . \tag{2.12}$$

Here τ_c is the decay time constant, and C_{post} the postsynaptic spike evoked jump in calcium concentration.

2.2.2   Spike based hebbian learning

In this section a mathematical formulation of correlation-based hebbian learning for spiking neurons is sketched based on [41]. A neuron receives input from $N >> 1$ synapses with different peak conductances $g_{0;i,j}$ for $1 \leq i, j \leq N$ and $i \neq j$. Changes in the peak conductance are introduced in three possible ways [55]:

1. The nth incoming spike at time t_j^n changes $g_{0;i,j}$ by an amount ω_{in} independent of the spike timing of the postsynaptic neuron i,

a
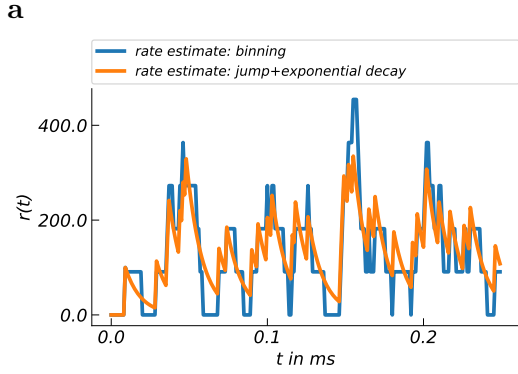
Fig. 2.6: The instantaneous firing rate of a neuron is well captured by a jump at the time of spike initiation and a subsequent exponential decay with right chosen amplitude and decay time constant.

2. the mth output spike at time t_i^m changes $g_{0;i,j}$ by an amount ω_{out} independent of the spike timing of the presynaptic neuron j,

3. the time difference between incoming and outgoing spike $\Delta t = t_i^n - t_j^m$ changes $g_{0;i,j}$ by $W(\Delta t)$.

Here $W(\Delta t)$ again defines the STDP learning window, which describes the dependency of the change in synaptic strength on the pre-/post- spike timing difference. Cases 1. and 2. describe mechanisms that do not depend on spike time correlations. They can either act global, if ω_{in} and ω_{out} are independent of $g_{0;i,j}$, or local in the case of such a dependence. For $\omega_{out} < 0$, case 2. can be interpreted as a mechanism for homeostatic downscaling.

The three mechanisms shall now be described in a more mathematical way, which closely follows [55]. A neuron i exhibits a spike train that can be formulated as follows:

$$S_i(t) = \sum_{spike} \delta(t - t_i^{spike}) . \tag{2.13}$$

Using this description of a spike train, the three types of synaptic change due to spiking of the pres-synaptic neuron j and postsynaptic neuron i can be formulated in one equation:

$$\Delta g_{0;i,j}(t) = \Big[\underbrace{\omega_{in}\, S_j(t)}_{case1} + \underbrace{\omega_{out}\, S_i(t)}_{case2} \Big] + \int_{-\infty}^{\infty} dt'\, \underbrace{W(t - t')S_j(t)S_i(t')}_{case3} . \tag{2.14}$$

Equation 2.14 correlates presynaptic and postsynaptic spike trains.

The analysis of equation 2.14 is in general rather complicated, because neurons exhibit spikes in a complex, stochastic manner. Therefore the change in synaptic conductance $\Delta g_{0;i,j}(t)$ is also a stochastic variable. An analytically more tractable formulation can however be found by focusing on the mean of $\Delta g_{0;i,j}$, which can be found by calculating the ensemble average of the process described by eq. 2.14. Taking the ensemble average of eq. 2.14, denoted by $\langle . \rangle$, and substituting $s = t - t'$, one obtains [55]:

$$\langle \Delta g_{0;i,j} \rangle (t) = \left[\omega_{in} \, \langle S_j \rangle (t) + \omega_{out} \, \langle S_i \rangle (t) \right] + \int_{-\infty}^{\infty} ds \, W(s) \langle S_j(t+s) S_i(t) \rangle \ , \tag{2.15}$$

where $\langle S \rangle (t)$ is called the instantaneous firing rate.

$$r_j(t) = \langle S_j(t) \rangle \ , r_i(t) = \langle S_i(t) \rangle \ . \tag{2.16}$$

The cross correlation function is defined by:

$$C_{cross;i,j}(s;t) = \langle S_j(t+s) S_i(t) \rangle \ . \tag{2.17}$$

Then, the ensemble averaged learning equation reads

$$\langle \Delta g_{0;i,j} \rangle (t) = \omega_{in} \, r_j(t) + \omega_{out} \, r_i(t) + \int_{-\infty}^{\infty} ds \, W(s) C_{cross;i,j}(s;t) \ , \tag{2.18}$$

Thereby, the average change in synaptic conductivity at a given point in time t can be calculated from the crosscorrelation function between the post- and presynaptic spike trains. This is a useful feature for the analysis of plastic networks with STDP since the crosscorrelation function can be easily estimated from long enough spike train data. Under some conditions also an analytical expression in linear approximation is known to the crosscorrelation function between pairs of LIF neurons.

2.3   Spatial learning

Some background on the theory of hippocampal learning and place cells has been given in the background section 1.4. Here a model for place cell learning introduced by [49] that sets the bases for memory representations in the current work will briefly be discussed. Each place encoding neuron i is assigned a place field P_i that is centered at x_i^{ctr}, which corresponds to a point in the space that our agent "explores". The width of this place field is described by Δw_i. The place field is randomly assigned to each encoding neuron by

$$P_i = [x_{ctr;i} - \frac{\Delta w_i}{2}, x_{ctr;i} + \frac{\Delta w_i}{2}] \ . \tag{2.19}$$

If during exploration the current position of our agent (e.g. a rat) is within the place field of some place cell i, the associated neuron receives a current pulse of width ΔT_{PF} and Amplitude I^{PF}. The amplitude of the current pulse depends on the distance of the current position to the center of the neurons place field

$$I_{PF}(\tilde{x}_i) = I_{max}(-(2 \ \tilde{x}_i(t) - 1)^2 + 1) \ , \tag{2.20}$$

where I_{max} is the maximum possible amplitude of the current pulse and

$$\tilde{x}_i(t) = \frac{x(t) - (x_{ctr;i} - \frac{\Delta w_i}{2})}{\Delta w_i} \ . \tag{2.21}$$

Here $x(t)$ is the position of the agent. The current pulses occur in time intervals that are time locked to a virtual theta oscillation with a frequency of 8 Hz. The theta oscillation starts at the beginning of a simulation and is not altered within, i.e. the current pulses occur in given time intervals, however slightly shifted depending on the position of the agent relative to the individual place cell center. This is motivated by the experimental finding that the timing of spikes during spatial learning depends on the position relative to the place-field center and on the phase of background theta oscillations [75]. The phase shift ΔT_{shift} is given by:

$$\Delta T_{shift}(\tilde{x}_i) = 0.9(1 - \tilde{x}_i^2) * T \ , \tag{2.22}$$
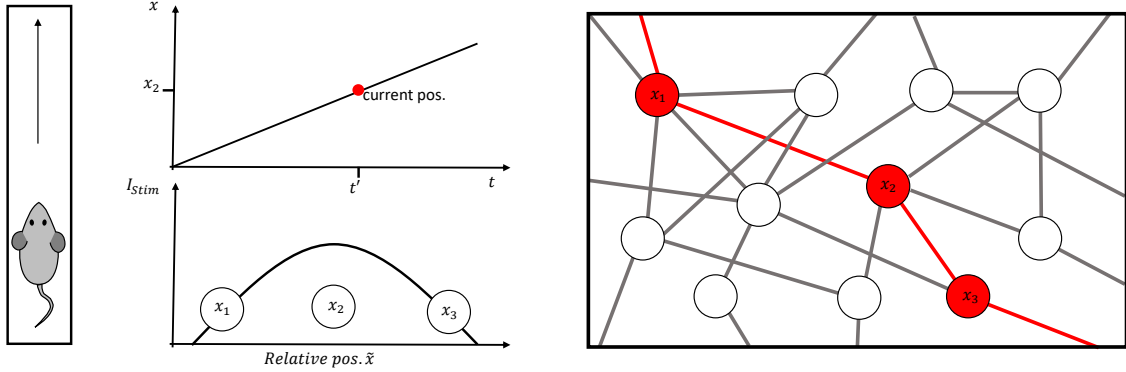
Fig. 2.7: The network is send down a linear track, here depicted by a mouse (left side). When the animal enters the place field of a neuron, the corresponding neuron gets an input pulse whose amplitude and timing depends on the distance to the place field center (eq. 2.20, 2.21, 2.22). The current pulse amplitude as a function of the relative position of the animal to the neurons place field center is sketched in the middle, bottom. Neurons with adjacent place fields that are connected via synapses alter their connectivity based on the different timing due to the phase shift in the current pulses they receive (right).

where T is the time of one oscillation period, i.e. 0.125 s. When the agent is send down a linear track, the phase shift between stimuli that is induced by 2.22 results in the development of a FeedForward- (FF) structure between neurons with place fields (Fig. 2.8, **a**). Synaptic connections between neurons become potentiated if the agent reaches the location of the presynaptic before the postsynaptic placefield. Therefore, because of the time shift $\Delta T_{shift}(\tilde{x}_i)$, the postsynaptic neuron will fire subsequent to the presynaptic neuron, which potentiates their connection due to STDP.

While this learning procedure from [49] produces memory representations of spatial tracks in a biologically motivated way that is in agreement with some experimental observations, the resulting FF -structure, whose width and height depends mainly on the parameter Δw_i, is predictable and can without strong assumptions be fitted by a function of exponentials. To reduce complexity and time consumption, the network topology will for further simulations be created by the function:

$$g_{ij} = \begin{cases} g_1\left(e^{-\frac{\Delta x_{ij}}{\tau_A}} - e^{-\frac{\Delta x_{ij}}{\tau_B}}\right) & \text{if } \Delta x_{ij} > 0 \\ g_2\left(e^{-\frac{\Delta x_{ij}}{\tau_C}} - e^{-\frac{\Delta x_{ij}}{\tau_D}}\right) & \text{if } \Delta x_{ij} < 0 \ , \end{cases} \tag{2.23}$$
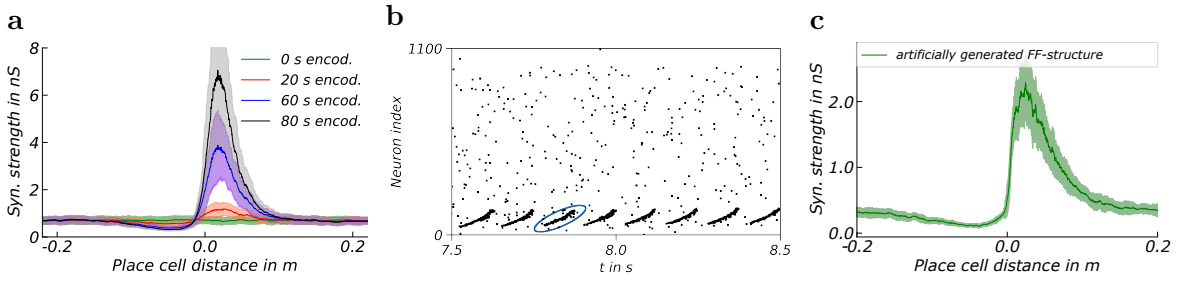
Fig. 2.8: A neural place cell model, with theta-oscillation time locked sensory stimuli pulses leads to FF-structures during training along a linear track. Panel **a** shows the evolution of the feed-forward structure after different simulation cycles, where in each cycle the system is ones send down the linear track. The neural response to sensory stimulus in the form of theta locked current pulses is shown in figure **b**. Instead of training the network to achieve a FF-structure as in **a**, equation 2.23 is used to achieve a equivalent network topology (**c**).

which qualitatively captures the result from the training procedure but is less time consuming. Here g_1 describes the amplitude of the FF-connections and g_2 the amplitude of the backwards connections which are depressed slightly due to the learning procedure.

2.4 Measures for the classification of neural network dynamics

2.4.1 Estimating the crosscorrelation function from spike data

As has already been pointed out in the course of this section, the crosscorrelation between post- and presynaptic spike trains plays an important role in STDP and therefore for its closer study. With long enough measurements of spike trains the crosscorrelation function can easily be estimated. Analytical expressions are however hard to derive, as will be shown in the last section.

The cross correlation for positive and negative times can be estimated from the simulated spike trains in terms of the firing rate at time Δt before and after a presynaptic spike:

$$C_{Cross}(t) = \frac{1}{\Delta t} \frac{\int_{t_{pre}+t}^{t_{pre}+t+\Delta t} \sum_j \sum_f \delta(t - t_j^f) dt}{N} = \frac{Prob[Neuron\ to\ spike\ n\ times\ in\ \Delta t](t)}{\Delta t} \ , \ (2.24)$$

where t_{pre} is the time of the presynaptic spike arriving at the synapse. When calculating the crosscorrelation function in terms of the factor by which the rate changes relative to the mean firing rate r_0 (and thereby the probability to fire), the following relationship holds:

$$C^*_{Cross}(t) = \frac{C_{Cross}(t)}{r_0} - 1 \ . \tag{2.25}$$

The key benefits of evaluating the crosscorrelation function from simulated data are that the analysis of the crosscorrelation itself leads to a better understanding of the synaptic dynamics. Moreover, ones the crosscorrelation function is known, different correlation based plasticity mechanisms can be analyzed via integration without the need of any further simulation (eq. 2.18).

2.4.2 Quality of replay

The quality of a replay event is quantified by measuring the sequence of spiking for neighboring neurons within the ff-structure. If in a neuron pair the post synaptic neuron fires within a time window of $\Delta T = 20ms$ after the presynaptic neuron, the order of spiking is in agreement with the local connectivity. If the postsynaptic spike occurs before the postsynaptic spike, the order is opposite to the local connectivity. The replay quality is measured using the matching index M, which has also been used to quantify the quality of replay in [50] and [49].

$$M = \frac{n_{true} - n_{false}}{n_{true} + n_{false}} \ , \tag{2.26}$$

where n_{true} is the number of spike pairs that occurred in the correct order and n_{false} the number of spike pairs that occurred in the wrong order. Therefore, if there is no preferred direction of spiking, $n_{true} = n_{false}$ and the matching index goes to zero, while for growing n_{true} and shrinking n_{false}, M converges to 1 (or -1 for the opposite case). The matching index is a measure similar to the crosscorrelation as it detects the order of spiking in a similar way. The difference is that crosscorrelation does this in theory in continuous time (not in practice, where simulations are done in discrete time steps, and cross correlation is estimated via small bins), while the matching index counts the occurrence of spikes within in a large binning window ($\Delta T = 20ms$) where the information of the exact timing is lost. Further the matching index gives

the normalized fraction between the number of events that occurred after and before a presynaptic spike, therefore the total number of events is lost too. However, the matching index requires far less data and is therefore a good indicator for how activity distributes in a network when simulating large networks which is time consuming. Note that crosscorrelation and matching index M are both a measure of correlation, not causality!

2.5 Analytical expression for the crosscorrelation of a weakly coupled LIF pair

To be able to analytically study the dynamics of the plastic neural network using the learning equation 2.18, an expression for the cross correlation function between spiking neurons (here LIF model neurons) is needed. This is a very difficult task, as the change in probability of emitting a spike has to be calculated depending on the input current received by a presynaptic neuron in the presence of stochastic noise that mimics the input from the thousands of other connected neurons. The approach proposed by S. Ostojic and N. Brunel [78, 18], which gives the crosscorrelation in linear approximation, will be sketched below. Notice however, that this approach is only able to describe the crosscorrelation between neuron pairs. Further, the linear approximation only holds for small PSC amplitudes, strong connections are not accurately described.

Given a single neuron pair of LIF neurons that is unidirectionally connected and only receive a constant current and Gaussian white noise (diffusion approximation), the dynamics of the presynaptic membrane potential is given by

$$\tau_m \frac{du_{pre}}{dt} = u_{rest} - u_{pre} + R_m \ I_{0;pre} + \frac{\sigma_{pre}}{\sqrt{\tau_m}} \eta_{pre} \ , \tag{2.27}$$

where $I_{0;pre}$ is the constant background current and $\frac{\sigma_{pre}}{\sqrt{\tau_m}}\eta_{pre}$ describes the white noise (see section 2.1.3 , diffusion approximation). The membrane potential of the post-synaptic neuron further receives spiking input from the presynaptic neuron. Therefore the dynamics of the postsynaptic membrane potential are described by

$$\tau_m \frac{du_{post}}{dt} = u_{rest} - u_{post} + R_m \ I_{0;post} + \frac{\sigma_{post}}{\sqrt{\tau_m}} \eta_{post} - R_m \ g(t)[u_{post} - E_{syn}] \ , \tag{2.28}$$

where the postsynaptic conductance change $g_{tot}(t)$ imposed by the presynaptic spike-train $S_{pre}(t)$ (see section 2.1) is given by:

$$g_{tot}(t) = \int_0^\infty d\tau g(\tau) \, S_{pre}(t - \tau) \ . \tag{2.29}$$

Here, we have written g instead of $g_{post,pre}$ for better readability. Note however that g is specific for the individual pre- postsynaptic connection. The formulation chosen in 2.28, splits the state equation up into an unperturbed part (leak term, base current+noise) and a perturbation, caused by the presynaptic neuron.

We now may ask, how does the probability that the postsynaptic neuron fires change due to the arrival of a presynaptic spike? This question can be reformulated by asking, how does the instantaneous firing rate of the postsynaptic neuron change after the arrival of a presynaptic spike, which has basically the same meaning as the first formulation. One finds that this question is actually not that easy to answer, because we deal with a system, where the response (in terms of the firing rate) of a LIF neuron to an input current is nonlinear. However, a linear approximation to the rate response is in good agreement with the actual response in a certain regime of the input current amplitude. Fourcaud-Trocme et al. [38] showed that, in the limit where $g_{tot}(t)[u_{post} - E_{syn}]$ is small, the instantaneous firing rate can be approximated by a linear relationship:

$$r_{post}(t) = r_{0;post} + \int_0^\infty d\tau R_I(\tau) g_{tot}(t - \tau)[\mu - E_{syn}] \ , \tag{2.30}$$

where $R_I(\tau)$ is some linear filter that is called the rate response function to an arbitrary input current. $r_{0;post}$ is the firing rate for a constant driving-current I_0 with Gaussian white noise (diffusion approximation). With equation 2.30 we now have a starting point for deriving an expression of the crosscorrelation function. In section **??**, the definition of the crosscorrelation function has been given as the ensemble average of the product of the pre- and postsynaptic spiketrains S_{pre}, S_{post} (Eq. 2.17) (the indices's pre, post in C_{cross} are left out for readability):

$$C_{cross}(s; t) = \langle S_{pre}(t) S_{post}(t + s) \rangle \ . \tag{2.31}$$

Further, the instantaneous firing rate is defined by $r_i(t) = \langle S_i \rangle$ and for a constant input current we write $r_{0;i}(t) = \langle S_{0;i} \rangle$. Therefore, we may rewrite equation 2.30 as

$$r_{post}(t) = \langle S_{post}(t) \rangle = \langle S_{0;post} \rangle + \int_0^\infty d\tau R_{I;post}(\tau) g_{tot}(t - \tau)[\mu - E_{syn}] . \qquad (2.32)$$

With the presynaptic spiketrain S_{pre}[1] and combining equations 2.31, 2.32 , we derive at an expression for the crosscorrelation function in terms of the rate response function $R_{I;post}(\tau)$

$$C_{cross}(s;t) = \langle S_{0;pre} \ S_{0;post} \rangle + \int_0^\infty d\tau R_{I;post}(\tau)(\mu - E_{syn})\langle S_{pre}(t+s) \ g_{tot}(t-\tau) \rangle$$
$$(2.33)$$

and expressing $g_{tot}(t - \tau)$ with equation 2.29

$$= \langle S_{0;pre} \ S_{0;post} \rangle + \int_0^\infty \int_0^\infty d\tau d\tau' R_{I;post}(\tau) g(\tau')[\mu - E_{syn}] \ \langle S_{pre}(t+s)S_{pre}(t-\tau'-\tau) \rangle .$$
$$(2.34)$$

When taking the Fourier transform with respect to t and t+s, the convolution integral in 2.33 turns into products. The ensemble average over the product of the Fourier-transformed presynaptic spike train $\langle S_{pre}(\omega)S_{pre}(\omega') \rangle$ is the power spectrum of the presynaptic neuron $A_{pre}(\omega)$. Then the crosscorrelation function reads [78]

$$C_{Cross}^*(\omega) = \frac{r_{0;pre}}{r_{0;post}} R_{I;post}(\omega) g(\omega)[\mu - E_{syn}] A_{pre}(\omega) , \qquad (2.35)$$

where the crosscorrelation is given in terms of the factor by which the rate changes relative to the mean firing rate r_0 (see section 2.4.1). We derive the crosscorrelation in terms of the change in the firing rate in the time domain via back-transformation and subsequent multiplication and addition of $r_{0;post}$.

$$C_{Cross}(t) = FT^{-1}(C_{Cross}^*(\omega)) \ r_{0;post} + r_{0;post} \qquad (2.36)$$

---

[1] We now assume that the input to the presynaptic neuron can be described in the diffusion approximation

To be able to calculate a solution for equation 2.35 we need an expression for $r_{0,pre}$ (or $r_{0,post}$), $A_{pre}(\omega)$ and $R_{I,post}(\omega)$.

To calculate the rate response function and the firing rate r_0 to a constant input current I_0, we need to solve the Fokker-Planck equation for the probability distribution of the LIF membrane potential. In detail, we need to know the probability that the membrane potential u crosses the spiking threshold u_{th} Δt second after the last reset, given some input current $I(t)$.

Expression for r_0

Let $P(u,t)$ be the probability distribution to find the membrane depolarization potential at u at time t . The time evolution of the probability distribution can be described by the Fokker-Planck equation (see e.g. [18]):

$$\tau_m \frac{\partial P(u,t)}{\partial t} = \frac{\sigma^2(t)}{2} \frac{\partial^2 P(u,t)}{\partial u^2} + \frac{\partial}{\partial u} \Big[(u - \mu(t))P(u,t) \Big] \; , \tag{2.37}$$

where $\mu(t)$ is the effective mean membrane potential. The first term on the r.h.s. describes the fluctuations of size σ and the second the drift due to the stochastic synaptic input. The probability flux $J(u)$ through u is then given by [37]:

$$J(u) = -\frac{u - \mu}{\tau_m} P(u,t) + \frac{\sigma^2}{2\tau_m} \frac{dP(u,t)}{du} \tag{2.38}$$

The probability flow through the threshold u_{th} gives the firing rate at time t $J(u_{th}, t) = r(t)$. As the membrane potential is reset after a spike, an absorbing boundary has to be introduced, setting $P(u_{th}, t) = 0$. The probability current through the boundary therefore gives the probability of emitting a spike [18]:

$$\frac{\partial P(u_{th}, t)}{\partial u(t)} = -\frac{2r(t)\tau_m}{\sigma(t)^2} \; , \tag{2.39}$$

Further, due to the resetting, the probability current flow through u_{reset} from below is given by the current flow from above minus the current flow through u_{th}:

$$\frac{\partial P(u_{reset-}, t)}{\partial u(t)} = \frac{\partial P(u_{reset+}, t)}{\partial u(t)} - \frac{\partial P(u_{th}, t)}{\partial u(t)} = \frac{\partial P(u_{reset+}, t)}{\partial u(t)} + \frac{-2r(t)\tau_m}{\sigma(t)^2} \ . \quad (2.40)$$

Additional conditions are $\lim_{u \to -\infty} = 0$ and $\int_{-\infty}^{u_{th}} P(u, t)du = 1$. With these conditions, solutions for $P(u)$ can be derived for the stationary state, i.e. when the neuron only receives a constant stimulus and white noise ($\mu(t) = \mu_0$, $\sigma(t) = \sigma_0$ and $P(u, t) = P_0(u)$). The solutions for $P_0(u)$ can be given in integral form, from which the stationary firing rate r_0 is be determined (Eq. 2.39) [18]

$$r_0 = \left[\tau \int_0^\infty du \ e^{-u^2} \left[\frac{e^{2y_{th}u} - e^{2y_{reset}u}}{u} \right] \right]^{-1}, \quad (2.41)$$

where $y_{th} = \frac{u_{th} - \mu_0}{\sigma_0}$ and $y_{reset} = \frac{u_{reset} - \mu_0}{\sigma_0}$.

Rate-response function

Brunel et al. derived a solution for $R_I(\omega)$ in linear approximation in [17].

$$R_I(\omega) = \frac{r_{0;post}}{g_m \sigma(1 + i\omega\tau_m)} \frac{\frac{\partial U}{\partial y}(y_{th}, \omega) - \frac{\partial U}{\partial y}(y_{rest}, \omega)}{U(y_{th}, \omega) - U(y_{rest}, \omega)}, \quad (2.42)$$

with

$$y_{th} = \frac{(u_{th} - I_0)}{\sigma}, \quad (2.43)$$

$$y_{rest} = \frac{(u_{rest} - I_0)}{\sigma} \ . \quad (2.44)$$

$U(y, \omega)$ is given by the following differential equation (Kummer's differential equation):

$$\frac{d^2 U}{dy^2} = 2y \frac{dU}{dy} + 2i\omega\tau_m U \ . \tag{2.45}$$

For which the following analytical solution in terms of the special mathematical function, the confluent hyper-geometric function is know [17]:

$$U(y, \omega) = \frac{e^{y^2}}{\Gamma((1 + i\omega\tau_m)/2)} M(\frac{1 - i\omega\tau_m}{2}, \frac{1}{2}, -y^2) + \frac{2ye^{y^2}}{\Gamma((i\omega\tau_m)/2)} M(1 - \frac{i\omega\tau_m}{2}, \frac{3}{2}, -y^2) \ , \tag{2.46}$$

where $M(y, \omega)$ is the confluent hyper-geometric function [4].

The response is given relative to the unperturbed stationary firing rate $r_{0;post}$. Its unit is therefore $\frac{Hz}{pA}$ and $\frac{R_I(\omega)}{r_{post,0}}$ would therefore give the fraction of change in rate per pA of input. When the firing rate is interpreted as the probability of the neuron to fire, $\frac{R_I(\omega)}{r_{0;post}}$ basically describes the change in firing probability in response to an input.

Power spectrum of a LIF neuron

If the input signal is Poissonian, the power-spectrum of the incoming current would be a constant. For the case of a presynaptic LIF neuron, driven by a constant current I_0 and Gaussian white noise, the power-spectrum is not a constant. An analytical expression can be given in terms of the Fourier transform of the inter-spike interval distribution $P_{ISI}(\omega)$ [41]. It is given by [78]:

$$A(\omega) = \frac{(1 + 2Re(A_+(\omega)))}{r_{0;pre}} \ , \tag{2.47}$$

where

$$A^+(\omega) = \frac{P_{ISI}(\omega)}{1 - P_{ISI}(\omega)} \ . \tag{2.48}$$
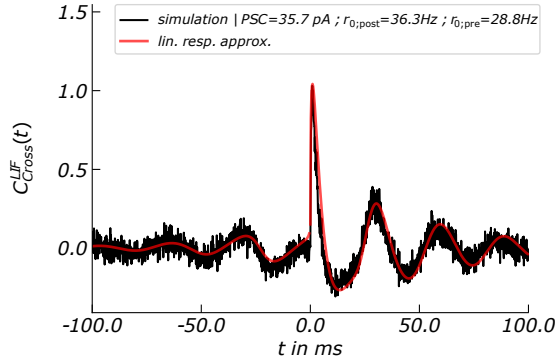
Fig. 2.9: The crosscorrelation between a neuron pair receiving white noise input, estimated from spike train data compared to the analytical solution of the crosscorrelation function in linear approximation. The red curve shows the inverse Fourier transform of the solution to equation 2.35, which has been calculated using the fast Fourier algorithm. The coupling between the pre- and postsynaptic neuron is weak with an PSC amplitude of $35.7pA$. In this regime the analytical solution is in good agreement with the estimation from spike data. For PSC amplitudes above $100pA$ the linear approximation starts to heavily underestimate the primary peak in the crosscorrelation at $t = 0$.

In the time domain, equation 2.47 describes the change in probability to observe a spike t seconds after the last spike.

The Fourier Transform of the inter-spike interval distribution can be expressed analytically for the LIF neuron model [103], [78]:

$$P_{ISI}(\omega) = \frac{U(y_{rest}, \omega)}{U(y_{th}, \omega)} \ . \tag{2.49}$$

We thereby have everything needed to calculate the crosscorrelation function from equation 2.35. The linear response approximation of the crosscorrelation function is in good agreement with results from simulations for the case of weak coupling (See fig. 2.9).

Calculating the transmission probability from the crosscorrelation function

The crosscorrelation functions can be interpreted as the probability of the postsynaptic neurons to fire at time t before or after the arrival of a postsynaptic spike. Thereby we can calculculate the probability P_{transm} that a postsynaptic neuron fired in response to a presynaptic spike from the crosscorrelation function. Note however that the term

'response' in this case is used to describe correlation, not causality[2] P_{transm} is calculated by first multiplying the crosscorrelation function by the postsynaptic baseline firing rate, which gives the ensemble averaged change in the instantaneous firing rate. Integrating over the positive part of this function for positive times gives P_{transm}:

$$P_{transm} = \int_0^\infty dt\ C_{Cross}^+(s;t) * r_{0;post}\ . \tag{2.50}$$

2.6   Information on procedures

All simulations and calculations were done using python 3.5. Simulations have been done with 0.1 ms precision and ran on a i5 7200 processor with a simulation- to real-time ratio of ≈ 4 at a network size of 480 neurons. In the methods section all parameter have been given as they were measured experimentally. However, we find it more neatly to set the resting potential u_{rest} of the neuron to $0mV$ instead of $-70mV$. Therefore in the results of this work the following parameter are set to different values: $u_rest = 0mV$, $u_{reset} = 10mV$, $u_{th} = 20mV$, $E_{syn}^{ex} = 70mV$, $E_{syn}^{in} = 0mV$. If in the following sections, input currents (e.g. I_0) are given in nAmV, the leakage resistance $R_m = 40M\Omega$ has been absorbed into the current variable. Otherwise, currents are given in A.

---

[2] One could argue whether response is therefore the correct term. However, from the 'perspective' of the STDP mechanism, whether the postsynaptic neuron fired after the presynaptic spike due to causality or just due to correlation does not make a difference.

Chapter 3

Results

3.1 Outline

The current work addresses the question whether spike-timing-dependent plasticity (STDP) in combination with synaptic scaling (SS) can lead to distinct up and down-scaling of synaptic connections in a network with dendritic amplification. We are specifically interested in how a memory representation in form of a FeedForward-structure (FF-structure) evolves under the influence of our plasticity model. We first show that the network model produces replay activity in combination with ripples. Next, the properties of the plasticity model for different widths of the STDP rule's LTP domain and different network parameter are examined for a single synaptic connection. Then, the results from simulating a larger network with embedded FF-structure are shown. The last part of the results section stands out from the rest of the work, where we compare the properties of STDP in analytical calculation with simulation results.

3.1.1 Ripples and replay in a feedforward network

In their paper, Jahnke et al. [49] have shown that a network with strong FF-connectivity (Fig. 3.1) and dendritic spiking, exhibits ripple like activity in combination with memory replay. Their network model sets the basis in which our plasticity model will be tested. In contrast to Jahnke et al., in the current work, the network does not receive any directed stimuli but is solely driven by a constant background current I_0 and Gaussian white noise with SD σ. Nevertheless, we find that pronounced ripples and and replay events are generated (Fig. 3.2, **a,b**). The replay is expressed by an upwards spread of activity, going from the neurons at the beginning of the FF-structure to its end. Further, we find that the mean activity of the individual neuron increases with its

position down the FF-structure (with rising neuron index in Fig. 3.2, **a**). The replay is, on a smaller timescale, divided into sharp cluster (ripples) of synchronously active neurons (Fig. 3.2, **b**). The single ripples are separated by a time-interval of $\approx 10ms$, i.e. they occur at a rate of $\approx 100Hz$, which is of the same order they are observed in experiments [69]. The time interval is approximately of the order of the PSC delay (here $3ms$) plus the dendritic spike delay ($\tau_{dendr} = 3ms$). The missing time interval can be explained by the rising time of the EPSP that it takes until the spiking threshold is reached.

a

b
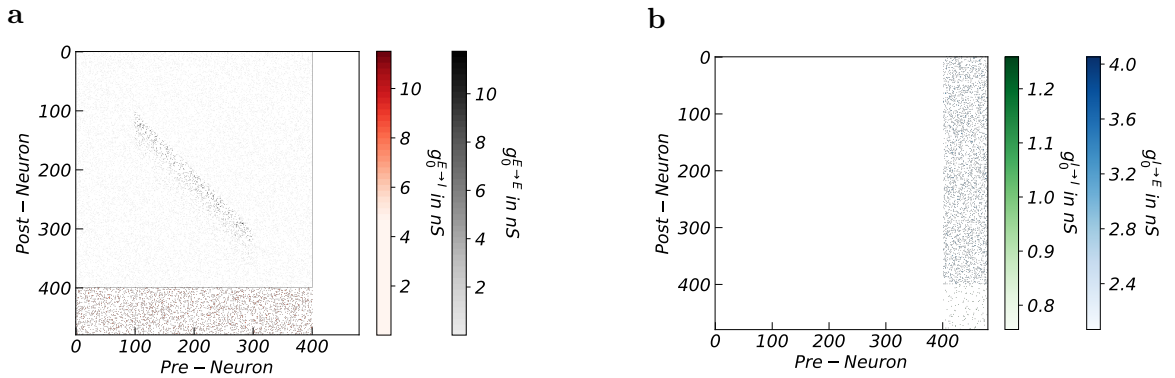
Fig. 3.1: Weight matrices for excitatory connections (**a**) and inhibitory connections (**b**). Memories are represented in the network via a FF-structure, which results in stronger connections in the lower diagonal of the excitatory weight matrix. Excitatory-excitatory connections are presented by the upper left submatrix $g_0^{ex}[0, 400; 0, 400]$. Excitatory connections to the inhibitory neurons are presented by the lower submatrix $g_0^{ex}[401, 480; 0, 400]$, where neurons 401-480 are inhibitory. In panel **b**, the inhibitory connections to the excitatory neurons are presented by the upper right submatrix $g_0^{inh}[0, 400; 401, 480]$. Inhibitory-inhibitory connections are presented by the lower right submatrix $g_0^{inh}[401, 480; 401, 480]$

If not stated otherwise during the course of this work, $I_0 = 3.6nA$ and $\sigma = 3mV$. In total, the network consisted of 480 neurons, where 80 were inhibitory and 400 excitatory. The network is initialized as described in the methods section 3.3, using the experimental synaptic weight distribution found in the hippocampus. The mean synaptic strength of this distribution is at $0.35nS$. We will refer to this as the groundstate. A memory is represented by a set of 100 strongly FF-connected neurons, such that the synaptic weight distribution is unimodal and long-tailed. The strength of this FF-structure is referred to as FF-strength and is defined as the average maximum synaptic strength of connections within the FF-structure. The inhibitory feedback loop is adjusted on the basis of the FF-strength. The mean Excitatory to Inhibitory connectionstrength

$(E \rightarrow I)$ is set to equal the FF-strength. Inhibitory to Excitatory connections $(I \rightarrow E)$ take a strength of $0.4 * FF - strength$. Inhibitory to inhibitory connections are not changed. The FF-structure is drawn into the network using equation 2.23 (Fig. 3.1).
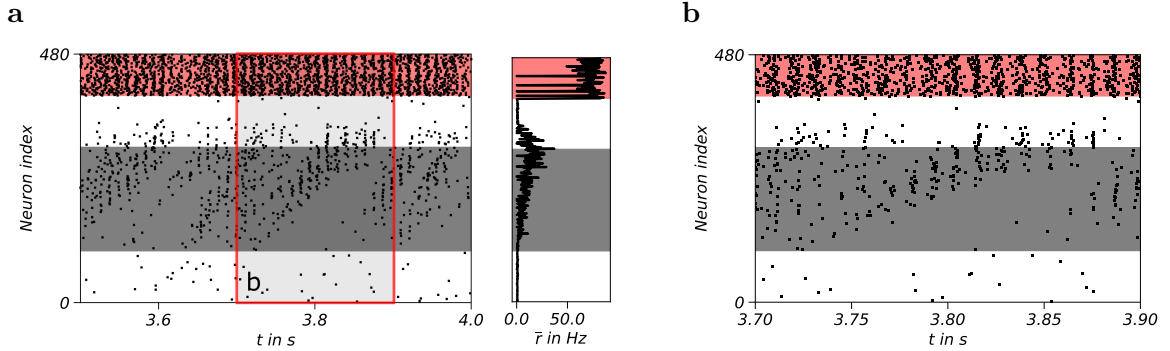
Fig. 3.2: After the embedment of a FF-structure, the neuronal population shows pronounced replay behavior, seen by the upwards diagonal spread of activity (**a**). The inhibitory neuron population is highlighted in red, the FF-connected set in grey. Excitatory neurons that do not have strong output connections are left with a white background. The high activity in the inhibitory population keeps the overall network activity in a stable state as it counterbalances the excitatory signaling. We find that the activity increases, the further a neurons lies within the FF-structure (higher neuron index). The slight spread of activity across the upper border (white to grey) originates from neurons that receive strong input but do not have strong output connections. On a smaller time scale, the replay observed in **a** is split into clusters of synchronous activity which show close resemblance to hippocampal ripples (**b**) [21].

Stability of the synaptic weight distribution

Before we show the results from studying the properties of the plasticity model, an adjustment to the STDP rule is motivated.

We find that the synaptic weights distribution drawn from the experimentally found hippocampal data (methods section 3.3) is not stable if the STDP rule is balanced or LTD-dominated (independent of whether SS is linear or convex) (Fig. 3.3). When STDP is LTD-dominated or balanced, synapses get potentiated only, if the associated post- and presynaptic neurons are sufficiently positively correlated. In a spontaneously active network without external stimuli this is only the case if the synaptic connection between these two neurons is strong. The initial state or groundstate of the network analyzed in the current work (based on the hippocampus), is however weakly coupled. Thereby, many of the connections decay towards zero (Fig. 3.3, **a**). We adjusted the STDP rule such that LTP dominates for weak synapses but becomes LTD-dominated

or balanced with increasing synaptic strength, depending on what parameter τ_s is chosen (methods section 2.2.1). This is achieved by making τ_S weight-dependent in the sense that its is large ($> 5ms$) for weak synapses but quickly converges to a given value (e.g. $\tau_S = 3ms$) when the synaptic strength rises.

$$\Delta g_0 = W(\Delta t) = \eta \begin{cases} e^{-\frac{\Delta t}{\tau_S^*(g_0)}} \left[A_+ \left(1 - \frac{\Delta t}{\tau_{+,1}} \right) + A_- \left(1 - \frac{\Delta t}{\tau_{-,1}} \right) \right] & \text{if } \Delta t \leq 0 \\[2ex] A_+ \, e^{-\frac{\Delta t}{\tau_{+,0}}} + A_- \, e^{-\frac{\Delta t}{\tau_{-,0}}} & \text{if } \Delta t > 0 \, , \end{cases} \tag{3.1}$$

where

$$\tau_S^*(g_0) = \tau_S + \gamma e^{-g_0 \beta}. \tag{3.2}$$

With $\beta = 8$ and $\gamma = 2$. These values show to keep the groundstate of the network approximately stable such that it matches the initial distribution even after longer plastic periods with spontaneous network activity (Fig. 3.3, **b**).
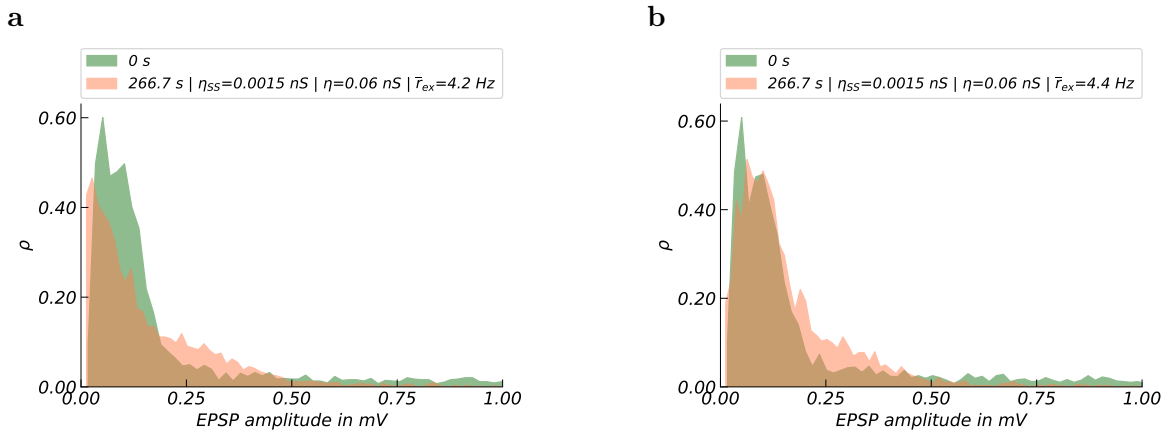
Fig. 3.3: The initial weight distribution (green) is oriented on experimental EPSP data in the hippocampus (see methods section). After 266.7 seconds of simulation (orange), the synaptic weight distribution shows a shift towards zero in the case of additive LTD dominated STDP (panel **a**). In order to remain a biologically more accurate distribution, the width of the LTP domain is set to depend on the synaptic weight, resulting in a weight distribution that is not much distorted even after longer periods of simulation (panel **b**).

3.2 Synaptic plasticity in a network of two single LIF neurons

Before studying consolidation in larger networks, we believe it is important to show the properties of our plasticity model for the single synapse. The knowledge gained from this study is then used to tune the parameters for the larger network simulations and also to help interpret the results. We address the following two questions:

1. How does τ_s influence potentiation and depression?

2. How do STDP and SS depend on the synaptic strength, pre- and postsynaptic activity and dendritic amplification?

We studied STDP and STDP with SS separately for a single neuron pair with a unidirectional connection (Fig. 3.4). The two neurons each received a constant input current I_0 and Gaussian white noise with SD σ. The model has been simulated for different input current amplitudes I_0 and synaptic strengths, while the noise level has been held constant at $3mV$.
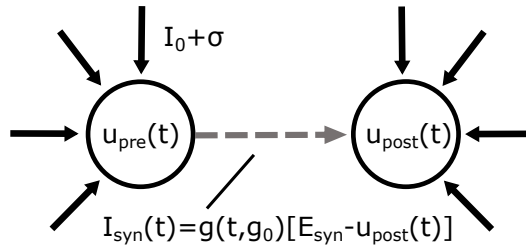
Fig. 3.4: A single excitatory neuron pair, receiving Gaussian white background noise with standard deviation σ and a constant stimulus current I_0, serves as an approximation a neuron pair embedded in a large network. Correlated input, inhibitory feedback and the shot noise character of synaptic input are ignored or approximated by Gaussian white noise.The postsynaptic current I_{syn} is determined by the synaptic conductance transient $g(t)$ and the membrane potential $u_{post}(t)$.

Due to the stochastic nature of the spiketrains, a pre-/postsynaptic spike pair can either result in depression or potentiation of the connection, thereby the synaptic strength fluctuates. We are only interested in the expected change. Therefore, the crosscorrelation function between the two neurons is estimated (methods section 2.4.1) using at least $16.67min.$ of spiketrain data. Equation 2.18 (methods section 2.2.2) is then used to calculate the expected synaptic change. The strength of the synapse is

either given in terms of its conductivity in pS or in terms of the PSC amplitude in pA. The PSC induced by a presynaptic somatic spike is described by equations 2.3, 2.2 (methods section 2.1.2) and dendritic spikes by equation 2.8 (methods section 2.1.3).

3.2.1 STDP without SS

Does the fact, whether STDP is LTD-dominated, balanced or LTP-dominated have any major impact on the expected change of a synaptic connection over a wide range of synaptic strengths and constant background current amplitudes? We indeed find that this is the case (Fig. 3.5). For defining the STDP rule, the following three values for τ_S were used:

- $\tau_S = 3ms$: LTD dominated

- $\tau_S = 4ms$: balanced

- $\tau_S = 5ms$: LTP dominated

Interestingly, our simulations show that LTD-dominated STDP depends on I_0 in a nonlinear, concave way (Fig. 3.5, **a,d,g**). Synapses are only potentiated if, first, the synaptic strength is above $\approx 100pA$ in terms of the PSC amplitude, and second if the background current I_0 is below $\approx 18.4mV$. For higher background currents or weaker PSC amplitudes, the synapse experiences depression (Fig 3.5, **a,d**). This is in contrast to LTP-dominated STDP, where potentiation is always stronger than depression (Fig. 3.5, **c,f**). Further, potentiation increases approximately linear (slightly nonlinear, convex) with I_0 for LTP-dominated STDP and does not converge to a maximum within the examined range (Fig. 3.5, **c,f,i**). When STDP is balanced, potentiation reaches a maximum or at least seems to converge within the examined range for I_0 (Fig. 3.5, **b,e**). Further, potentiation dominates over depression for almost all values of synaptic strength. Depression only occurs for very weak synapses at background currents above $16mV$. (This however means that our STDP rule is not balanced in a very strict sense, because it is not odd but asymmetric).

Similarly, LTD-dominated, balanced and LTP-dominated STDP differ in their dependence on the synaptic strength. They however share the property that potentiation increases sigmoidal with the synaptic strength and not e.g. linear (what one might naively expect). This can be explained by two properties of the model. First, the probability that a presynaptic spike evokes a response from the postsynaptic neuron

P_{transm} (methods section 2.5) does grow concave with the PSC amplitude (Fig. 3.6, **a**). Second, apart from P_{transm}, the timing is important for STDP.
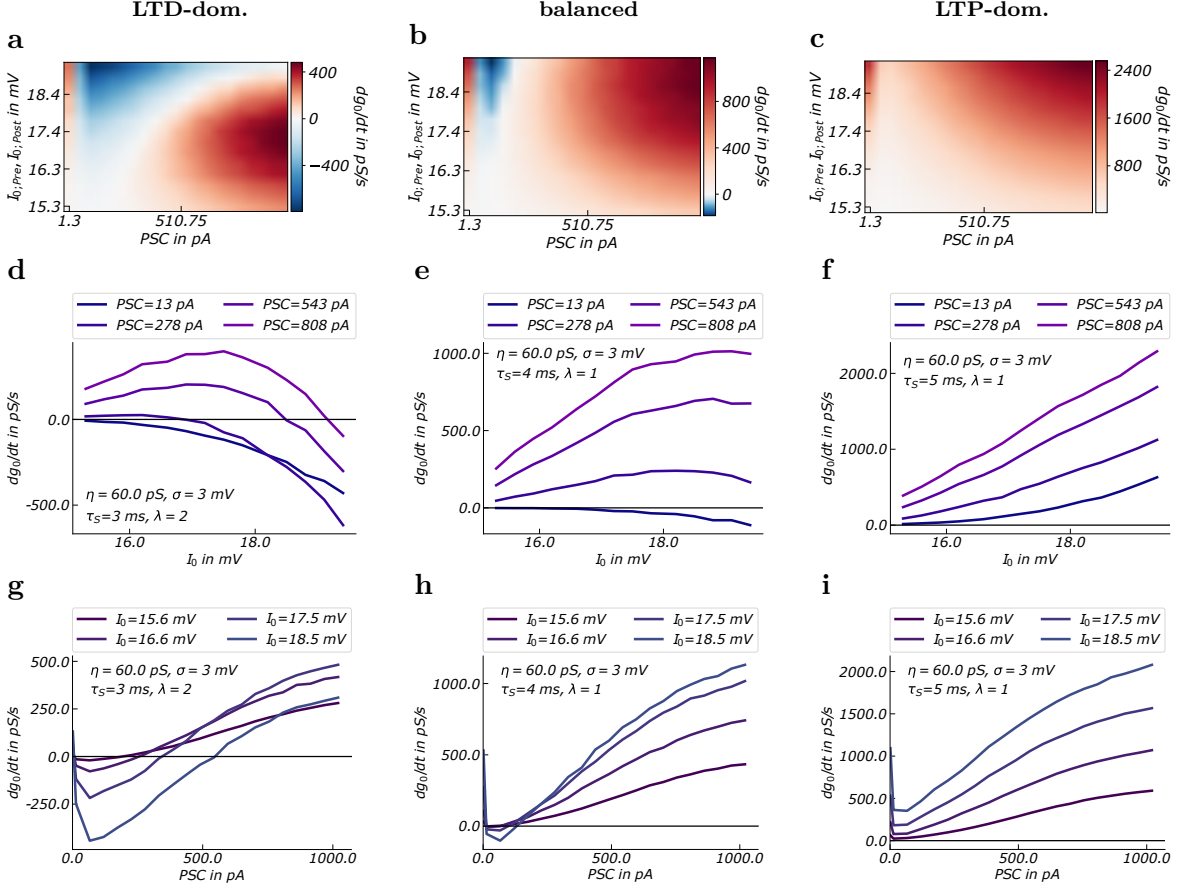
Fig. 3.5: STDP induced potentiation or depression varies depending on whether STDP is LTD-dominated, balanced, or LTP-dominated. The expected synaptic change has been estimated for different background currents I_0 and PSC amplitudes for a single neuron pair receiving Gaussian white noise with SD σ. This has been done by calculating the crosscorrelation function from spike train data and subsequent integration with the STDP learning window to receive the synaptic change in $pS/Spike$. The synaptic change in pS/s is derived via multiplication with the presynaptic firing rate. LTD-dominated STDP (**a,d,g**) leads to depression for small PSCs and for high I_0, while for balanced STDP (**b,e,h**) depression can only be found for very weak synapses at high I_0. LTP-dominated STDP (**c,f,i**) always potentiates synapses. STDP depends concave on I_0 for LTD-dominated and balanced STDP but linear (slightly convex) for LTP-dominated STDP (**d,e,f**). However, all three STDP rules show a sigmoidal dependence on the PSC amplitude. λ in the legend is the power of g_0 in the SS function.

When the PSC increases, the postsynaptic response occurs at earlier times, which, due to the exponential shape of the STDP rule, results in a nonlinear growth of

LTD-dominated

a

b

c

d
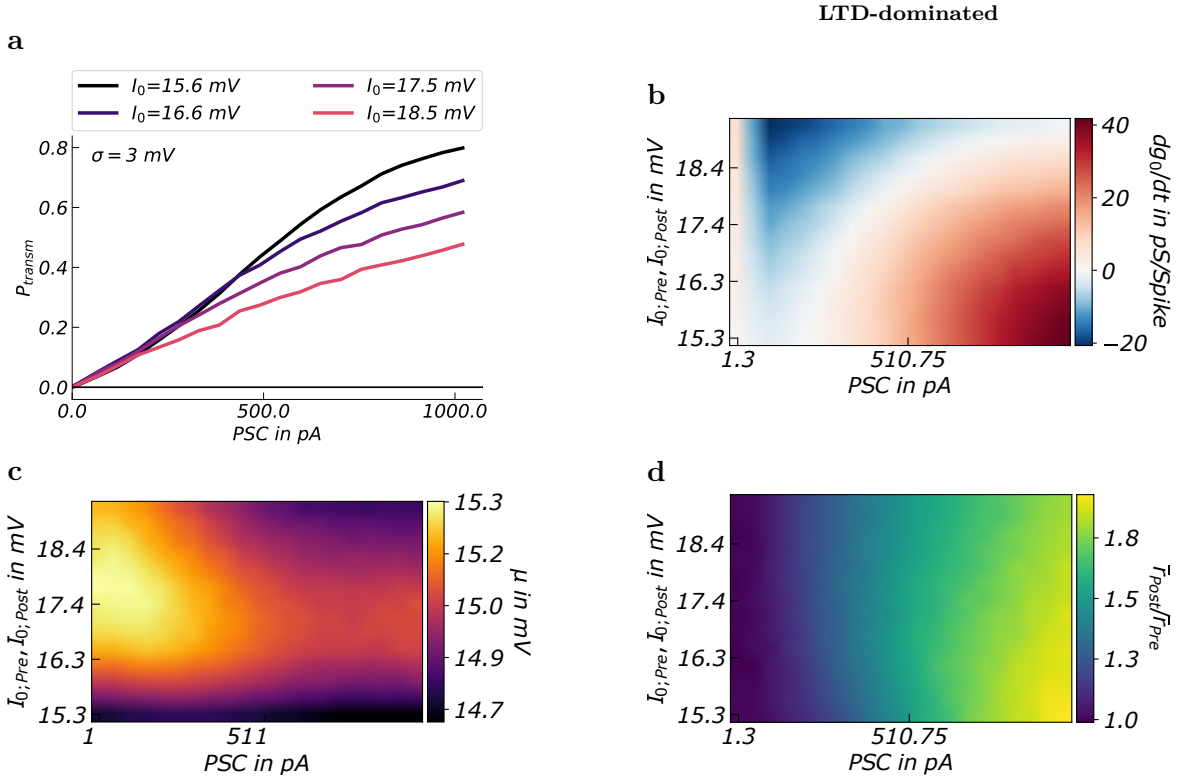
Fig. 3.6: The transmission probability in terms of the PSC amplitude follows a concave function and is higher for low background currents I_0 (**a**). Thereby, STDP induced potentiation is always strongest for strong PSCs at low I_0 (**b**). However there seems to be no correlation between the effective ,membrane potential and the transmission probability (**c**). The postsynaptic activity increases significantly with the strength of its presynaptic connection and up to doubles at strong PSCs (**d**). The synaptic change has again been calculated via the crosscorrelation function and integration with the STDP learning window.The transmission probability P_{transm} has been calculated by integrating over the positive part of the crosscorrelation function at positive times (see methods section 2.5).

potentiation, reaching its maximum if the postsynaptic response occurs instantly. Interestingly, P_{transm} does not reach 1 even for strong PSC amplitudes. This is the case, because there is always a certain probability that the neuron is driven over the spiking threshold by the background current directly before the arrival of presynaptic spike. In that case the subsequent refractory period prohibits a direct response to the PSC. A PSC evoked response directly after the refractory period is also not possible since the membrane potential has to recover from the reset potential ($u_{th} - u_{reset} = 10mV$). Thereby, the higher the postsynaptic activity (equivalent to high I_0), the lower the probability that a stimulus evokes a response. This effect is also examined in the synaptic change per spike (figure 3.5 is in pS/s), which is highest at low I_0 and strong

PSCs (Fig. 3.6, **b**). Note that P_{transm} shows no correlation with the effective membrane potential (Fig. 3.6, **c**), which one could expect, since a higher effective membrane potential means that the average distance between membrane potential and spiking threshold is lower. At last, we find that at low I_0 and strong PSCs, the postsynaptic rate up to doubles relative to the postsynaptic rate (Fig. 3.6, **d**).

3.2.2   STDP with SS

In the preceding section the properties of STDP were studied. It is now appropriate to expand the model by SS and dendritic spikes. We address the following question: Does STDP and SS lead to distinct up (potentiation) and downscaling (depression), such that memory consolidation is possible? We state that it is only possible to consolidate a memory if we find at least three distinct regimes of potentiation and depression:

1. Depression for weak synapses (to the groundstate not to zero),

2. potentiation for intermediate synaptic strength,

3. depression for strong synapses.

Otherwise, synapses would either all decay or grow towards one state, which is equivalent to loosing the memory that is decoded in a network.

We studied synaptic plasticity for LTD-dominated, balanced and LTP-dominated STDP in combination with either linear or convex SS. Further, simulations were done with and without dendritic amplification. The dendritic spiking threshold was set to $\theta = 43nS$, which lead to the emission of dendritic spikes at PSCs of $\approx 200pA$. The individual learning rates for STDP (η) and SS (η_{SS}) define how much each mechanism changes the synaptic strength respectively. They were set such, that the maximum potentiation is around $100pS/s$, while synaptic depression starts at PSCs of $\approx 400pA$ with dendritic spikes and $\approx 700pA$ without dendritic spikes (Fig. 3.8). Remember that dendritic spikes introduce a strong and fast current and thereby significantly enhance the correlation between neurons. As before, the expected synaptic change has been estimated for different I_0 and synaptic strengths ($PSCs$), while $\sigma = 3mV$.

We find that synaptic plasticity is partitioned into three regimes regarding the PSC amplitude if STDP is LTD-dominated or balanced (Fig. 3.8, **a-h**). For LTP-dominated STDP three regimes are only found with dendritic amplification and if SS is linear

(Fig. 3.8, **i**). This result is explained in the following (However, only LTP- and LTD-dominated STDP are discussed, the explanation for balanced STDP should follow intuitively as a boarder case).
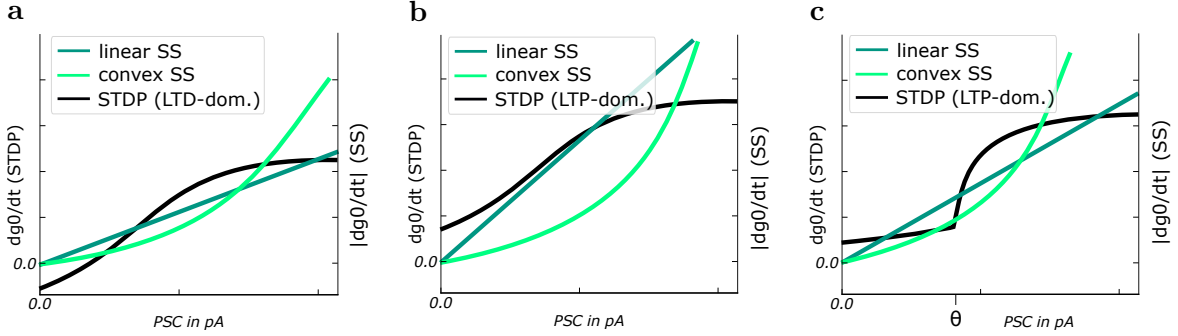
Fig. 3.7: Because of the way STDP depends on the synaptic strength/PSC (nonlinear/sigmoidal), three distinct regimes of depression and potentiation are only possible under certain conditions. If STDP is LTD dominated (**a**, black curve), i.e. weak synapses experience STDP induced depression, linear (dark green) as well as convex (light green) SS can be set such that STDP induced potentiation is stronger than SS induced depression in an intermediate regime of the synaptic strength, while a lower and upper regime induce depression. If STDP is LTP dominated (**b**), SS-induced depression is not strong enough for weak synapses to predominate depression. However when dendritic spikes are evoked at some threshold θ (**c**), SS might still not predominate very weak connections but generate a depression regime for intermediate strengths before the inset of dendritic spikes.

LTD-dominated STDP+SS: If LTD is dominated, depression occurs for weak synapses due to STDP and SS. If η_{SS} is chosen such that SS induced depression increases slower with the synaptic strength than STDP-induced potentiation, synapses with intermediate strengths experience potentiation. However, since STDP depends sigmoidal on the PSC, SS will eventually predominate STDP (Fig. 3.7, **a** (sketch)).

LTP-dominated STDP+SS: If the LTP regime in the STDP rule is however too brought, such that even weak synapses experience a lot of potentiation, the first depression regime cannot be established (Fig. 3.7, **b** (sketch)). Dendritic spikes however introduce a sudden increase in the correlation between pre- and postsynaptic neuron at the dendritic spiking threshold θ. Thereby, η_{SS} can be highly increased, such that weak synapses get downscaled even if STDP is LTP-dominated, while we still find a potentiation regime for intermediate synaptic strengths (Fig. 3.7, **c** (sketch)). However this is only true for linear SS and for the parameters chosen here. If $\tau_s > 5ms$ the three regime structure will eventually break also with dendritic spikes.
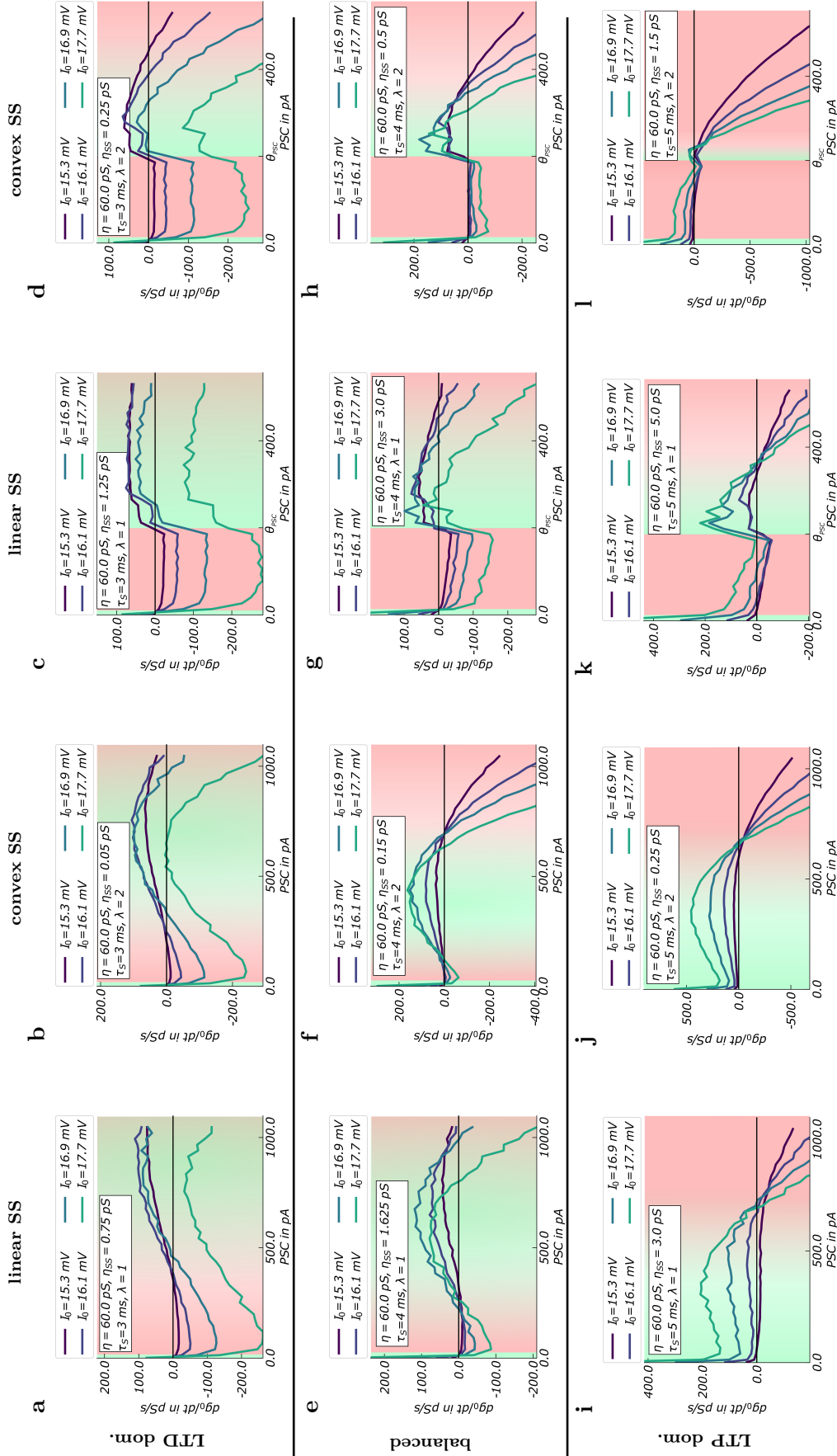
Fig. 3.8: Synaptic potentiaion (highlighted in light green) and depression (highlighted in light red) induced by STDP and vary on whether STDP is LTD-dominated, balanced or LTP-dominated. The results shown in the different panels are divided into models with I_0 and vary on whether STDP is LTD-dominated, balanced or LTP-dominated. The results shown in the different panels are divided into models with dendritic spiking (**c,d,g,h,k,l**) and those without **a,b,e,f,i,j**. Results are further subdivided into LTD-dominated, balanced and LTP-dominated STDP in combination with either linear or convex SS. We find that synaptic change is divided into three regimes (two of depression, one potentiation), except if STDP is LTP dominated in the absence of dendritic amplification (**i,j**). The start of the potentiation regime can be set precisely via the dendritic spiking threshold ($\theta = 200pA$) (**c,d,g,h,k,l**), because these increase the crosscorrelation between neurons significantly. High I_0 results in the loss of the potentiation regime for LTD-dominated STDP(**a,b,c,d**), whereas potentiation always increases with I_0 for LTP-dominated STDP. Whether SS is linear or convex influences how fast SS induced depression predominates potentiation with increasing PSC.

Further, a different threshold for the emission of dendritic spikes could also result in the loss of either the first depression regime or the potentiation regime.

Whether SS is linear or convex mainly only effects at what rate SS starts to dominate over STDP with increasing PSC. This leads to broader potentiation regimes in the case of linear SS compared to convex SS. Further, we find that LTP-dominated, balanced and LTD-dominated STDP with SS depend different on I_0 (As follows from the preceding section). When STDP is LTD-dominated, the potentiation regime is completely lost at high $I_0 > 17mV$ (Fig. 3.8, **a-d**). In the case of LTP dominated STDP, potentiation increases continuously with I_0 for synaptic strengths that lie below the regime in which SS induced depression dominates (Fig. 3.8, **i-l**).

Based on the results shown in figure 3.8 we chose the most promising parameter sets that might enable the consolidation of a FF-structure with dendritic amplification.

1. LTD-dominated STDP + convex SS+dendritic amplification (Fig. 3.8, **d**)

2. balanced STDP +convex SS+dendritic amplification (Fig. 3.8, **h**)

3. LTP-dominated STDP+linear SS+dendritic amplification (Fig. 3.8, **k**)

Note however that the parameter for η_{SS} has been slightly adjusted for network simulations. Results for networks without dendritic amplification will only be shown at the very end of the section.

3.3   Consolidation of FF-memory representations

We find that FF-structures in a spiking neural network get scaled up or down during spontaneous network activity, depending on the FF-strength, using our plasticity model. This process of up- and downscaling will be referred to as consolidation. We find however, that depending on the model parameter, the FF-structure may not entirely be preserved but gets fractured during consolidation.

The previous section has given an overview over how different STDP rules in combination with either linear or convex SS change the synaptic strength between two neurons. In this section, the results from simulating a network under balanced and LTD-dominated STDP with convex SS and LTP-dominated STDP with linear SS are presented.
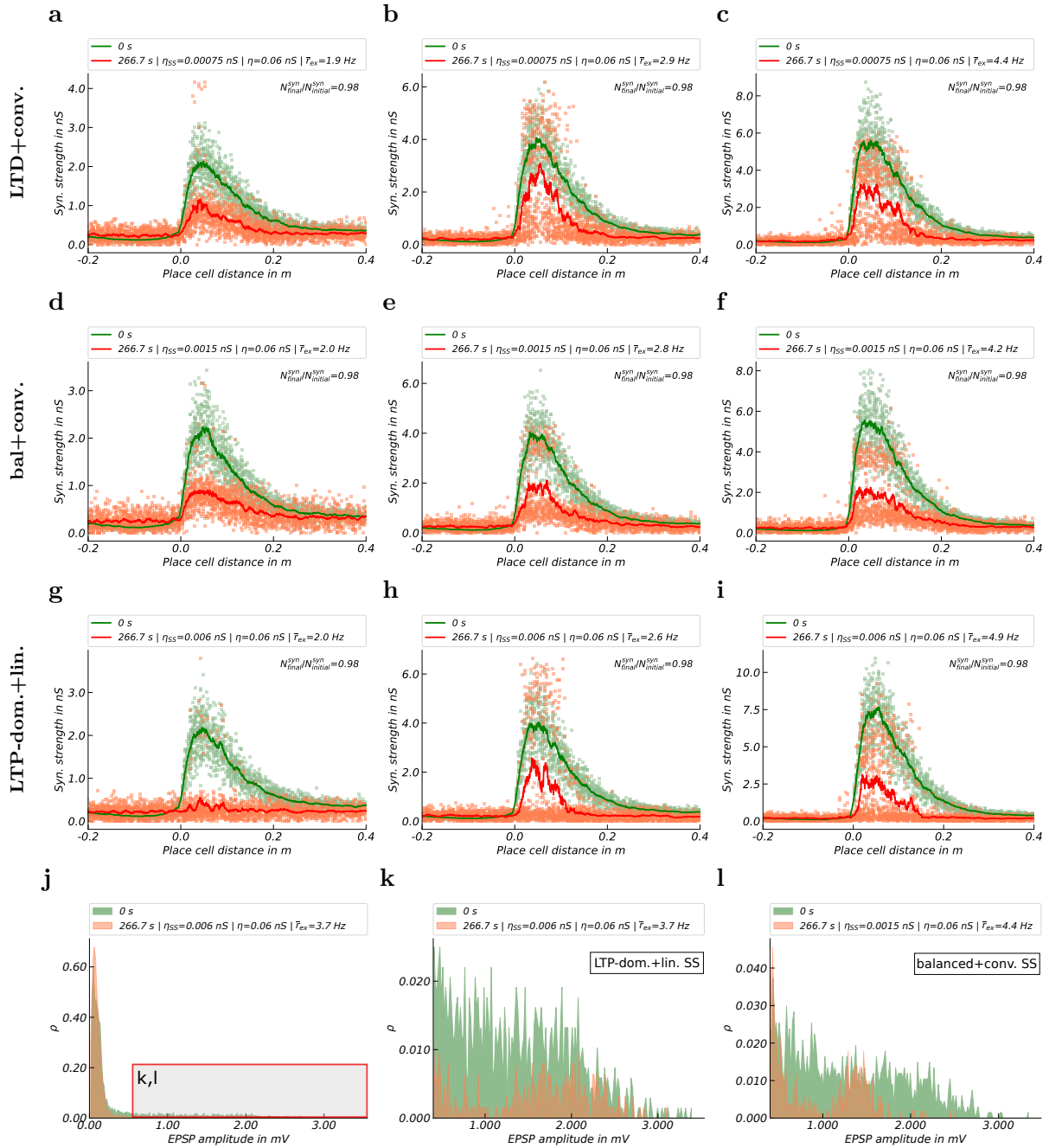
Fig. 3.9: STDP with SS in a spiking neural network with active dendrites distinctively up- and downregulation connections in the FF-structures, thereby transforming the initially long-tailed unimodal into a bimodal distribution (**j,k,l**). We simulated a network of inhibitory and excitatory LIF neurons, where a subset of the excitatory neurons had strong FF-connections with neurons with neighboring place fields. Panels **a-i** show the synapses within the FF-structure as a function of the place cell distance (In green before the simulation, in red after). The STDP and SS learning rates and mean excitatory activity are given in the legends. We studied the three cases of LTD-dominated and balanced STDP with convex SS and LTP-dominated STDP with linear SS. We find in all three cases that the FF-structure gets downregulated on average (red line). FF-structures that lie above the dendritic spiking threshold however retain a number of strong connections (get consolidated) (**b,c,e,f,h,l**), whereas those below get completely downregulated to the groundlevel, which is associated with the loss of the of the memory encoded in the FF-structure (**a,d,g**).

The learning rates η and η_{SS} for STDP and SS are chosen such, as to lead to an upper limit for synaptic growth that lies around $4 - 6nS$. This choice has been made to keep the synaptic strengths in a biologically plausible regime.

Synaptic plasticity is only activated after a certain runtime ($\approx 67s$). During the first static simulation period, quantities such as mean activity and matching index are collected. The plastic period ends when the synapses in the network have approximately reached a steady state. Subsequent, the matching index and other quantities are again measured for $\approx 67s$. Experiments show that the firing rate of pyramidal neurons in the hippocampus lie around $0 - 10Hz$, with population mean firing rates of $1 - 2Hz$ during wake and SWS [46]. Therefore, the constant background current is set to a value such that this average firing rate is approximately reached. This is found to be the case for $I_0 = 0.36nA$ at a background noise value of $\sigma = 3mV$. Neurons within the FF-structure have higher firing rates and the mean firing rates change depending on the strength of the FF-structure, I_0 is however not adjusted.

Our network simulations show that after a plastic simulation period of $266s$, the synapses in the FF-structure are clearly divided into a set that retains a certain strength above, while the rest returns to the ground state (Fig.3.9). Thereby, a bimodal weight distribution evolves (Fig. 3.9, **j,k,l**). Synapses are however only consolidated if the FF-structure has a minimum strength. Weak structures decay entirely back to the groundstate (Fig. 3.9, **a,d,g**). We find that linear SS leads to a broader synaptic distribution of consolidated synapses than convex SS (compare Fig. 3.9 **k** with **l**). This is the case because a small shift in the synaptic strength enters convex SS quadratically. Thereby the upper bound for the synaptic strength is sharper than for linear SS, where the depression magnitude increases more gradually (linear) with the synaptic strength. Synapses can get consolidated if their initial synaptic strength lies above the dendritic spiking threshold which is set to $\theta = 43nS$ (corresponding to a PSC amplitude of $200pA$ or a FF-strength of $\approx 3nS$). In the following, results are only shown for the model with balanced STDP and convex SS, as most of the results are the same for the other models. If this is not the case, the results for LTP-dominated or LTD-dominated STDP will be added.

Fracturing of the FF-structure

While some synapses get consolidated, we find that the majority of synaptic connections within the FF-structure actually get back to the ground state. The ratio of strong

synapses that get consolidated to those that decay to the groundstate defines the consolidation index C (Fig. 3.10, **c**). We find that even strong FF-memory representations have a consolidation index of at maximum 0.3, i.e. on average each neuron looses around 70% of its strong connections. This leads to an average downscaling but also fractures the feed-forward structure. The probability distributions for the number of strong input and output connections per neuron show that while around 75% of the neurons preserve a strong input connection, more than 40% do not retain a strong output connection (Fig. 3.10, **a,b**). The expected length of a feedforward-structure after consolidation can be calculated from these two distributions.
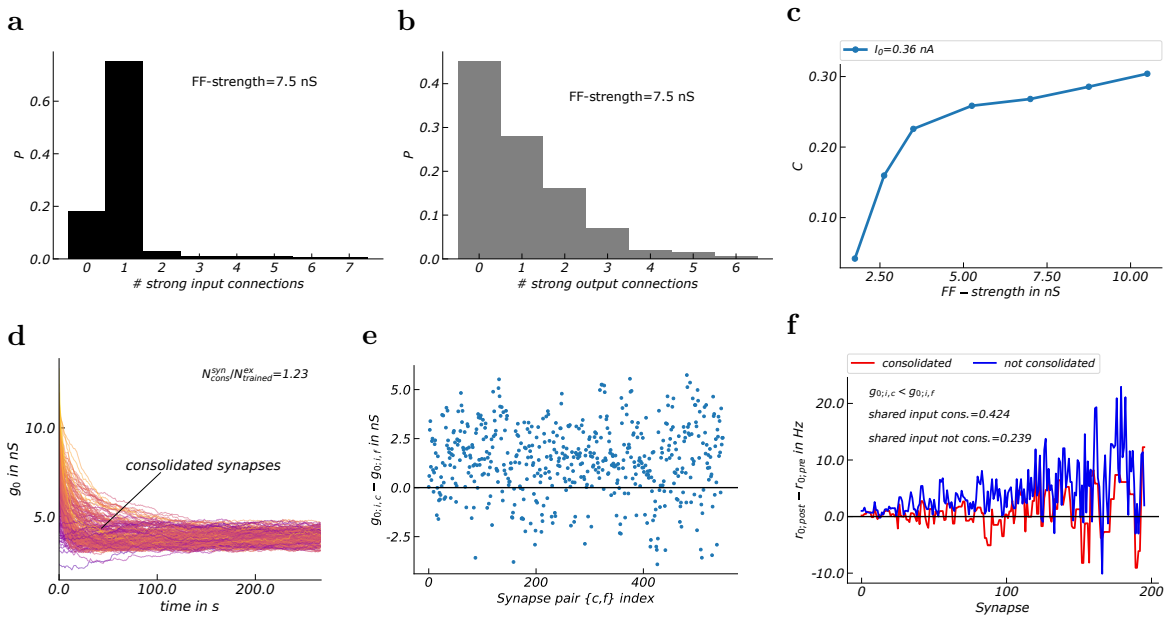
Fig. 3.10: Consolidation results in the loss of most strong synapses. A small subset of strong synapses that belong to the presynaptic neuron with the smallest firing rate difference to the postsynaptic neuron is however retained. Panels **a, b** show the probability of a neuron to retain a strong (>2 nS) input or output connection after consolidation (for FF-strength=$7.5nS$). The number of consolidated synapses increases with the FF-strength but converges to a level of 30% of consolidated synapses (**c**), which corresponds to ≈ 1 synapse per neuron with the here chosen number of intial strong connections (set by the FF-width). Panel **d** shows the trajectories of consolidated synapses for 266 s of simulation. The difference in synaptic strength between the consolidated synapse $g_{0;i,c}$ and its opponent synapses that did not get consolidated $g_{0;i,f}$ show that while consolidated synapses are stronger than the average, there are synapses that are stronger but did not consolidate (**e**). The difference in pre- and postsynaptic activity for these cases is shown in panel **f**, from which we conclude that a small difference in activity is the critical factor in our consolidation model that determines whether a synapse consolidates or returns to the groundstate.

We find that, under the condition that a neuron has only one output connections, the expected number of strong synaptic connections that would start out from this connection is only 3.1. In other words, after consolidation a FF-structure would fracture into smaller ones, which on average contain 3 strong (consolidated) connections. Even if the initial condition is changed, such that the first neuron of the FF-structure has 6 strong output connections, the expected length is ≈ 8.7.

As each neuron retains only one strong input connection, we address the question, when do synapses consolidate and when not? First, we find that under all the strong synaptic connections a neuron receives, the stronger ones are more likely to consolidate (Fig. 3.10, **e**). However, synaptic strength alone does not guarantee that a synapse wins in the competition for consolidation against opponent input connections. In many cases, the synapse that gets consolidated is above the mean synaptic strength but is not the strongest one. A second important factor is the difference in pre- and postsynaptic firing rate. We find that whenever the stronger synapse does not consolidate, the difference between post- and presynaptic firing rate is higher than for the weaker synapse that does consolidate (Fig. 3.10, **c**). Note that the synapses that consolidate do reach a steady state (Fig. 3.10, **d**)
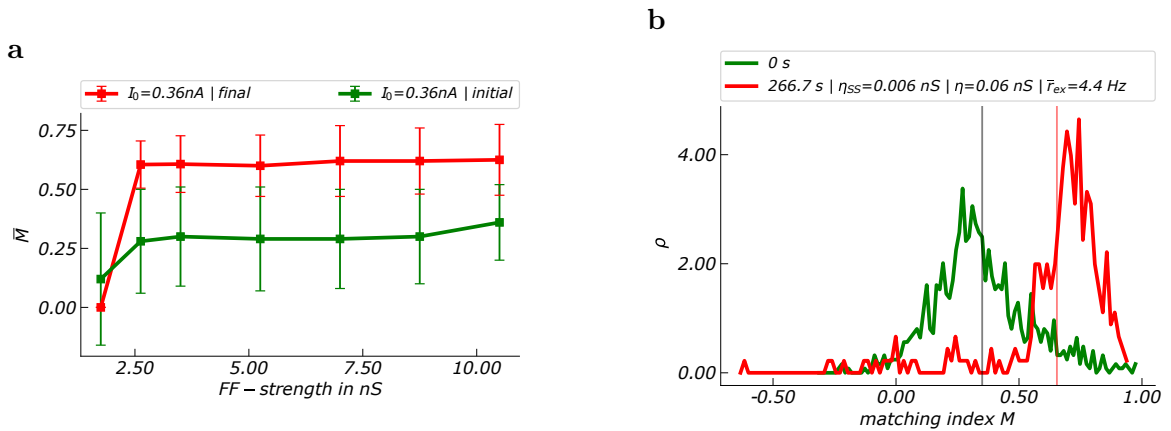
Fig. 3.11: Despite the general down regulation of the FF-structure, the replay quality of synapses that lie above the ground state increases significantly during consolidation (**a**). The replay quality measured in terms of the matching index doubles on average, independent of the initial FF-strength. The mean and variability of the matching indices's are calculated from the matching index distribution over all potentiated synapses (**b**).

Consolidation enhances memory replay

We find that the replay of memory representations in form of a FF-structure is enhanced after consolidation. To measure the quality of memory replay, the matching index M is used (methods section 2.4.2). The matching index is calculated before and after consolidation for each strong synapse (i.e. not for those synapses that got set back to the ground state after consolidation). From the matching indices's we get the matching index distribution over the synapses (Fig. 3.11, **b**). After consolidation there is a clear shift in the matching index distribution towards one, i.e. towards the correct order of replay at the single neuron pair level. It does however say nothing about the higher order correlations in the network activity. The mean matching index always converges to ≈ 0.6, compared to a mean matching index of ≈ 0.25 before consolidation, independent of the initial FF-strength (Fig. 3.11, **a**).

3.4 Influence of different parameters on the consolidation dynamics

3.4.1 Different FF-structure-widths

We find that the number of consolidated synapses does not change significantly with the FF-width (Fig. 3.12, **a-c**)(The observed fluctuations were only around $\Delta \frac{N_{cons}^{syn}}{N_{cons}^{syn}} \approx 0.2$ and not enough data has been gathered that would allow any statement). The FF-width has however a greater influence on the spiking dynamics of the network. Narrow FF-structures show less pronounced ripples with less participating neurons (Fig. 3.12, **d** compared to **e**). This is however to expect as a narrow FF-structure couples (and therefore synchronizes) less neurons. The matching index is influenced only very little but decreases slightly with the FF-width (Fig. 3.12, **f**). The slight decrease can be explained by the higher network activity for broader FF-structures. A higher activity means that each neuron receives more spikes from different presynaptic neurons, this perturbs the communication between individual neuron pairs and thereby the order of firing.
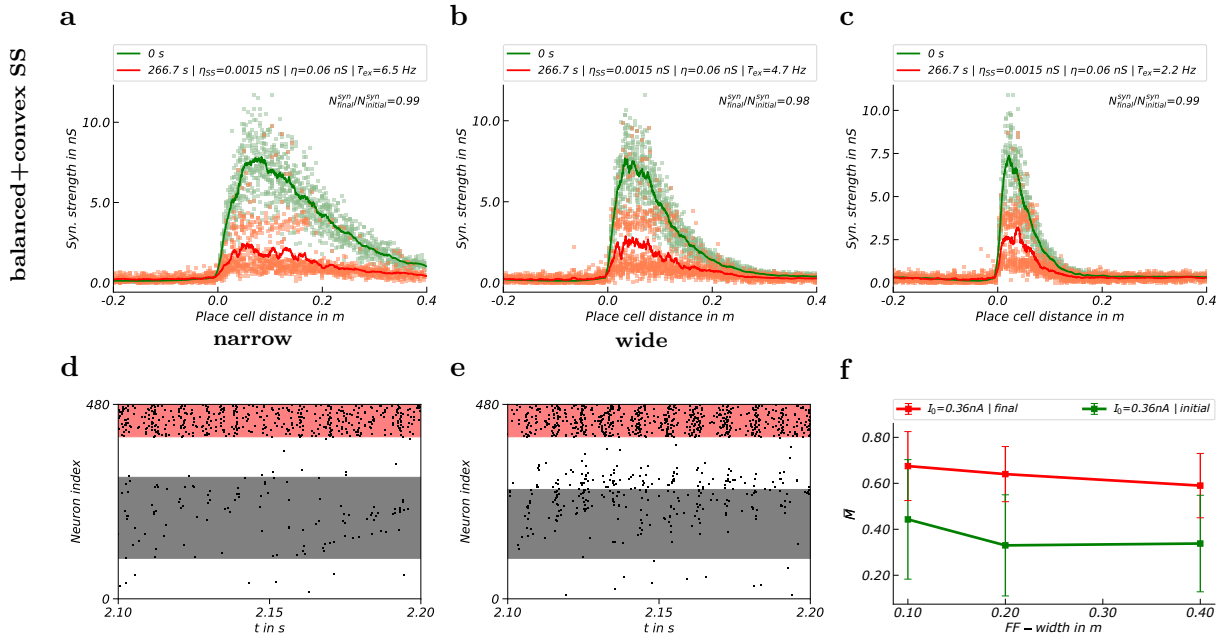
Fig. 3.12: The width of the FF-structure has no major impact on the number of consolidated synapses or the replay quality (**a,b,c**). The ripple generation however varies depending on the FF-width (**d,e**). Narrow structures result in smaller clusters of synchronized neurons, firing simultaneously. Thereby the ripples are smaller (less pronounced) in **d** (narrow) compared to **e** (wide). The replay quality in terms of the matching index M is however not significantly changed by the FF-width (**f**). The width has been decreased in steps of 50% from panel **a**-**c**.

3.4.2 Multiple memory representations and recurrent assemblies

Our network simulations show that STDP and SS not only enable a network with a single strong FF-structure to consolidate a subset of its synapses, but that the same holds true for networks with multiple distinct FF-structures (Fig. 3.13 **a**, 3.14). Further, even random recurrent cell assemblies can get consolidated (Fig. 3.13 **b**, 3.15), however different for LTP-dominated STDP than for balanced or LTD-dominated STDP.

A network with two distinct FF-structures, where one is weak (such that the dendritic spiking threshold is not reached) and the other strong, results in the deletion of the weak structure (Fig. 3.14 **b**), while a subset of synapses of the strong one is preserved strong (Fig. 3.14 **a**). Pronounced replay is limited to the neurons that are

part of the strong encoded FF-structure (Fig. 3.14 **c**).
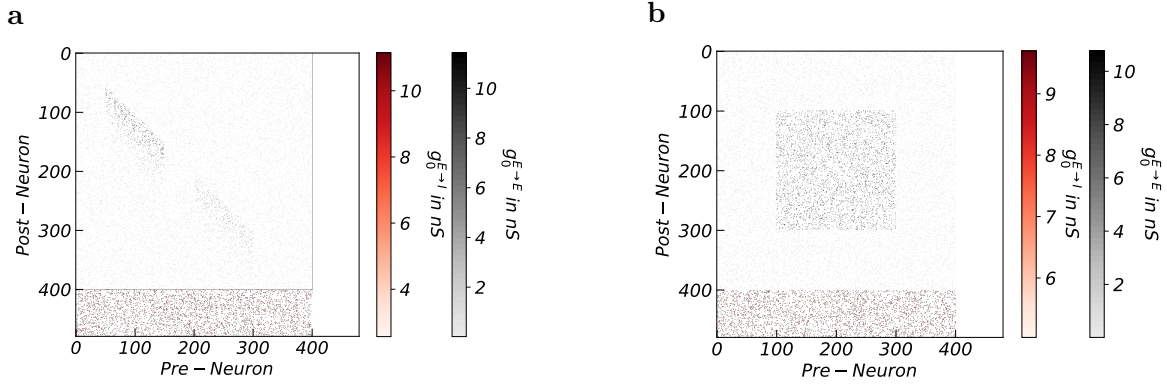
Fig. 3.13: Panel **a** shows the excitatory weight matrix of a network that inhabits two distinct FF-structures. One represented by the lower diagonal in the upper left, the other represented by the lower diagonal in the lower right. The upper structure has been strongly encoded with weights reaching up to $10nS$, while the lower structure has only been weakly encoded. Panel **b** shows the excitatory weight matrix for a random recurrent assembly, inhabiting 200 neurons.
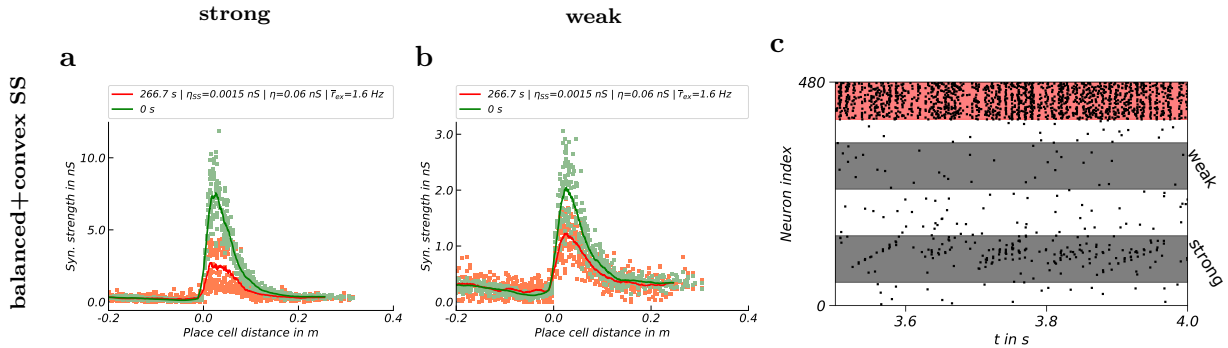
Fig. 3.14: STDP with SS enables networks with multiple distinct FF-structures to consolidate or delete these independent of each other. Two FF-structures have been embedded into the network such that there is no overlap in the placefields between the neurons associated with one or the other FF-structure. One FF-structure is strong with a mean maximum synaptic strength of $\approx 8nS$ (**a**), the other weakly with a mean maximum strength of $\approx 2nS$ (**b**). After 266.7 s of simulation the strong FF-structure retained a number of strong synapses, while the weak one got consistently downregulated across all stronger synapses. Further, both structures exhibit different spike dynamics. The neurons belonging to the strong FF-structure show pronounced replay and ripple generation while the weak FF-structure does not (**c**).

The spontaneous activity in a network with random recurrent cell assemblies leads to different consolidation results for LTD-dominated and balanced STDP compared to LTP-dominated STDP (Fig. 3.15). We find that a cell assembly containing 200 neurons does not consolidate in the case of LTD-dominated and balanced STDP but for LTP-dominated STDP, if η_{SS} is not changed compared to previous simulations (Fig. 3.15, **a,b,c**).
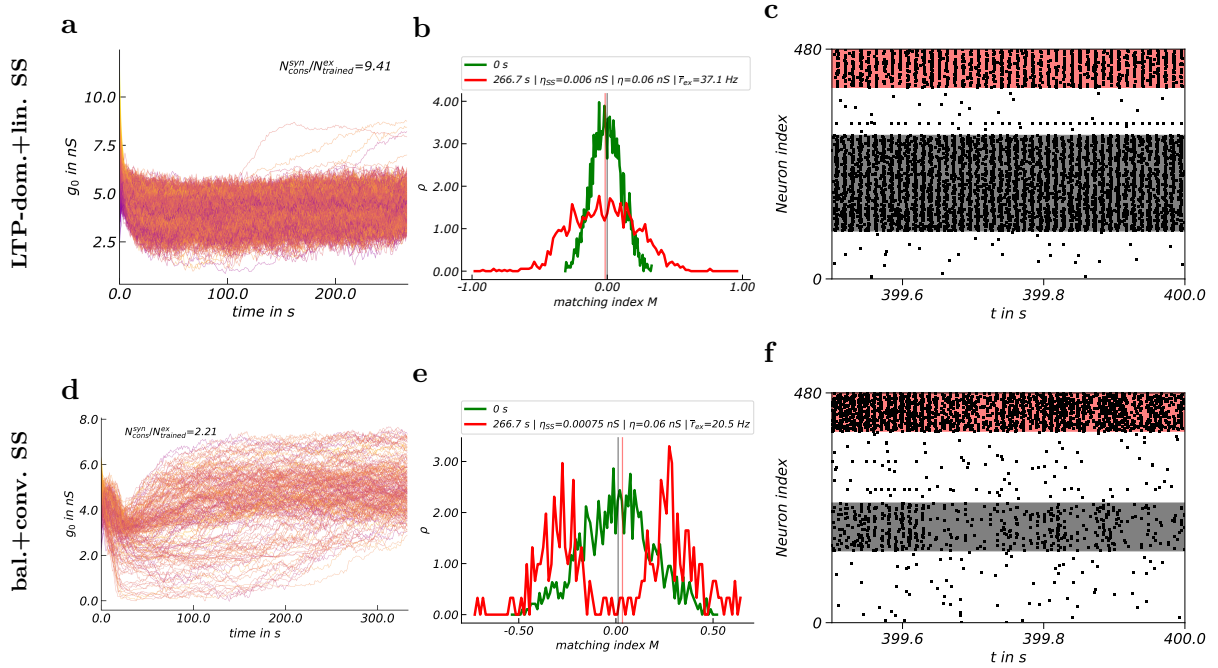
Fig. 3.15: Random recurrent cell assemblies consolidate different depending on their size, the SS learning rate and whether STDP is LTP-dominated or not. A strong recurrent cell assembly has been embedded into a random network and simulated for 266.7 s under the influence of LTP-dominated STDP and linear SS (**a,b,c**). When STDP is LTP-dominated, neurons in large recurrent assemblies (containing 200 neurons) retained around 9.4 strong input connections that converged to a steady state between 2.5 and $6nS$ (**a**). Further, the matching index distribution broadened, indicating an increment in the temporal structure of the replay (**b**). The replay was periodic, ripple-like and consistent (**c**). Balanced and LTD-dominated STDP were only able to consolidate a recurrent assembly if the learning rate η_{SS} was decreased by half compared to previous FF-structure simulations. Despite, only about 2 strong connections per neuron were retained (not shown here). Decreasing the assembly size to 100 neurons led to the same result (**d,e,f**). However, the assembly exhibited pronounced replay and ripples that was not consistent but occurred in temporally separated phases (**f**). Moreover, the matching index distribution became bimodal, indicating highly temporally ordered firing of strong connected neuron pairs.

We find these different results, because the STDP rules respond different to the self-amplification of activity in a recurrent assemblies. It has been shown in section 3.2 (see figure 3.8) that higher background currents (which raise the network activity), lead to weaker potentiation in the case of LTD-dominated and balanced STDP, while potentiation stays relatively strong for LTP-dominated STDP. Thereby, if the self-amplificatory effect of activity is too strong, depression will dominate for LTD-dominated STDP and balanced STDP, which leads to the down-regulation of the recurrent assembly to the groundstate. If, in the LTP-dominated case, the recurrent assembly consolidates, we find that the replay quality enhances (Fig. 3.15, **b**). Because in a recurrent assembly, the order of firing has no true or false direction, this shows up in an increase in variance of the matching index distribution, not in a shift of the mean towards one. Despite, we find no splitting of the distribution into neuron pairs that fire in one or the other direction. Further, the number of consolidated synapses is a lot higher than in the FF-case with ≈ 9 consolidated synapses per neuron. As in the FF-case, the assembly shows ripple like activation (Fig. 3.15, **c**), which is however regular and persistent. If we decrease the assembly size to 100 neurons and at the same time decrease η_{SS} by half, we find that also LTD-dominated (therefore also balanced STDP) leads to the consolidation of the assembly (Fig. 3.15, **d,e,f**. However, the number of consolidated synapses is much smaller (≈ 2 synapses per neuron). Further, the consolidation process has a stronger effect on the replay. While in the LTP-dominated case, the matching index distribution solely broadened, here we find that the distribution splits into a bimodal distribution (Fig. 3.15, **e**). This means that after consolidation the order of firing is very distinct in either one or the other direction for single neuron pairs. Moreover, the network exhibits ripple like activity, which is not regular but occurs more randomly than in the case of LTP-dominated STDP (Fig. 3.15, **f**).

3.4.3   Changing the background noise

We find that the background noise σ the network receives biases the outcome of the network consolidation process. In the before shown simulation results, σ has always been set to $3mV$. If we increase the noise to $\sigma = 5mV$, we find that all synapses within the FF-structure decay to the groundstate, i.e. no synapses consolidate (Fig. 3.16, **a**). Further, the network activity and FF-replay become noisy and in conclusion the distinct ripples disappear (Fig. 3.16, **b**).

Interestingly however, the matching index distribution (before consolidation) does not change much compared to when $\sigma = 3mV$ (Fig. 3.16, **c**). If the background noise level is decreased to $\sigma = 1mV$, a subset of synapses stays above the groundstate (Fig.
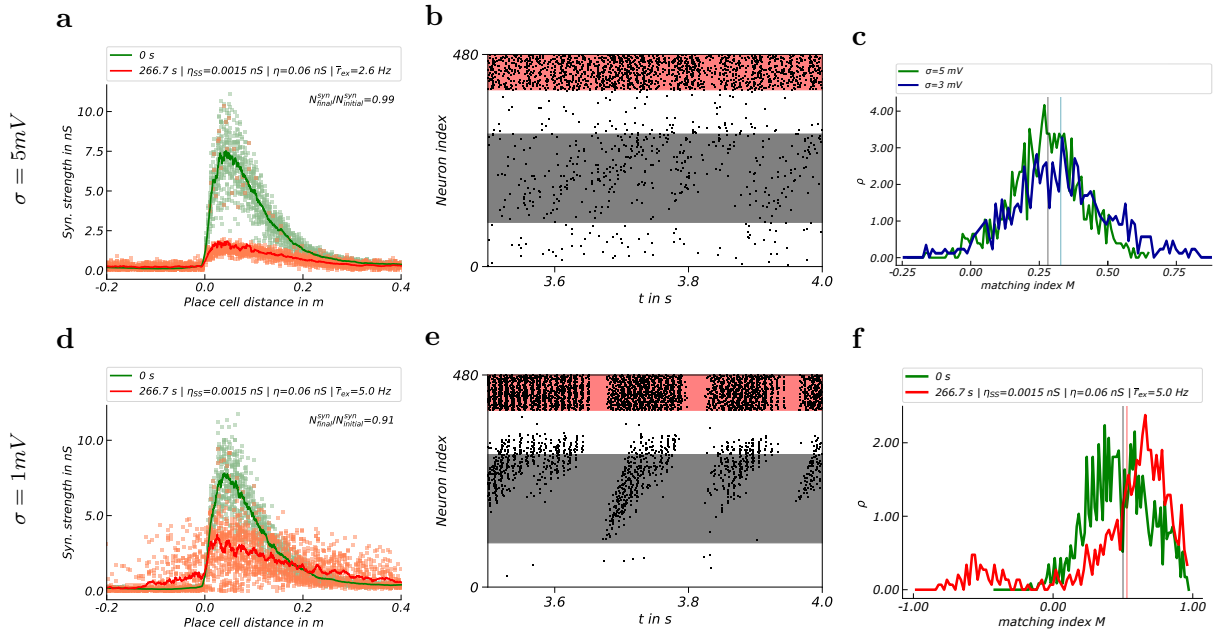
Fig. 3.16: The background noise magnitude influences whether and how FF-structures consolidate. A network with strong FF-connectivity has been simulated with background noise ($\sigma = 1mV$) (**d-f**) and high background noise ($\sigma = 5mV$) (**a-c**). The background current has been adjusted such that in both cases the mean excitatory firing rate lies around $2Hz - 5Hz$. At high background noise, the FF-structure does not get consolidated (**a**). Further, the memory replay in the initial state is weak and unpronounced (**b**). The matching index distribution however only changes slightly compared to $\sigma = 3mV$ (**c**). Low background noise 'blurs' the FF-structure and results in the growth of strong recurrent connections (**d**). The replay occurs in strong bursts (**e**). The matching index distribution shows a small shift towards 1 and the growth of a second mode at negative values, associated with the new strong recurrent connections (**f**).

3.16, **d**). However, the FF-structure is broadened and strong recurrent connections evolve. This change in the consolidation process occurs, because the lower noise level allows the neurons to fire more synchronous and activity spreads though the FF-structure with less disturbance (Fig. 3.16, **e**). The more synchronized activity however also results in more STDP induced potentiation. This supports the growth of weak synaptic connections that belong to neurons in the FF-structure, such as recurrent connections. At low noise levels, the matching index distribution evolves a second mode during consolidation which has its mean at negative values of the matching index (Fig. 3.16, **f**). The new mode accounts for the increased occurrence of activity spread in opposite direction (to the FF-structure), because of the new strong recurrent connections. The mode accounting for the activity spread in direction of the FF-structure however still shows a shift towards one (Fig. 3.16, **e**).

3.4.4 Impact of background current and inhibitory feedback

Inhibition and the background current have similar effects on consolidation but different for LTD-dominated and balanced STDP compared to LTP-dominated STDP. If in the following shown results, the background current is changed, the inhibitory feedback is held at $I \rightarrow E = 0.4 * FF - strength$ and $E \rightarrow I = FF - strength$. If the inhibitory feedback is changed, the background current is held at $I_0 = 0.36nA$ and $I \rightarrow E$ and $E \rightarrow I$ are changed by the same factor. Lowering the background current amplitude and increasing the inhibitory feedback strength both decrease the network activity and increase the memory-replay quality. On the other hand,increasing the background current and lowering the inhibitory feedback both increase the network activity but result in slightly different network dynamics and consolidation results (Fig. 3.17). However this difference is small.

Increased activity

We find that if the background current is high (here $I_0 = 3.9nA$), such that the mean excitatory firing rate is around $9Hz$, the FF-structure no longer consolidates in all three cases of STDP. Moreover, the replay is noisy and ripples are almost gone (Fig. 3.17, **a, e**). In contrast, if the inhibitory feedback is low, such that the mean excitatory firing rate is also at about $9Hz$, synapses still consolidate and while the replay also becomes noisy, ripples are , while also spread, less noisy than for high I_0 (Fig. 3.17, **b, f**). However, if STDP is LTP-dominated, lowering the inhibition leads to strong recurrency (see following subsection).

Decreased activity

If the network activity is decreased to low values around $2Hz$, the ripples become more pronounced and the replay less noisy. However, whether the activity is decreased by adjusting the inhibitory feedback or the background current shows to make no major difference in the consolidation process or the network dynamics (Fig. 3.17, **c, g and d,h**). In general (whether the network activity is altered via inhibition or the background current), a higher network activity results in a worse matching index before the consolidation. If the FF-structure gets consolidated, the matching index is however enhanced (Fig. 3.18). We find that, if the inhibitory feedback is above $1nS$ (corresponding to a network activity of $\approx 7Hz$), the mean of the matching index distribution always converges to ≈ 0.6 during consolidation, independent of the inhibitory feedback strength (Fig. 3.18, **b**).
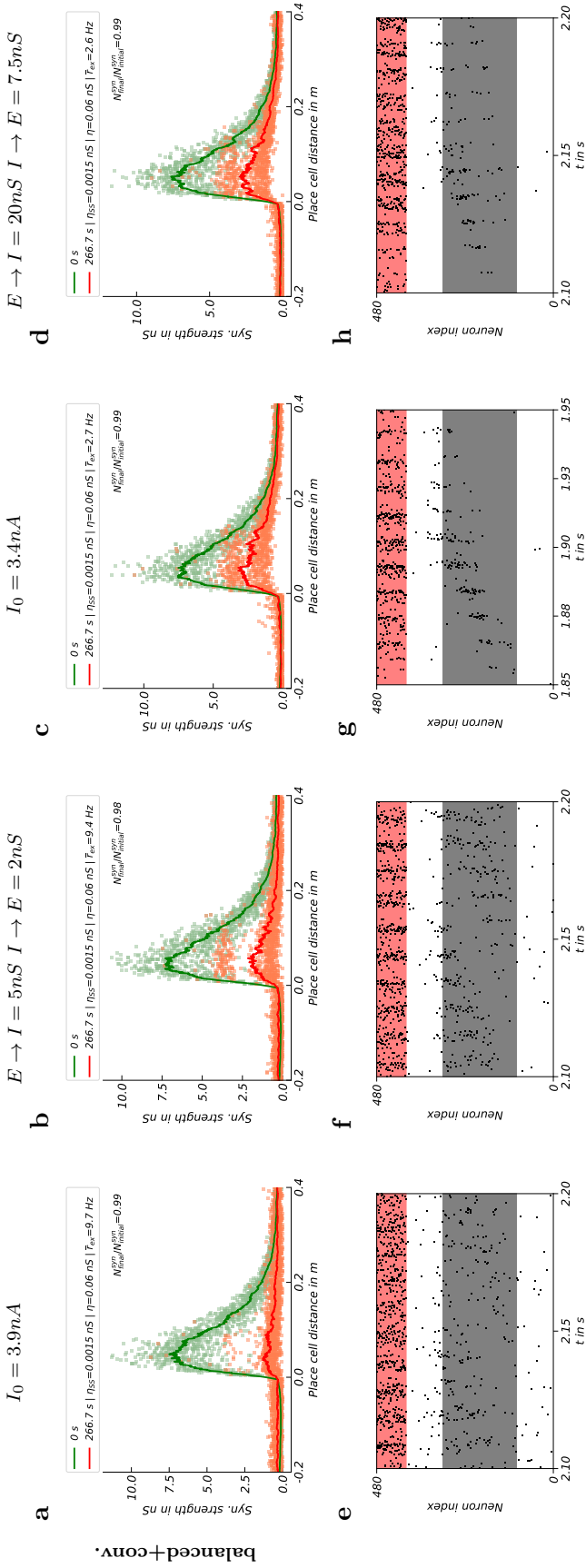
Fig. 3.17: Inhibitory feedback and background current have similar effects on the network dynamics, but can lead to slightly different consolidation results. When I_0 is changed, the inhibitory feedback is held constant at $E \rightarrow I = FF - strength$ and $I \rightarrow E = 0.4 * FF - strength$. The FF-strength is set to $7.5nS$. When the inhibitory feedback is changed, $I_0 = 3.6nA$. Higher network activity induced by higher I_0 impedes consolidation (**a**), while higher network activity induced by lower inhibitory feedback still enables consolidation (**b**). Weak inhibitory feedback and high I_0 further have a slightly different impact on the spiking dynamics of the network. While both worsen the replay and 'blur' the ripples, ripples are more pronounced at low inhibitory feedback (**e**, **f**). High inhibition (**d**) and low I_0 (**c**) result in the consolidation of the FF-structure. The ripple generation is in both cases very pronounced (**g**,**h**).
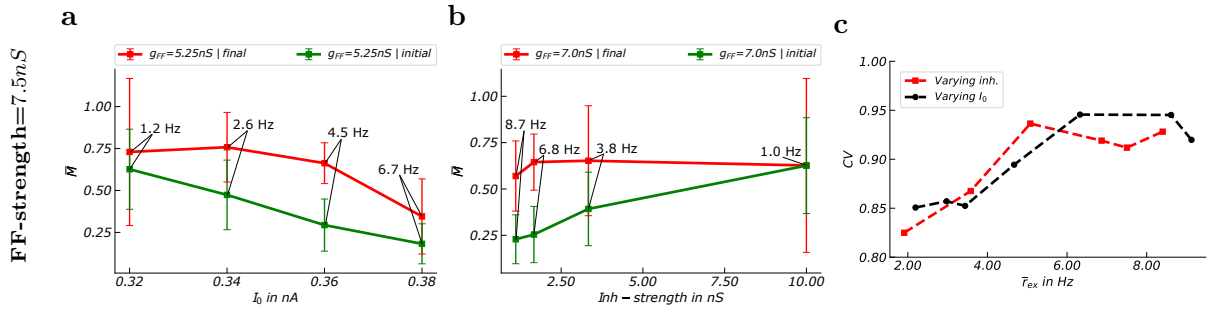
Fig. 3.18: The mean matching index ($\overline{M}$) decreases with increased activity induced by lower inhibition or increased background current I_0. The mean matching index and its variance are calculated from the matching index distribution over all strong synapses ($> 2nS$). Inhibition and I_0 influence the network activity. Therefore the activity is the network property upon which the replay quality due to I_0- or inhibition-changes are compared. Increasing I_0 (**a**) results in a noticeable change in $\overline{M}$ after consolidation (red line) already at network activities $> 4Hz$, while decreased inhibitory feedback (**b**) does not change $\overline{M}$ up to at least $6.8Hz$ (**b**). The inh.-strength on the x-axes is the $I \to E$ strength, however $E \to I$ is changed with the same factor. The coefficient of variation (CV) of the inter-spike-timing intervals (before consolidation) increases with the firing rate, i.e. also the single neuron fires less regular (**c**).

In contrast, raising the background current leads to a drop in the mean matching index already at a network activity of $\approx 3Hz$ (Fig. 3.18, **a**). In comparison, if the inhibitory feedback is such that the network activity is at $6.8Hz$, the mean matching index is still at 0.6 after consolidation. For an adjusted background current, the matching index lies at ≈ 0.4 at a network activity of $6.7Hz$. The coefficient of variation (CV [1]) of the inter-spike-timing intervals (before consolidation) increases with the firing rate ((Fig. 3.18, **c**). Therefore not only the temporal structure of activity between neurons decreases with the network activity but also the firing of the single neuron becomes less autocorrelated.

lowering the inhibition and increasing I_0 for LTP-dominated STDP

We find that in the case of LTP-dominated STDP, low inhibitory feedback results in the transformation of the FF-structure to a recurrent cell assembly (Fig. 3.19, **b**). Further, while at a background current of $I_0 = 3.9nA$, the FF-structure vanishes (as in the balanced/LTD-dominated case), increasing the background current further to $I_0 = 4.2nA$, results in the hole network scaling up drastically if STDP is LTP-dominated

---

[1]The CV is defined as the ratio of the standard deviation to the mean

(Fig. 3.19, **a**). Note that in the case of lowered inhibition not the hole network scaled up but only synapses belonging to neurons within the FF-structure.
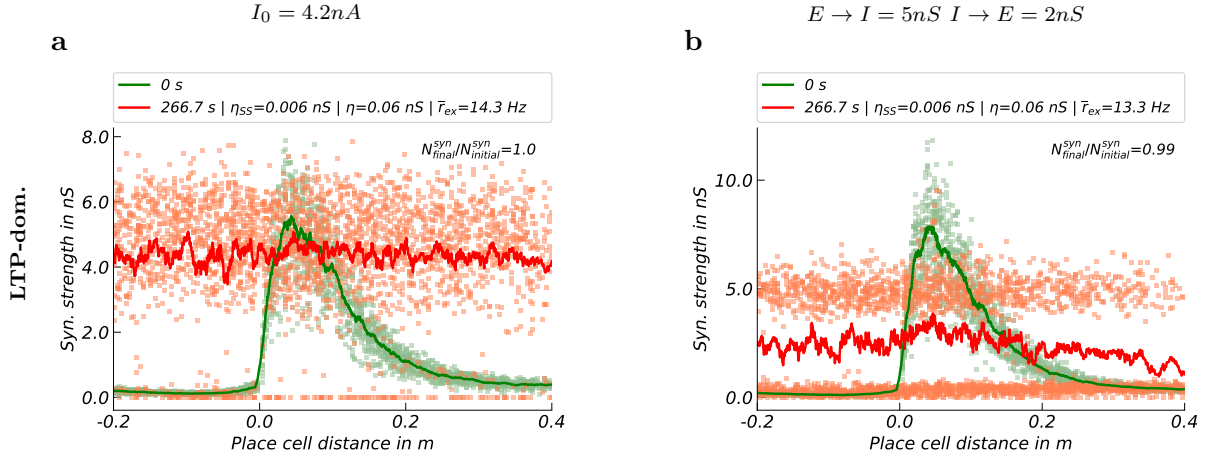
Fig. 3.19: When STDP is LTP-dominated, lowering the inhibition or increasing I_0 can result in the growth of large recurrent assemblies. I_0 has been increased to $4.2nA$ (**a**), resulting in the potentiation of the hole network. Lowering the inhibition (**b**) also lead to the growth of recurrent connections, however limited to connections belonging to neurons within the FF-structure.

3.4.5 Fragmentation of the FF-structure during consolidation

We found that STDP in combination with SS can consolidate FF-structures and result in an enhanced memory replay. However with the downside that most of the strong connections are lost, which fractures the FF-structure. A small microcircuit with STDP and with STDP and SS has been simulated to shed some light on this issue. 16.67 min. of spiketrain data has been captured from the simulations to get an estimate for the crosscorrelation function, from which the synaptic change in pS/s has been calculated. The microcircuit consisted of a single postsynaptic neuron, receiving dendritic spikes and input from a number of presynaptic neurons, where all connections had the same strength. Simulations were done for a number of $1-6$ presynaptic neurons and for different connectionstrengths (Fig. 3.20). All neurons received a background current $I_0 = 16.5mV$ and noise with $\sigma = 3mV$. We find that the magnitude of potentiation a synapse experiences decreases with the increasing number of opponent presynaptic neurons (Fig. 3.20, **a**).Moreover, the ratio of postsynaptic to presynaptic firing rate up to doubled for each additional connection at the inset of dendritic spikes ($\approx 200pA$) (Fig. 3.20, **c**).

balanced (No Dendr.)   **balanced+conv. SS**

a   **b**

c
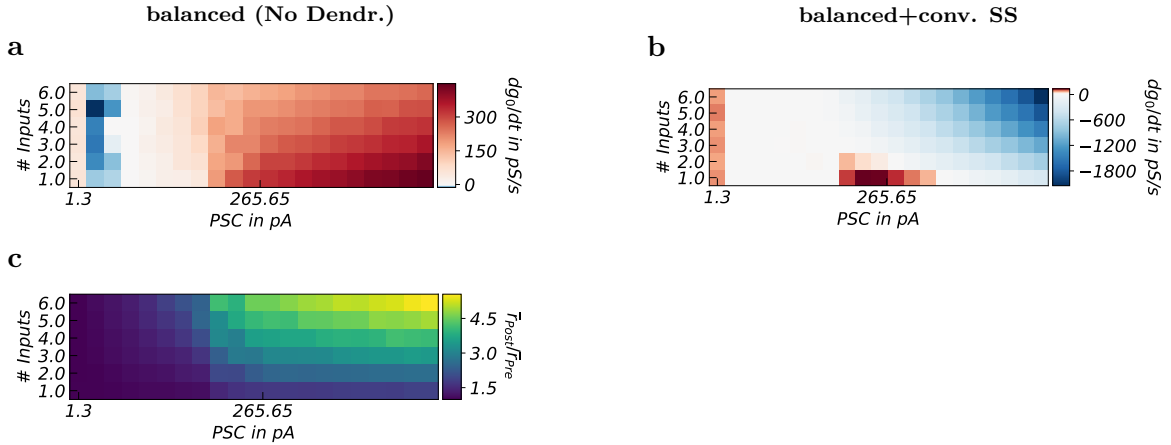
Fig. 3.20: Each additional strong input a neuron receives lowers the potentiation per synapse (**a**) and up to doubles the postsynaptic activity (**c**). Therefore SS induced depression highly increases, such that potentiation is only present in the case of a single strong input (**b**). The synaptic change has been estimated via the crosscorrelation function which has been estimated from spiketrain data. We did simulations for a single postsynaptic neuron and varied the number of presynaptic inputs from $1 - 6$ (synaptic strengths were equal for all connections). Panel **a** shows the synaptic change for balanced STDP without SS, panel **c** the ratio of postsynaptic to presynaptic firing rate depending on the number of inputs and the PSC amplitude. Panel **b** shows the synaptic change with balanced STDP and convex SS. The learning rates were $\eta = 60pS$ and $\eta_{SS} = 0.05pS$.

The higher postsynaptic firing rate in turn increases depression due to SS by up to a factor of two for each additional connection. This finding states the general problem with SS, as it depresses connections to presynaptic neurons that fire slower than the postsynaptic neuron. In our model, the amount, by which SS scales down connection does not depend on the difference between pre- and postsynaptic neuron but solely on the postsynaptic rate. However, potentiation is induced by STDP only around a small time window, when the presynaptic neuron fires. Therefore, if the presynaptic activity is low compared to the postsynaptic neuron, potentiation is slow compared to depression via SS. This becomes a problem in FF-structures, where the neural activity increases, the further down a neuron 'sits' within the structure. We therefore here propose two adjustments that could be made to the model:

1. the reduction of the learning rate η_{SS} for SS

2. intrinsic plasticty

Intrinsic plasticity [58] describes the mechanism of an adaptive spiking threshold that changes such that the neuron fires at a target rate. The mechanism is implemented

as follows: Each time the neuron fires, its firing threshold is increased by an amount $\Delta u_{th} = 0.3mV$. As long as the neuron does not exhibit a spike, the spiking threshold decreases with a time-constant $\tau_{IP} = 0.2s$ according to

$$\frac{du_{th}}{dt} = -\frac{\Delta u_{th}}{\tau_{IP}} \tag{3.3}$$

The target firing rate is thereby set by the decay time constant via $r = 1/\tau_{IP} = 0.2s = 5Hz$, because τ_{IP} is the time it takes for the threshold to get back to the level at which the last spike was evoked.

Thereby, intrinsic plasticity adjusts the firing rate of each neuron to a target firing rate, independent of the input the individual neuron receives.

Both approaches result in a larger number of synapses experiencing potentiation (Fig. 3.21).
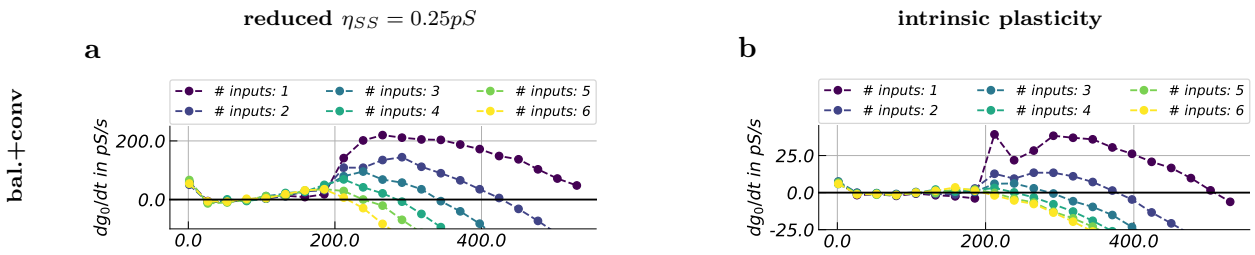
Fig. 3.21: Lowering the SS learning rate or setting a target firing rate for the neurons via intrinsic plasticity increases the number of consolidated synapses. The simulations with intrinsic plasticity have been done for a target firing rate of $5Hz$ (**b**). The simulation for reduced SS (**a**) were done with η_{SS} decreased by half ($\eta_{SS} = 0.75pS$). STDP has been balanced in both cases.

Lowering the SS learning rate

We find that lowering the learning rate η_{SS} for SS results in a larger set of consolidated synapses in the case of LTD-dominated and balanced STDP but leads to the growth of a recurrent cluster in case of LTP-dominated STDP (Fig. 3.22). η_{SS} has been reduced by half, compared to previous simulations. This decreases the competition between STDP and SS and therefore results in a broader synaptic weight distribution with stronger synapses and also leads to the consolidation of more synapses.

However, the larger pool of strong synapses in the network also increases the activity. The activity is highest at the end of the FF-structure, where it results in the growth of
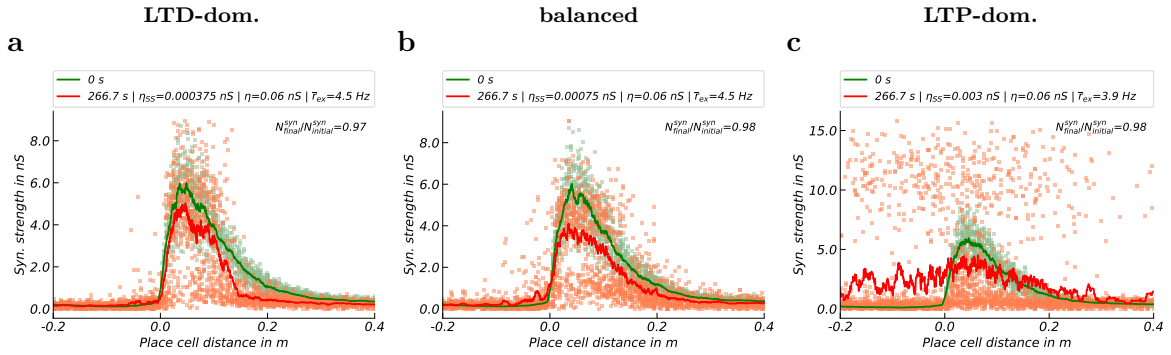
Fig. 3.22: Lowering η_{SS} by half results in the consolidation of more synapses. However, the FF-structure is only retained if STDP is balanced or LTD-dominated. The consolidation process is best for LTD-dominated STDP (**a**), where mainly strong synapses within the FF-structure retain strong. Balanced STDP also consolidates the FF-structure, however the distribution becomes more 'fuzzy', and strong recurrent connections (place cell distance < 0) start to emerge (**b**). For LTP-dominated STDP, consolidation is no longer stable and breaks the FF-structure (**c**).
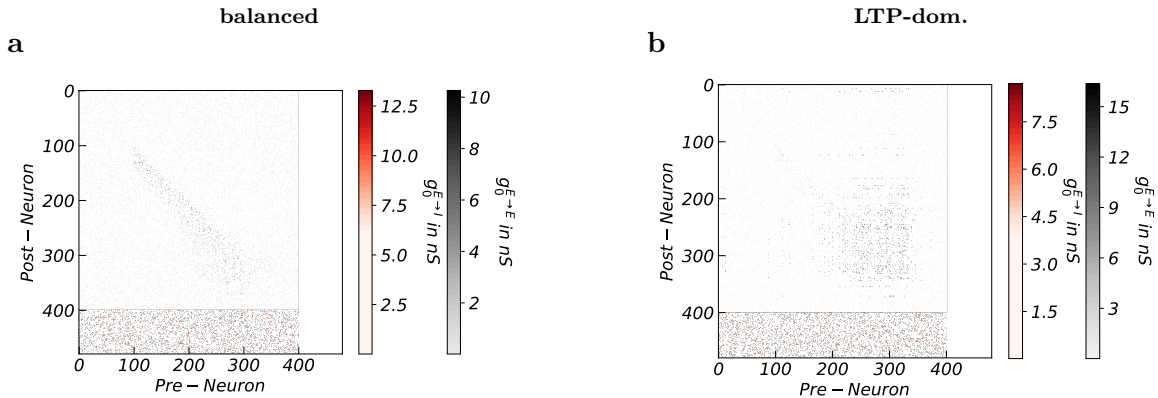
Fig. 3.23: When η_{SS} is divided by half, the emergence of strong recurrent connections occurs mainly at the end of the FF-structure, where the network activity is highest. Panel **a** shows the excitatory weight matrix for balanced STDP after consolidation. As seen, the FF-structure is retained. Panel **b** shows the excitatory weight matrix for LTP-dominated STDP after consolidation where first, the beginning of the FF-structure is almost dissolved and second, the end of the FF-structure evolved into a random recurrent assembly.

strong recurrent connections in the case of LTP-dominated STDP (Fig. 3.22 **c**, 3.23 **b**).The evolution of strong recurrent connections can also be found for balanced and LTD-domianted STDP, where this effect is however not as strong and the FF-structure is retained (Fig. 3.22 **a,b**). The replay quality (of the strongly connected neurons) in terms of the matching index is only slightly enhanced after consolidation , in contrast to when the network lost most of its strong connections (Fig. 3.24, **a**) (each additional

strong connection that drives a neuron changes the spike-timing and therefore perturbes the order of firing from the perspective of other presynaptic neurons). However, the probability that a neuron retains at least one strong output and input connection is greatly enhanced (Fig. 3.24 **b,c**). Thereby the FF-structure is preserved and most probably continuous instead of fractured.
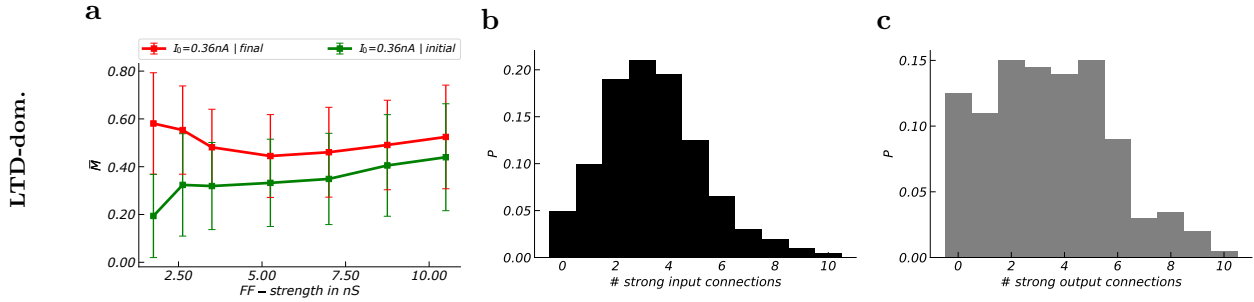
Fig. 3.24: A lower SS learning rate consolidates more synapses but increases the mean matching index only slightly (**a**) compared to when fewer synapses are retained strong (compare Fig. 3.11). The probability distributions for the number of strong input and output connections per neuron (**b,c**) lets us suggest that the FF-structure no longer fractures during consolidation.

Introducing intrinsic plasticity to the model

We find that intrinsic plasticity results in the consolidation of most synapses within the FF-structure. In contrast to the approach of lowering η_{SS}, the FF-structure is retained even for LTP-dominated STDP. However, the intrinsic plasticity mechanism impairs the generation of pronounced ripples (Fig. 3.25). Moreover the matching index is low compared to previous results without intrinsic plasticity. This makes sense, because a intrinsic plasticity mechanism biases the correlation between neurons by forcing each neuron to fire after a certain time interval set by τ_{IP}.
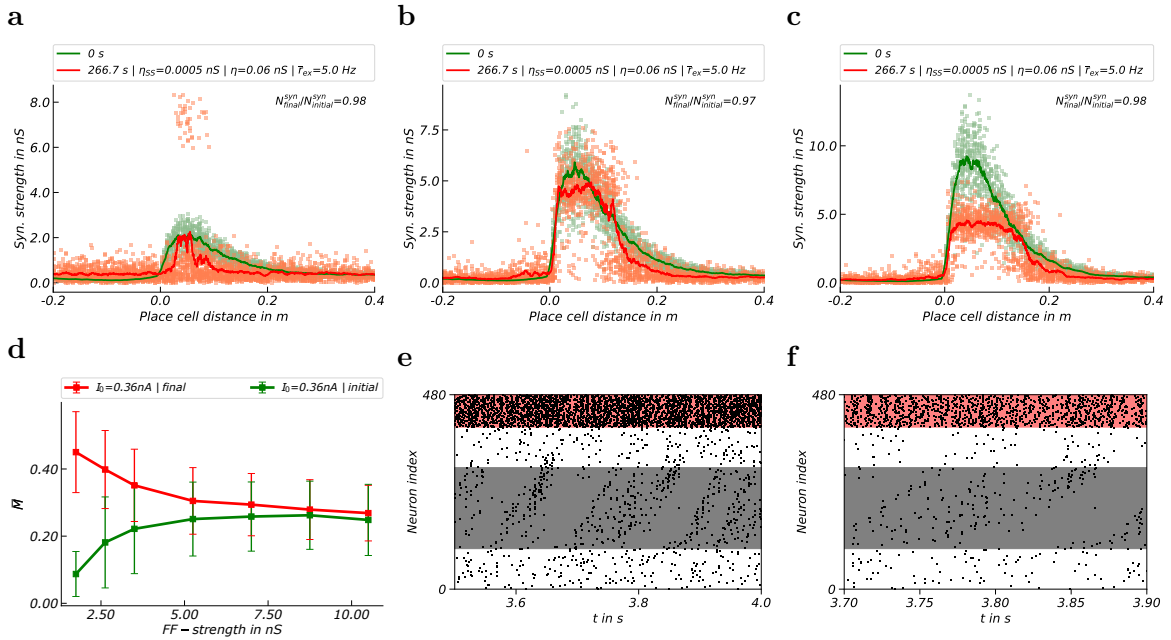
Fig. 3.25: Intrinsic plasticity increases the number of consolidated synapses if the target rate is not too high but worsens replay and ripple generation. The intrinsic plasticity has a target firing rate of $5Hz$. FF-structures get consolidated at various FF-strengths (**a,b,c**). For weak FF-structures however only the strongest synapses consolidate, while the rest decays to the groundstate (**a**). The matching index only increases significantly for FF-structures up to $5nS$. For higher FF-strengths, the number of consolidated synapses is too large to cause significant change compared to the initial state (**d**). Memory replay is present (**e**) but exhibits less pronounced ripples (**f**).

3.4.6 Consolidation without dendritic spikes

In the absence of dendritic spikes FF-structures consolidate, however in a regime that is biologically less plausible.

The results from section 3.2.2 showed that consolidation would only be possible for LTD-dominated or balanced STDO since LTP-dominated STDP does not support bimodal distributions. We therefore did not study LTP-dominated STDP without dendritic spikes. Our simulation results show that due to the much reduced SS learning rate that is needed in order to retain a potentiation regime results in a much slower convergence rate of the network to a steady state. Consolidation did occur, however, the regime in which synapses consolidated was at synaptic strengths around $30-40nS$, which we would consider rather unrealistic (Fig. 3.26, **a-f**). Morover, most synapses did not consolidate but decayed to the groundstate. While this is not directly visible from figure 3.26, **a-f**, where simulation time has been $533s$, simulating $2000s$ was
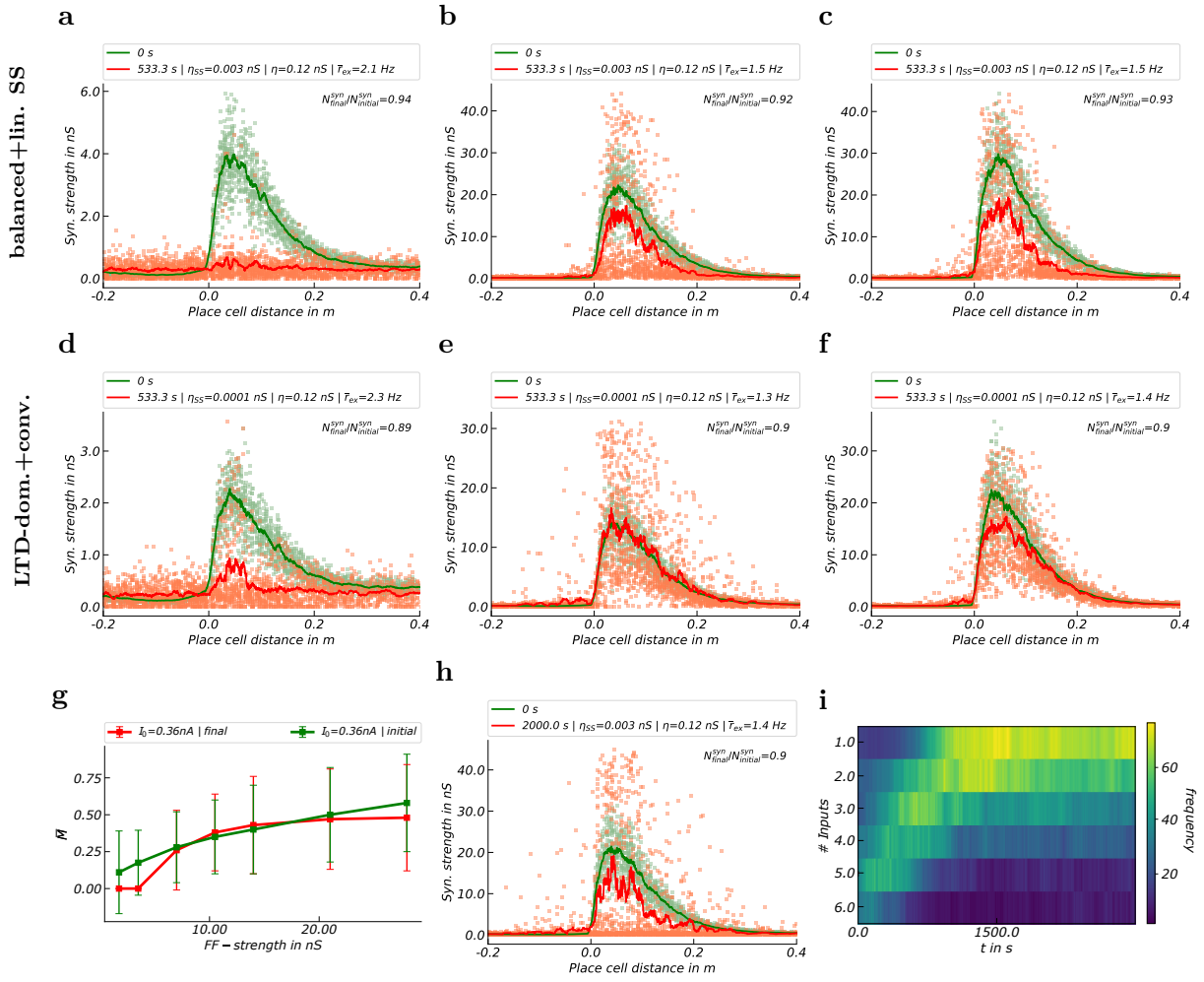
Fig. 3.26: The network model without dendritic amplification shows slow convergence to a steady state and unrealistic broad synaptic distributions. Balanced STDP (**a,b,c**) and LTD-dominated STP (**d,e,f**) consolidate a subset of strong synapses for FF-strengths above $7nS$ (**b,c,e,f**). However the consolidated synapses have strengths up to $40nS$. Weaker structures decay to the groundstate (**a,d**). The matching index is not much improved during consolidation and converges to ≈ 0.3. The network reaches a steady state only after around $2000s$ (**h**). During this consolidation period, the neurons loose most of their strong inputs (# inputs) (**i**).

enough for the network to reach a steady state, in which only ≈ 1 strong synapse per neuron was retained (Fig. 3.26, **h,i**). Lowering the SS learning rate would probably result in a larger number of synapses but also at an even higher consolidation regime above $40nS$. Further, the matching index did not change much during consolidation but converged towards ≈ 0.3 (Fig. 3.26, **g**) The reason why only roughly 1 strong synapse per neuron gets consolidated is the same as for the model with dendritic spikes.

a

b
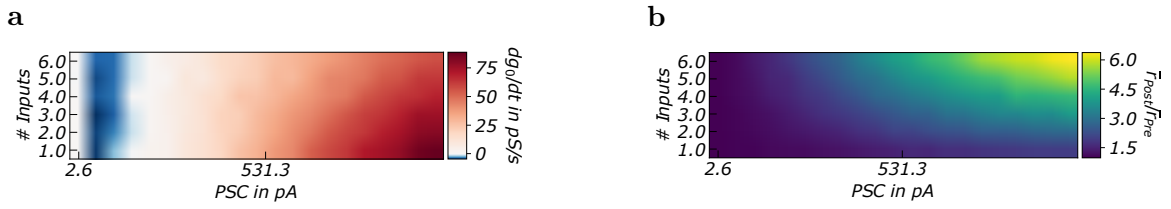
Fig. 3.27: Each additional strong input a neuron receives lowers potentiation per synapse and up to doubles the postsynaptic activity. The synaptic change has been estimated via the crosscorrelation function which has been estimated from spiketrain data. We did simulations for a single postsynaptic neuron and varied the number of presynaptic inputs from $1-6$ (synaptic strength were equal for all connections). Dendritic spikes were turned off. Panel **a** show the synaptic change for balanced STDP without SS, panel **b** the ratio of postsynaptic to presynaptic firing rate depending on the number of inputs and the PSC amplitude.

Because the upper limit for the synaptic growth is at $\approx 30-40nS$, PCs are very strong ($> 2nA$). The strong PSCs up to double the postsynaptic activity and thereby significantly increase depression induced by SS (Fig. 3.27). However, lowering η_{SS} would result in synapses growing larger than $40nS$ and increasing η_{SS} in the deletion of the FF-structure. Therefore, consolidation of more synapses would better be achieved via a different SS rule, which has a different dependence of the synaptic strength or the postsynaptic activity. Alternatively intrinsic plasticity would probably lead to better consolidation. Both these suggestions have however not been tested in the current work.

3.5   Summary

1. We found STDP and SS combined are able to drive the synaptic distribution of a network with dendritic amplification into two distinct, stable regimes, forming a bimodal weight distribution, which we propose is necessary to retain memories. In our model this works for FF-structure as well as recurrent assemblies. However, this consolidation process highly depends on the form of the STDP rule and and the learning rates of STDP and SS. LTP-dominated STDP e.g. potentiates connections at high drives, while LTD-dominated STDP depresses connections. Moreover FF-structures are less stable under LTP-dominated STDP, because high activity can result in the potentiation of weak synapses and in strong recurrency. The number of strong synapses per neuron the network retains after consolidation depends on the exact balance between the learning rates of SS and STDP. High

SS learning rates lower the number of strong synapses, however significantly increase the temporal order of spiking for those connections that retain strong. It should be noted however that this result should not be over-interpreted and that it is questionable if the used matching index is a good measure to quantify the quality of memory replay, because it only considers the correlation between single neuron pairs and not the hole population representing the memory.

2. A network without dendritic amplification is also able to consolidate its memory, however only if STDP is not LTP-dominated. Further, if connections consolidate,the synaptic weights become large, such that they are at the edge of what is considered biologically plausible. Moreover, most of the strong synaptic connection are lost.

3. We derived results for STDP and STDP+SS induced change in a single connected neuron pair over a wide range of input current amplitudes and connection strengths. We found that the probability of a presynaptic neuron to evoke a postsynaptic response increases concave with the connection strength and that therefore STDP induced potentiation increases nonlinear (sigmoidal) with the synaptic strength. Also, the form of the STDP rule influences how potentiation changes with the background current. For LTD-dominated STDP, this dependence is highly concave, while for LTP dominated STDP it is slightly convex.

Chapter 4

STDP: Comparison of analytical methods and simulations

4.1 Introduction

The motivation for this chapter, while a little bit out of the focus of this works, comes from two arguments. An analytical solution to a problem gives a clear view on how different variables/parameter of a system interact to give a certain result. Second, numerical simulations often take much more time than analytical calculations. Therefore, in order to better understand the dynamics of neural networks it is appropriate to look for such analytical solutions. The basis for the results in this section come from Ostojic et al.[78], who derived an expression for the crosscorrelation between two LIF neurons (Eq. 2.35) in terms of

1. the rate response to a constant input,

2. the autocorrelation function

3. the rate response function (which is the rate response to an oscillating input)

For the rate response function an analytical expression has been derived by Brunel et al.[18] (methods section 2.5) . While some of the analytical results shown in this section are reproduced from their work, we here do a more extensive comparison to simulation results. Analytical solutions to the rate response function are compared to simulation results over a wide range of osculating current amplitudes. Further the analytical expression for the inter-spike-interval distribution of a LIF is directly compared to simulation results, as well as the autocorrelation function for different

levels of noise σ and input currents I_0. At last, analytical results for the STDP induced synaptic change are compared to simulations, which has not been done before in the known literature.

4.2 The rate response to a constant input current and white noise

The simplest input a LIF neuron can receive is a constant background current. Then, the response is simply given by the differential equation 2.1. In the presence of Gaussian white noise as additional input, the solution to the Fokker-Planck equation, describing the evolution of the membrane potential probability distribution, is known and given by equation 2.41 (Fig. 4.1).
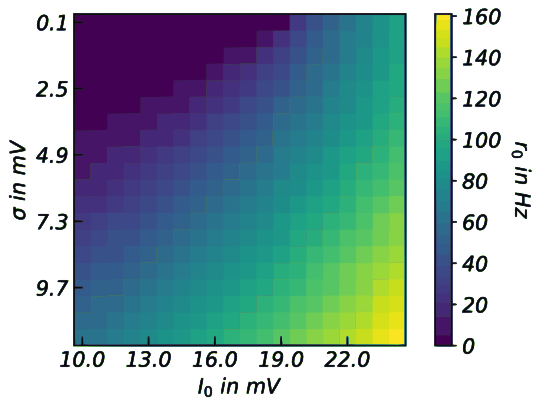
Fig. 4.1: The firing rate r_0 of a LIF neuron in response to a constant input current I_0 and Gaussian white noise with SD σ.

4.3 The rate response function to an oscillatory input current

We find that the analytical solution in linear approximation to the rate response functions is in good agreement with simulations if the the amplitude of the oscillating

input current is not too small nor too strong. We simulated a unconnected population [1] of 1000000 LIF neurons receiving an oscillating input current

$$I_{osc} = I_1 \; cos(\omega t) \; , \tag{4.1}$$

where I_1 has been set from $0.5 - 5mV$ and ω from $1 - 200Hz$. Apart from I_{osc}, the neuron population received a constant input current $I_0 = 20.3mV$ and Gaussian white noise with $\sigma = 0.5$, which drives the neuron population to a firing rate of $\approx 30Hz$. The response of a LIF neuron highly depends on the baseline firing rate r_0 and the background noise the neuron receives [17, 88], simulations have however only been done for the mentioned noise and input current values (Fig. 4.2 **a**). The analytical solutions (Eq.2.42) were done for a baseline firing rate of $30Hz$ and at different levels of Gaussian white noise $\sigma = 0.5, 1, 3, 6mV$ (Fig. 4.2, **b**). While it has already been argued in [17] that the linear approximation is only valid for small amplitudes of the oscillating input current, the linear approximation of the response function has never been directly compared to results from simulation at different current amplitudes (at least not to the knowledge of the author). While equation 2.42 that gives the response in Hz/A does not depend on the the current amplitude, simulations (Fig. 4.2, **a**) show that there is a dependency and that the analytical solution (Fig. 4.2, **b** red curve) are in approximate agreement with simulations only if $I_1 \geq 1.5mV$. The assumption on which the linear approximation of the rate-response function is based is, that the response of the neuronal population can be approximated by $r(t) = r_0 + r_1 * cos(w * t)$ when the input is of the form $I(t) = I_0 + I_1 cos(\omega t)$ with I_1/I_0 being small, but $I_1 > \sigma$. We find that for $1.5mV > I_1 > 0.5mV = \sigma$, the rate response is overestimated by the linear approximation. For strong amplitudes, the amplitudes of the resonance modes are in good agreement with what is found analytically, however the modes seem to broaden and slightly shift towards higher ω. The response in the firing rate exhibits resonance effects when the frequency of an oscillating input current is N times the baseline firing rate r_0, where $N = 1, 2, 3, ..$ (Fig. 4.2, **a**, **b**). However in the presence of noise this resonance effect quickly decays for frequencies of the input higher than $2 * r_0$ (Fig. 4.2, **b** Please note that the analytical results have already been shown in [78] and were reproduced for the current work.) However, we find a resonance mode at $r_0/2$ (Fig. 4.2 **a**), which is not predicted by the linear approximation.

---

[1]A neuron population has been simulated to be able to more efficiently calculate the ensemble average, note, the neurons were not connected in a network!
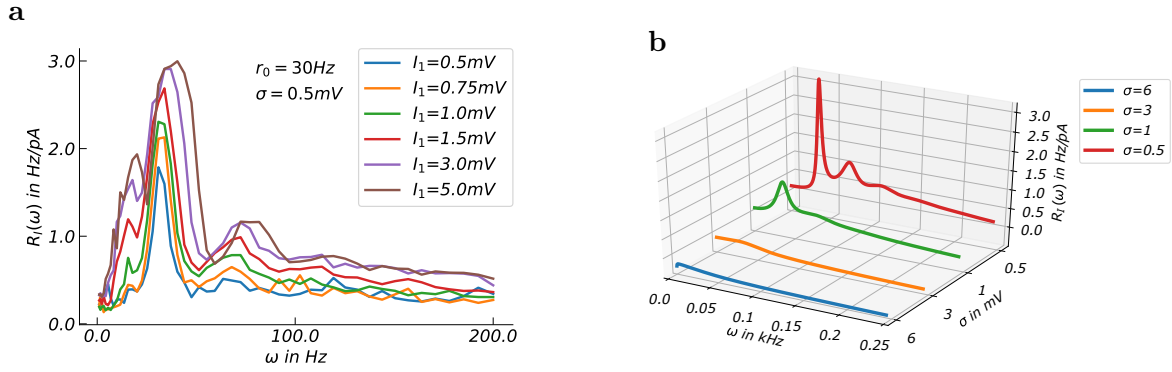
Fig. 4.2: a: The rate response function of a LIF neuron to oscillatory currents of different amplitude I_1 as a function of the oscillation frequency. The background noise has been set to $\sigma = 0.5mV$. Analytical results from linear response theory are valid for current amplitudes ($I_1 \geq 1.5mV$, compare red curve in **b**). A resonance mode at low ω is found that is not predicted analytically. The analytical solutions to the rateresponse function show that the resonance modes found at low background noise fade with increasing noise (**b**).

4.4 PISI, Auto-correlation function and the cross-correlation function

We find that the analytical solutions for the LIF inter-spike-interval (ISI) distribution (Eq.2.49) which can be calculated from solutions to the Kummer's differential equation[2] 2.45 are in excellent agreement with simulations (Fig. 4.3, **a**). So are the analytical solutions for the LIF autocorrelation function (Fig. 4.3, **b,c**) which can be expressed in terms of the ISI-distribution (Eq.2.47).

It should be mentioned however that the accuracy was only present for noise levels up to $3mV$. For higher levels of σ the analytical solution began to differ from the simulation. The reason for this discrepancy at higher noise levels has not clearly been identified but probably originates from numerical errors when solving the Kummer's differential equation. The equation has been solved numerically instead of using its solution in form of confluent hyper-geometric functions as it has been found that common algorithmic implementations that solve the confluent hyper-geometeric function are less accurate and do not lead to good results.

---

[2]Note that we solved Kummer's differential equation numerically using Eulers method instead of solving its solution in terms of the confluent hyper-geometric function, because we found this lead to very different results (This is probably due to the accuracy with which the confluent hyper-geometric function is solved in the scipy implementation that we used).
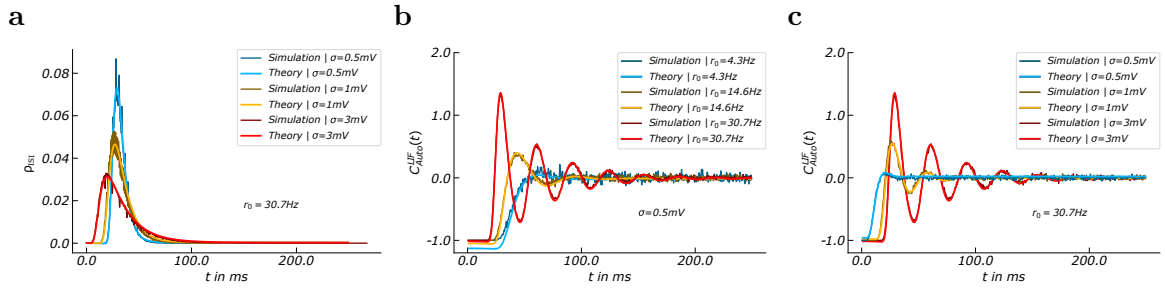
Fig. 4.3: Panel **a**: Inter-spike interval distribution of a LIF neuron at a mean firing rate of $\approx$ 30 Hz for different level σ of the background noise. Analytical results are in very good agreement with simulations. The distribution broadens with the amount of background noise, i.e. the neuron fires less regular. Further, the maximum of the distribution shifts towards smaller inter-spike-intervals. Note that the refractory period is not taken into account. Panel **b**: The autocorrelation function of a LIF neuron, driven by different constant background currents and white noise ($\sigma = 0.5mV$). Analytical results are again in very good agreement with simulations. The harmonic modes occur at integer multiples of the baseline firing rate r_0 and start to disappear with lower firing rates .Panel **c**: The Autocorrelation function of a LIF neuron at a constant firing rate of $30Hz$ for different amounts of background noise. The harmonic modes become weaker with the amount of noise.

PSC

To calculate the crosscorrelation function between two LIF neurons the synaptic current across a synapse with conductance g_0 needs to be defined. As before in the current work $I_{syn}(t) = g(t)(E_{syn} - u(t))$. Since with the crosscorrelation function, the ensemble averaged response to a input current is calculated $I_{syn} = g(t)(E_{syn} - \mu)$ (Fig. 4.4, **b**), where the effective membrane potential μ has been set to $17mV$. To solve the convolution integral in equation 2.35, the Fourier transform $I_{syn}(f)$ is determined (Fig. 4.4, **b**)

Crosscorrelation

The crosscorrelation function can now be expressed as a double convolution integral of the rate response function (Fig. 4.2) over the input current of a spike and the autocorrelation function of the presynaptic LIF neuron or equivalently in the frequency domain by the product of the respective Fourier transforms. Here, the crosscorrelation function is defined as the factor by which the instantaneous firing rate changes relative to the baseline firing rate after the inset of a PSC/Spike. The analytical results are

a

b
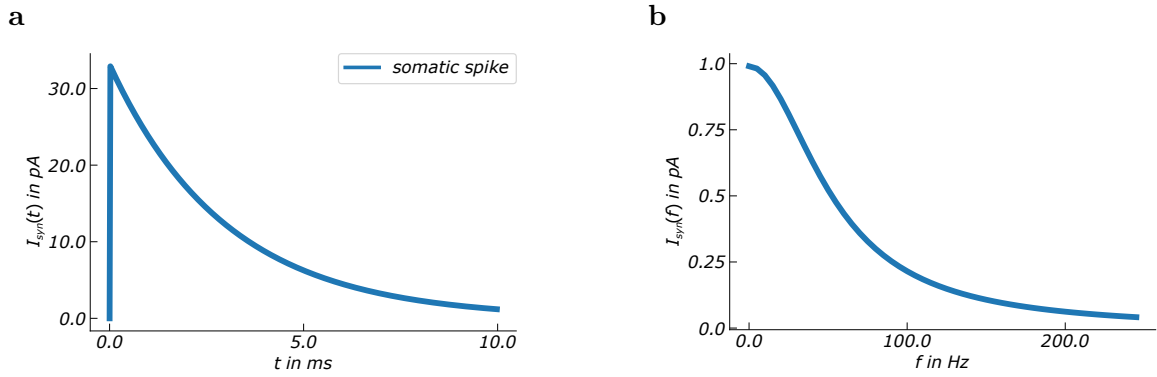
Fig. 4.4: panel **a,b**: The synaptic spike current that is evoked whenever a presynaptic spike occurs. The Fourier transform is used to calculate the convolution integral with the rate response function (**b**).

in good agreement with the simulation (Fig. 4.5). This has already been verified in [78] and is just included to show the agreement between the implementation of the method in this work with [78]. In the next section, the crosscorrelation function is used to determine the synaptic change for different forms of the standard STDP learning window over a wide range of pre- and postsynaptic firing rates. The advantage of calculating the synaptic change from the crosscorrelation function lies in the fact that once the crosscorrelation function is known, the synaptic change for different STDP rules can be calculated by a simple integral.

a

b
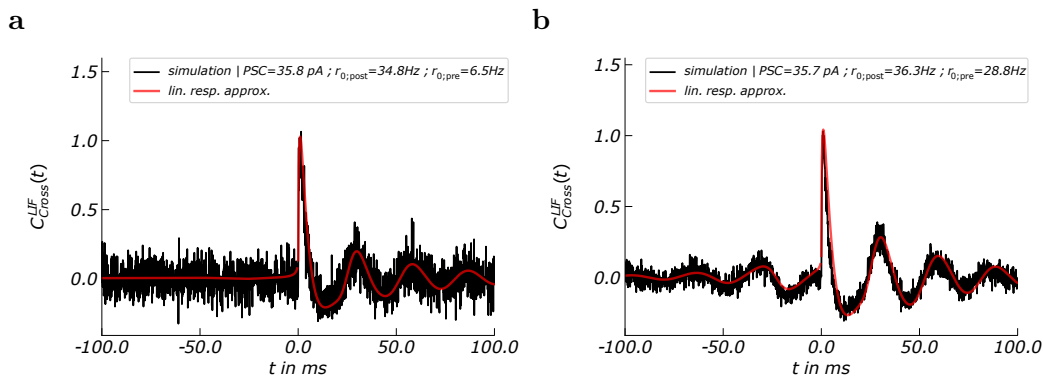
Fig. 4.5: The analytical crosscorrelation function (red curve) is in good agreement with simulations (black curve) for large differences in pre- and postsynaptic rate (**a**) as well as for similar rates (**b**). Pre- and postsynaptic neuron both received white noise with $\sigma = 0.5mV$. These results match with those from [78].

4.5 STDP dependence on the pre- postsynaptic firing rates

We find that potentiation and depression induced by STDP depend significantly on the pre- and postsynaptic firing rate (Fig. 4.6). Especially at low noise, properties are found that are explicitly a result of the autocorrelation function of the LIF neuron (Fig. 4.6, **a-d**). Further, analytical results are in very good agreement with simulations over a wide range of I_0 and the noise level σ, however only for low PSC amplitudes ($< 100pA$). We studied the following 4 model cases:

- a balanced STDP rule at low noise levels,

- a LTD dominated STDP rule at low noise levels,

- a balanced STDP rule at low noise with direct recurrency,

- a balanced STDP rule at intermediate noise levels.

We chose these cases as they shed light on the dependents to the width of the STDPs LTP-domain, the noise and the network topology (recurrency). For each of the above cases, analytical results are compared to simulations. The refractory period after the spike is not taken into account. The analysis is restricted to the case of a single neuron pair that receives a constant background current I_0 and Gaussian white noise with a standard deviation σ. No other connections such as inhibitory feedback are considered (Despite a recurrent connection). The connection strength is set to a low value of $g_0 = 1nS$ which corresponds to a PSC amplitude of approximately $55pA$. At much higher synaptic strengths, the linear approximation will not hold anymore and the analytical result deviate from simulations (Fig. 4.8). While these cases do not account for the hole spectrum of synaptic dynamics in the presence of STDP, they contribute to clearing the view on STDP.

Case 1 (Fig. 4.6, a,b):

In the presence of low background noise ($\sigma = 0.5mV$) and an approximately balanced STDP rule, STDP induced potentiation displays a sharp maximum when the pre- and postsynaptic firing rates are close (Fig. 4.6 **a,b**). Synaptic change in pS/s is highest at high firing rates, in terms of $pS/spike$ however highest at low firing rates (Fig. 4.7 **a**). This is explained by the stronger first mode in the crosscorrelation at low rates compared to high rates (Fig.4.7, **c,d**).
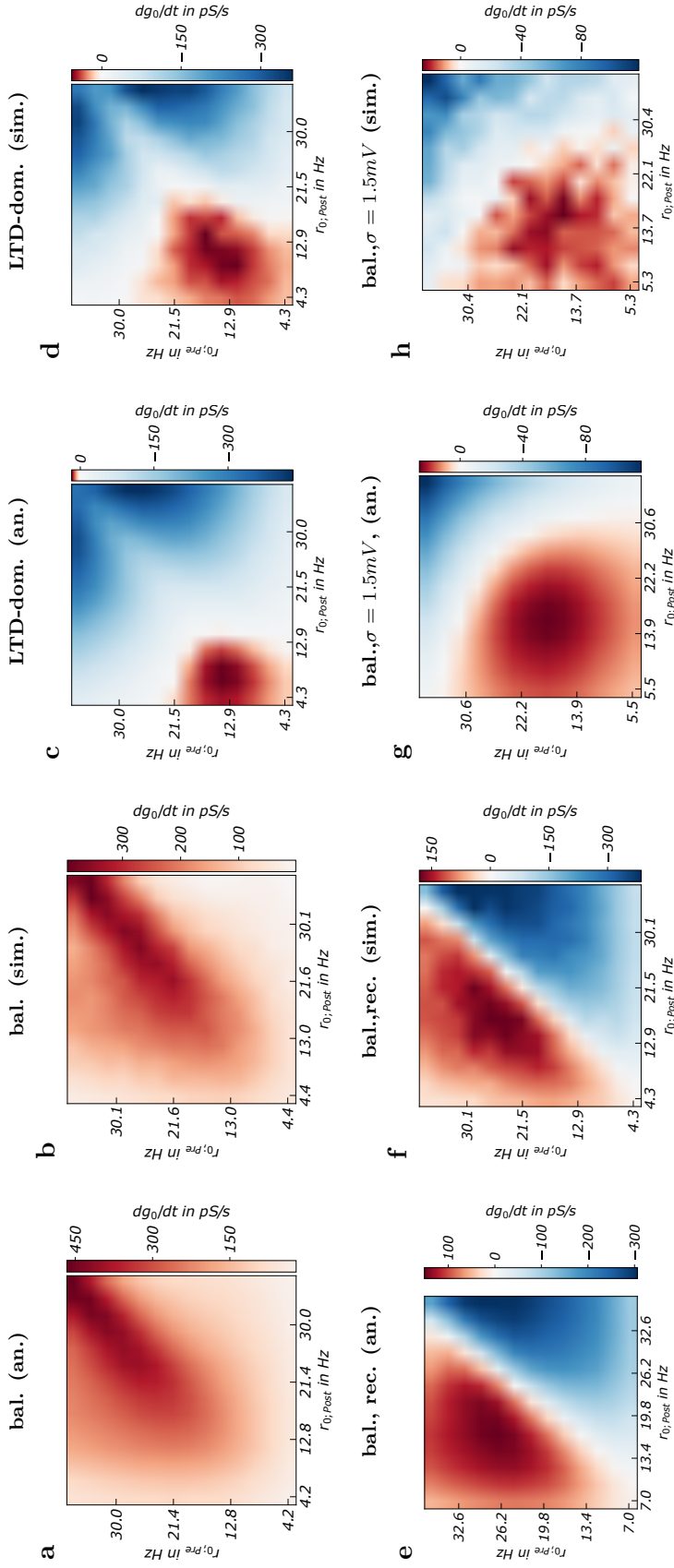
Fig. 4.6: Panels **a,b**: The synaptic change in pS/s is analyzed for a balanced STDP rule ($\tau_S = 4ms$) at low background noise ($\sigma = 0.5mV$). The synaptic connection strength is set to $g_{0;Post,Pre} = 1nS$. Analytical results in linear approximation (**a**) are compared to results from simulations (**b**). There is a strong dependence of synaptic potentiation on the alignment of pre- and post-synaptic firing rate. panels **c,d**: When changing the STDP rule from balanced to LTD dominated ($\tau_S = 3ms$), synaptic plasticity carries out major qualitative changes. Depression dominates for high firing rates, induced by stronger background currents, while potentiation is limited to low rates. With stronger synaptic connections, potentiation will spread towards higher firing rates and eventually result in a similar picture as in **a,b**. Panels **e,f**: Direct recurrent connections result in a competition, where the neuronal connection gets potentiated that belongs to the presynaptic neuron with the higher firing rate. The other connection experiences depression.The STDP rule is again set to be balanced. Panels **g,h**: Synaptic change at an increased amount of background noise ($\sigma = 1, 5mV$m, $\tau_S = 4ms$)

Further the maximum of potentiation appears sharper at high firing rates than at low rates (Fig. 4.7 **a**). An explanation for this phenomenon can be derived from examining the autocorrelation function (fig. 4.3, panel **b**). At higher firing rates, the auto-correlation function of the LIF neuron shows more and stronger modes at the N-fold of its mean firing rate (N=1,2,3,...). This means, that the neuron fires more regular. Therefore, if the two neurons emitted a spike synchronously, the probability that the next spike is evoked again synchronously is higher when pre- and postsynaptic neuron share the same high firing rate.
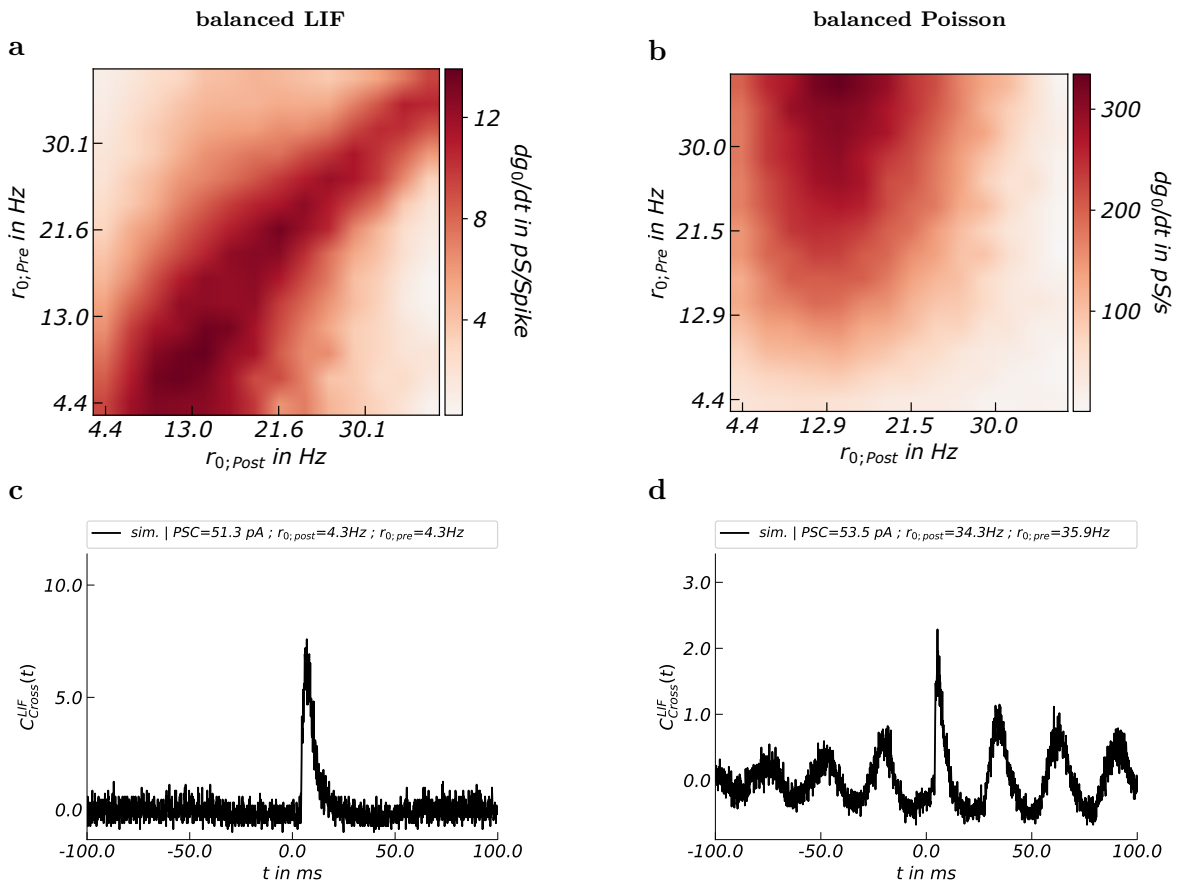
Fig. 4.7: Panel **a**: The synaptic change given in $nS/Spike$ as a function of the pre- and postsynaptic firing rate respectively ($\tau_S = 4ms$, $\sigma = 0.5mV$). Panel **b**: When the presynaptic LIF neuron is exchanged by a poisson spiker, the dependence of the synaptic change on the post- and presynaptic firing rate changes, supporting the argument that the auto-correlation function of the LIF neuron has a major impact of correlation based synaptic plasticity. Panel **c,d**: The crosscorrelation function is shown for low and for high pre- and postsynaptic firing rates. The strong modes at high firing rates (**d**) are result from the LIF neurons auto-correlation.

Phase shifts, perturbing this synchrony, are introduced by noise, while the synaptic connection between both neurons brings them into phase at the emission of a presynaptic spike. To support our argumentation we simulated the same system but with a Poisson spiker as the presynaptic neuron (a neuron that generates a spiketrain that is a Poisson process and therefore is not autocorrelated) (4.7, **b**). We find that in this case, potentiation is maximal at the highest presynaptic firing rate and an intermediate postsynaptic rate of $\approx 13Hz$. A higher presynaptic rate here just means that there is a higher chance of evoking a response per second. With increasing postsynaptic firing rate, this probability however decreases (also see section 3.2.1).

Case 2 (Fig. 4.6, c,d):

When introducing a STDP rule that is LTD dominated, the picture changes. While in the balanced case, synaptic potentiation was strongest at high post- and presynaptic firing rates, here it is strongest at low firing rates and becomes negative at high firing rates. However, synaptic potentiation is still closer to or greater zero when the presynaptic rate is close to the postsynaptic rate. The explanation is the same as for the balanced case. That synaptic growth is strongest at lower rates is explained by multiple facts. The higher firing rate is induced by a stronger background current, i.e. spiking occurs mainly due to the background current and less due to presynaptic spiking. Increasing the presynaptic firing rate to the postsynaptic rate, will not lead to an equivalent increase in correlation between post-and presynaptic neuron (Fig. 4.7, **d**). While this effect is the same for LTP-dominated or balanced STDP, the wider LTP domain ensures that potentiation occurs even when correlation is low. Further, a wide LTP window can account for the second modes in the crosscorrelation function at high rates (fig. 4.7, **d**).

Case 3 (Fig. 4.6, e,f):

When introducing a direct recurrent connection between a neuron pair, the neuron with the higher firing rate will always dominate over the one with the lower rate, if both connections are equally strong, i.e. potentiation occurs only if the presynaptic rate is higher than the postsynaptic (This effect would become weaker when the recurrent feedback is delayed). This might explain why in section 3.4.2 the consolidation of the recurrent assembly led to the evolution of a strictly bimodal matching index distribution.

Case 4 (Fig. 4.6, g,h):

At increasing levels of noise, the dependence of STDP induced potentiation on the difference between pre- and postsynaptic rate decreases. This is in agreement with the argument that this phenomenon is mainly an effect of the LIF neurons auto-correlation function, which looses its distinct modes at higher noise levels (fig, 4.3, **c**). That the picture is still different from the case of a presynaptic Poisson spiker is explained by the time that the membrane potential needs to recover after the reset. Therefore, the autocorrelation is not constant even at high noise levels (see also Fig. 4.3 **a**). Further, the synaptic change becomes negative at higher pre- and postsynaptic firing rates. This results from the STDP rule not beeing perfectly odd (Eq. 3.1). Increasing the level of noise by a factor of 3 lead to a significant decrease in the maximum synaptic potentiation from $450nS/s$ to $-90nS/s$ at PSC amplitudes of $55pA$ (compare Fig. 4.6 **a**, **g**). This is in agreement with the outcomes for different noise levels in networks simulations of section 3.4.3. Therefore, decreasing or increasing the level of noise only slightly would always demand to adapt the parameters of STDP and synaptic scaling, since STDP is strongly influenced by the amount of noise and SS is not.
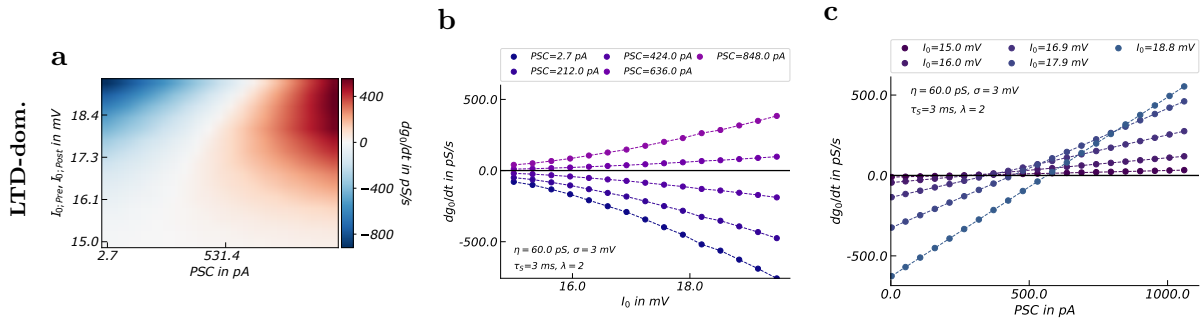
Fig. 4.8: Analytical solutions for the crosscorrelation function quickly quickly differ from simulations if the PSC increases. When comparing **a,b,c** to figure 3.5, panels **a,d,g**, one notices that potentiation and depression depend very different on I_0 and that high I_0 does not lead to depression for strong PSCs (**b**). Further, potentiation depends linear on the PSC and does not follow a sigmoidal functions (**c**)

At last we want to compare how the analytical solution depends on I_0 and the PSC amplitude in contrast to the simulation results from figure 3.5. Since the amplitude of the crosscorrelation in linear approximation does depend linear on the PSC amplitude instead of sigmoidal, the crosscorrelation and thereby potentiation is heavily overestimated for large PSCs (Fig. 4.8, **c**). Further the dependents on I_0 is different (Fig. 4.8, **b**) and only matches the results from simulations approximately for very weak synapses.

4.6 Summary

1. We have shown that the methods to calculate the expected synaptic change induced by STDP, which were presented in section 2.5 and 2.2.2, give estimations that are in very good agreement with simulations for low PSCs. This has not been done in the literature so far, using these methods. Further, we derived unknown properties of STDP such as the exact dependents on the difference between post- and presynaptic firing rate and were able to explain the findings through the LIF autocorrelation. This might be important in networks with very diverse activity, where post- and presynaptic rates differ and fluctuate (which is the case e.g. in strong FF-structures). Moreover we shed light on the quantitative and qualitative dependence of STDP on the background noise and the form of the STDP window for different pre- and postsynaptic activities.

2. In addition we delivered a direct comparison between the available analytical expressions for LIF rate-response function, inter-spike-interval distribution and autocorrelation function with simulation results.

Chapter 5

Discussion

Our simulation results show that STDP in combination with SS could be a possible mechanism that explains some of the experimental findings that have been made in the hippocampus during sleep and of which some seem contradictory:

1. during SWR in the hippocampus [86], synaptic connections that take part in SWR are down regulated [71]

2. SWR are accompanied by memory replay [91], [50];

3. sleep enhances memories [63].

These points can be viewed as contradictory because memory enhancement (3.) seems to contradict with the observation of downscaling (1.) of strong connections during sleep, if we assume that these strong connections are the representation of a memory. Moreover, memory replay (2.) implies a higher degree of correlation between neurons. However, this does not support the hebbian idea that neurons that are correlated should increase their synaptic strength, i.e. experience potentiation induced by STDP.

5.1 Stabilizing STDP and homeostatic plasticity

We found that the downscaling during replay activity could be explained by the SS mechanism, because it depresses connections between neurons, regardless of whether these neurons are correlated or not. However, SS and STDP have to be carefully balanced, such that a memory does not get lost during the network consolidation process.

Further, the exact functional shape of STDP plays an important role. If the STDP rule is LTP dominated, the ff-structure might evolve into a recurrent assembly, while recurrent assemblies are fragile if STDP is LTD-dominated. The simulation results suggest that a LTD-dominated STDP rule would be the best option for consolidating FF-structures, however not necessarily the best for consolidating recurrent assemblies. In general, FF-structures are less stable as there is always the possibility that strong recurrent connections evolve, whether it be due to spontaneous activity or due to directed external sensory stimuli. These recurrent connections could perturb the correct order of replay. Whether this would result in disturbed memories in 'practice' is an open question.

Other theoretical studies:

The problem that hebbian plasticity leads to unstable learning has been adressed in many studies, however it is still not completely understood how stabilzing mechanisms are implemented in the brain. In 1982 Bienenstock et al. proposed a model for learning in the visual cortex with a sliding threshold for LTP and LTD which lead to stable learning (also known as BCM rule) [12]. Miller and MacKay studied the implications of constraining hebbian learning via multiplicative and subtractive memechanisms that counteract LTP [67]. A similar study has been published in the same year by Goodhill et al. [43] that showed that such artificial weight constraints significantly affect the neural network dynamics and limit the performance of learning. Another method has been introduced by van Rossum et al. [108] who showed that stable learning is possible with a weight-dependent STDP rule. Their results indicate that stable correlation-based plasticity can be achieved without introducing competition, e.g. through synaptic scaling, or other multiplicative or subtractive mechanisms. However another study [93], where a weight dependent STDP rule was fitted to the data from Bi and Poo [85], found that stabilizing, weight dependent STDP rules lead to slow learning and that increasing the learning rate leads to rapid forgetting in the presence of realistic background noise. This is also what Jahnke et al. [49] found, where a similar weight dependent STDP rule was used that lead to the deletion of FF-structures. In [35], Abbott and Gerstner showed that homeostatic control of activity and correlation based synaptic change can both arise from STDP. Another approach to stabilize excitation has been studied by Fernando et al. [36], who showed that STDP together with short-term plasticity stabilizes weights in a network receiving Poisson input between 10-40 Hz. A more recent work [33] studied excitatory STDP and inhibitory STDP in combination with

homeostatic plasticity in form of synaptic weight normalization. Excitatory STDP was approximately balanced, inhibitory STDP LTP-dominated. They found that in an initially homogeneous network, small imbalances in the structure emerge to few driver neurons with strong excitatory connections. In addition they did simulations with synaptic scaling instead of synaptic weight normalization and showed that the network behaved the same, assuming equal mean presynaptic rates and slow time-scales of plasticity. Note however that this is not the case in the current work, where the firing rates differ a lot. Exchanging synaptic scaling with weight normalization (which is independent of the firing rate) would most probably lead to different results.

Experimental work:

Apart from synaptic scaling, there are a number of other proposed mechanisms that could be responsible for network activity regulation observed experimentally. Such mechanisms are intrinsic plasticity [28], change in synapse number [57], or metaplasticity that influences the ability to induce synaptic plasticity [2]. There is experimental evidence for all these mechanisms. However they are not found in all neurons [104] and only synaptic scaling is associated with altering the receptor content at synapses and thereby acts as a direct counter mechanism to LTP. However apart from the receptor number at the postsynaptic site there is evidence for homeostatic mechanisms that alter the neurotransmitter number and release probability at the presynaptic site [104, 25]. Note however that these different mechanisms are not present in all neuron types and not always combined [104]. Further it has been suggested that synaptic scaling does not only globally scale synapses [107] but may act local on synapses [95] or requires widespread changes in network activity that is not limited to single neurons [104] (In the current work, SS acted global on all incoming connections of a neuron). However most experimental studies modify the activity of all neurons in a network and therefore it is difficult to investigate the role of the individual neuron and to differentiate between global, local, pre- and postsynaptic mechanisms [104]. In conclusion, how exactly synaptic scaling and other mechanisms regulate neural excitability has not yet been completely clarified. This also shows that there is still a lot of theoretical work that can be done to test how these different homeostatic mechanisms would interact, what role the presynaptic expression of homeostatic plasticity might play, how different STDP rules like the symmetric/asymmetric may contribute to this, in what way presynaptic activity might be important (anti-hebbian learning). Moreover, are STDP and SS independent mechanisms or are they correlated in some way, what are the underlying

dynamics of activity dependent receptor trafficking?

Our work has contributed to answering some of these questions by showing the effects of postsynaptic activity dependent synaptic scaling on stabilizing new memories. We have shown that such a scaling rule would need to be tightly balanced with STDP in order to keep the number of strong connections in the required regime. Further we have shown that intrinsic plasticity could counterbalance the strong activity fluctuations found in networks with a high diversity of connection-strengths and thereby stabilizes a larger number of strong connections in combination with SS and STDP. Moreover, we shed light on the importance of balancing STDP towards LTP or LTD by showing that this can have a strong impact on the synapse dynamics. However, our model does not explain activity increases observed in experiments when network activity is low [104]. In our SS model, the chosen target firing rate of 0, higher target firing rates however result in the growth of synapses belonging to weakly active neurons, which we consider as biasing old memories. Moreover, increasing the synaptic coupling between low active neurons does not necessarily increase their activity if none of the neurons in the resulting stronger connected assembly gets enough input to drive the other neurons.

5.2 Memory stability and enhancement

The enhancement of memories after sleep (which in the current work is simulated by the absence of any specific external stimuli), is to a degree also observable in our model. However we want to emphasize that this statement is very vague. What we found is, that if the learning rate of SS is high enough, SS introduces a strong competition between synapses that belong to a certain postsynaptic neuron. Only connections from presynaptic neurons that have a firing rate close to the postsynaptic neuron consolidate, the rest decay to the ground-level. The deletion of most of the strong synapses results in an enhanced temporal order of spiking between neuron pairs that retain their strong connection. However this goes to the expense of a continuous memory representation. This again raises some unanswered questions such as, how many neurons or connections are actually involved in forming a certain memory, must a memory be a continuous structure or do spatially close cluster that are active on a similar timescales represent a memory equally well? However, one argument against a possible fragmentation of such structures is that it comes along with a highly reduced activity after consolidation. Experiments have shown however, that strong activity of hippocampal neurons in the form of sharp wave/ripples is retained over long time-periods during sleep and

doe not decay much even after 3 hours [46]. This would support the hypothesis that, while synapses might get down-regulated, the majority stays in a regime, where dendritic spiking is induced and with it ripple-like activity. Memory enhancement may be better explained by theories of system consolidation [32] or multiple trace theory [54]. Moreover, our model only explains the synaptic evolution during sleep/ripple-like activity, where connection strengths get redistributed. However, if the dendritic activity is shut down, the connections need to be stabilized by other mechanisms. We therefore suggest that subsequent to this process, synaptic consolidation [30] is needed that leads to long lasting alterations of synapse proteins and thereby fixes synapses or at least makes them less accessible to changes. The process of synaptic consolidation might also be connected to ripple-like activity and replay and therefore goes hand in hand with the reorganization of synaptic connections we studied in the current work.

5.2.1 Dendritic spikes necessary for network consolidation?

We found that the correlation that is induced between neurons by classical somatic spikes is not sufficient to enable a clear up and downscaling of connections within a plausible regime (Fig. 3.4.6), at least if synaptic changes are solely driven by STDP and SS. Therefore our work would suggest that reducing ripple-like activity by impairing dendritic amplification would result in a different redistribution of synaptic weights. Therefore, are SWR always accompanied by dendritic spikes? If yes, how do synapses change if dendritic spiking is impaired? There has been experimental work that suggests that dendritic spikes are indeed necessary for the induction of ripples in the hippocampus [24]. Further, Sadowski et al. [89] showed that the reactivated place cell firing patterns are able to induce LTP, but only if accompanied by ripple-activity and resulting dendritic depolarization. This supports our model, where potentiation only sets in if the dendritic spiking threshold is reached. Moreover, the contradiction between Sadowskis finding that ripples induce LTP and Norimotos finding [71] that synapses get downregulated during SWR is in part covered by our model. Sadowski demonstrated the induction of LTP for synapses that had a strength of $\approx 35pA$, which corresponds to a synaptic conductivity of about $0.65nS$. In our model, potentiation started only for synapses with a synaptic strength $> 2nS$, which however is set by the dendritic spiking threshold. A lower dendritic spiking threshold in our model would result in the potentiation of synapses that lie around $0.65nS$. For stronger ff-structures, we find an average downregulation just as Norimoto.

5.2.2   Other studies on memory stability

The synaptic stability versus plasticity dilemma [3] has been in the focus of several studies, addressing the question how memories could be retained in a network while still being able to encode new memories. Abraham et al. [4] suggested a regulated balance of synaptic stability and synaptic plasticity is required for optimal memory retention, criticizing that the ongoing synaptic change does imply that even long encoded memory could quickly become lost. This is also an important criticism to the current work, where consolidated synapses heavily rely on the momentary network activity. Slight changes to the pre- and postsynaptic firing could quickly result in the loss of previously consolidated synapses. However it is this property that also allows to integrate new memory into the network. The question is rather, how fast synaptic change should occur and if synapses that were in the consolidated regime for a long time should be stabilized in addition by other mechanisms that slow down plasticity (e.g. by making the learning rate depend on the time a synapse stayed in an upper regime (synaptic consolidation)). Work that investigates the role of STDP in memory retention has been done by Billings et all. [13], who showed that a soft-bound, weight-dependent learning rule has a very short retention time as compared to a learning rule that is independent of the synaptic weights (related to [108], [93], section 5.1). Theoretical work on how STDP could stabilize memories by having two stable fixed points has been done by Wei et al. [110] who studied the effects of ongoing STDP on the stability of memory patterns stored in synapses of an attractor neural network. In a recent work, Park et al. investigated weight dependent STDP and showed that, what they called asymmetric STDP leads to flexible memory that is volatile and easily overwritten, while symmetric STDP results in stable memory representations. Asymmetric STDP depends on the synaptic weight such that weak synapses are potentiated (STDP is LTP-dominated) and strong synapses are depressed (STDP is LTD-dominated). This rule has already been identified to lead to fast forgetting already by others ([93, 108]). Symmetric STDP is balanced, however the learning rate is strongest for intermediate synaptic strengths and decreases when the synaptic strength increases or decreases from the mid-value. Combining the two STDP rules, they could realized a hybrid memory type that operates in a way intermediate between stable and flexible memory.

5.3   Unimodal or bimodal synaptic distribution?

Experimental studies [9, 5, 68] have provided evidence that synaptic weights follow a unimodal, long-tailed distribution which can be approximated by a log-normal dis-

tribution. So does that mean that memories are stored in unimodal distributions? Theoretical works [79, 110, 93] (and the current work) suggest that synaptic plasticity rules that drive synapses into a unimodal distribution do not retain old memories. Further, [33] showed that their synaptic plasticity model that leads to long-tailed uni-modal distributions, amplifies small inhomogeneities in the synaptic weight distribution. While resulting in the experimentally observed unimodal long-tailed distribution, we propose that such a process would bias old memory representations. So how could our proposal that only synaptic plasticity that leads to bimodal distributions stabilizes memory fit into the experimental findings? First, the experimental data does not consider single memory representations but averages over all synapses, regardless of their function. In general we assume that the number of strong connections is small compared to the set of all synaptic connections, as it is the case in the current work. Therefore, if individual memories are stored in bimodal distributions but with slightly different shapes, the mean over all of these could look like a unimodal distribution. Seconds, if the number of strong connections is very low, this could, under high sub-sampling (which is the case in all experimental studies due to the overwhelming size of the brain) indeed lead to the observation that synapses are unimodal distributed. Third, in our model, synapses are initially also distributed in a long tailed unimodal distribution after training. The bimodal distribution only evolves during consolidation. Therefore, in a random subsample of synapses that contain consolidated and newly potentiated synapses that not yet consolidated, a bimodal distribution would again not be found. However, it might be that there are mechanisms that stabilize synapses and retain a long tailed unimodal distribution. One candidate could for example be metaplasticity [2] that slows down synaptic plasticity in synapses associated with older memories.

5.4   Measures for memory replay

What are good measures for the quality of memory replay activity? In the current work memory retrieval has been measured in terms of the matching index. But is this the right way to do it? The replay of memory has been identified as being crucial for memory consolidation. The disruption of memory replay in the hippocampus during sleep results in weaker memory, while enhanced replay strengthens memory [11, 10]. Enhanced replay is however often associated with an increased activity of neurons that encoded information during wake and not necessarily with temporally structured replay. However, structured replay of sequences that occurred during wake have been observed

during sleep in the hippocampus [50]. So, how much does the strength of a memory depend on the overall activity of neurons associated with it and how important is the temporal structure of the replay. We found that the temporal order of firing, measured by the matching index, increases significantly for individual neuron pairs, if the total number of strong inputs the postsynaptic neuron receives decreases. The question is, to what level does the enhanced order of spiking for single neuron pairs enhance memory and to what degree is the overall activity of neuron ensembles important for the memory retrieval? We suggest that there is a sweet spot between the right temporal order of replay that might be interpreted as the precision of a memory and the magnitude of activity that might be interpreted as the strength of that memory. However to shed more light on these questions more experimental studies are needed that look precisely at how much the connectivity in the hippocampus changes during sleep and how much this change influences the order and activity of replay. If the temporal structure of replay enhances during sleep, is this due to the loss of strong connections or due to the formation of new, enhanced memory traces in the network? Or is the downregulation that Norimoto observed during ripple-like activity not connected to the loss of any synapses after all? Further study has to go into how to quantifying the quality of such replay events. The matching index used in the current work only accounts for correlations between single neuron pairs, without taking into account the activity of the other neurons that make up the memory. It might be worth thinking about alternative measures that include higher order correlations. Moreover one could try to derive more appropriate measures from information theory. Another attempt to quantify memory replay in FF-structures that takes into account the population activity of small assemblies of neurons can be found in [23]. This method however neglects single neurons pair activity.

5.5   Conclusion

This work has shown that STDP in combination with SS and dendritic amplification reorganizes synapses within newly formed FF-memory representations. During spontaneous, ripple-like activity these memories are stabilized/consolidated as synapses are transfered into a bimodal distribution. This process however depends on the exact form of the STDP learning window as well as the timescales/learning-rates of STDP and SS and is closely linked to the emission of dendritic spikes. We find an average downregulation of strong FF-structures in agreement with the downregulation of synapses during ripple-like activity found in experiment [71]. Moreover our plasticity model

can be tuned to control the number of synapses that are retained in the consolidated memory representation, where synapses that belong to neurons with similar activities are favored. We find that the temporal structure of activity between single neurons enhances when the overall number of strong synapses within the memory representation is reduced. However, this also leads to a reduction of activity and therefore to weaker replay. Further, we showed that STDP depends sigmoidal on the synaptic strength and that the dependents on the pre- and postsynaptic activity is highly influenced by the form of the STDP window. We found that LTD-dominated STDP depends concave, while LTP-dominated STDP depends convex on the firing rate of the pre- and postsynaptic neuron, which has strong implications in how synapses react to stimuli of different strengths. At last we studied established methods for estimating the crosscorrelation function of LIF neurons to calculate the synaptic change induced by STDP and compared these results to simulations. We found that analytical and simulation results are in good agreement for weakly coupled neuron pairs. Further we showed that the LIF neurons autocorrelation impacts how STDP induced potentiation depends on the pre- and postsynaptic activity and moreover shed light on how background noise affects STDP. However, there is still a lot of theoretical and experimental work that has to be done to clarify our understanding about the different homeostatic and hebbian mechanisms that drive plasticity and may consolidate memory in the brain.

References

[1] Abbott, L. F. and Nelson, S. B. (2000). Synaptic plasticity: Taming the beast. *Nature neuroscience*, 3 Suppl:1178–1183.

[2] Abraham, W. C. and Bear, M. F. (1996). Metaplasticity: the plasticity of synaptic plasticity. *Trends Neurosci.*, 19(4):126–130.

[3] Abraham, W. C. and Robins, A. (2005). Memory retention – the synaptic stability versus plasticity dilemma. *Trends in Neurosciences*, 28(2):73–78.

[4] Abramowitz M., S. I. A. (1965). *Handbook of Mathematical Functions: with Formulas, Graphs, and Mathematical Tables (Dover Books on Mathematics)*. Dover Publications.

[5] Arellano, J. I. (2007). Ultrastructure of dendritic spines: correlation between synaptic and spine morphologies. *Frontiers in Neuroscience*, 1(1):131–143.

[6] Ariav, G., Polsky, A., and Schiller, J. (2003). Submillisecond precision of the input-output transformation function mediated by fast sodium dendritic spikes in basal dendrites of CA1 pyramidal neurons. *J. Neurosci.*, 23(21):7750–7758.

[7] Badel, L., Lefort, S., Brette, R., Petersen, C. C. H., Gerstner, W., and Richardson, M. J. E. (2008). Dynamic i-v curves are reliable predictors of naturalistic pyramidal-neuron voltage traces. *Journal of Neurophysiology*, 99(2):656–666.

[8] Bannai, H., Niwa, F., Sherwood, M. W., Shrivastava, A. N., Arizono, M., Miyamoto, A., Sugiura, K., Lévi, S., Triller, A., and Mikoshiba, K. (2015). Bidirectional control of synaptic GABAAR clustering by glutamate and calcium. *Cell Reports*, 13(12):2768–2780.

[9] Barbour, B., Brunel, N., Hakim, V., and Nadal, J.-P. (2007). What can we learn from synaptic weight distributions? *Trends in Neurosciences*, 30(12):622–629.

[10] Barnes, D. C. and Wilson, D. A. (2014). Slow-wave sleep-imposed replay modulates both strength and precision of memory. *J. Neurosci.*, 34(15):5134–5142.

[11] Bendor, D. and Wilson, M. A. (2012). Biasing the content of hippocampal replay during sleep. *Nature Neuroscience*, 15(10):1439–1444.

[12] Bienenstock, E. L., Cooper, L. N., and Munro, P. W. (1982). Theory for the development of neuron selectivity: orientation specificity and binocular interaction in visual cortex. *J. Neurosci.*, 2(1):32–48.

[13] Billings, G. and van Rossum, M. C. W. (2009). Memory retention and spike-timing-dependent plasticity. *Journal of Neurophysiology*, 101(6):2775–2788.

[14] Born, J. and Wilhelm, I. (2011). System consolidation of memory during sleep. *Psychological Research*, 76(2):192–203.

[15] Brodmann, K. (1909). *Vergleichende Lokalisationslehre der Grosshirnrinde in ihren Prinzipien dargestellt auf Grund des Zellenbaues*, volume 1. Barth.

[16] Brunel, N. (2000). Dynamics of sparsely connected networks of excitatory and inhibitory spiking neurons. *Journal of Computational Neuroscience*, 8(3):183–208.

[17] Brunel, N., Chance, F. S., Fourcaud, N., and Abbott, L. F. (2001). Effects of synaptic noise and filtering on the frequency response of spiking neurons. *Physical Review Letters*, 86(10):2186–2189.

[18] Brunel, N. and Hakim, V. (1999). Fast global oscillations in networks of integrate-and-fire neurons with low firing rates. *Neural Computation*, 11(7):1621–1671.

[19] Buchanan, K. A. (2010). The activity requirements for spike timing-dependent plasticity in the hippocampus. *Frontiers in Synaptic Neuroscience*, 2.

[20] Buzsáki, G. (1989). Two-stage model of memory trace formation: A role for "noisy" brain states. *Neuroscience*, 31(3):551–570.

[21] Buzsaki, G., Horvath, Z., Urioste, R., Hetke, J., and Wise, K. (1992). High-frequency network oscillation in the hippocampus. *Science*, 256(5059):1025–1027.

[22] Cajal, S. R. (1909). *Histologie du syst éme nerveux de l'homme & des vert ébr és*, volume 1. Maloine.

[23] Chenkov, N., Sprekeler, H., and Kempter, R. (2017). Memory replay in balanced recurrent networks. *PLOS Computational Biology*, 13(1):e1005359.

[24] Chiovini, B., Turi, G. F., Katona, G., Kaszás, A., Pálfi, D., Maák, P., Szalay, G., Szabó, M. F., Szabó, G., Szadai, Z., Káli, S., and Rózsa, B. (2014). Dendritic spikes induce ripples in parvalbumin interneurons during hippocampal sharp waves. *Neuron*, 82(4):908–924.

[25] Davis, G. W. (2006). Homeostatic control of neural activity: From phenomenology to molecular design. *Annual Review of Neuroscience*, 29(1):307–323.

[26] Dayan, P. and Abbott, L. F. (2005). *Theoretical Neuroscience: Computational and Mathematical Modeling of Neural Systems (Computational Neuroscience Series)*. The MIT Press.

[27] de Vivo, L., Bellesi, M., Marshall, W., Bushong, E. A., Ellisman, M. H., Tononi, G., and Cirelli, C. (2017). Ultrastructural evidence for synaptic scaling across the wake/sleep cycle. *Science*, 355(6324):507–510.

[28] Desai, N. S. (2003). Homeostatic plasticity in the CNS: synaptic and intrinsic forms. *Journal of Physiology-Paris*, 97(4-6):391–402.

[29] Droste, F. and Lindner, B. (2017). Exact analytical results for integrate-and-fire neurons driven by excitatory shot noise. *Journal of Computational Neuroscience*, 43(1):81–91.

[30] Dudai, Y. (2004). The neurobiology of consolidations, or, how stable is the engram? *Annual Review of Psychology*, 55(1):51–86.

[31] Dudai, Y. (2012). The restless engram: Consolidations never end. *Annual Review of Neuroscience*, 35(1):227–247.

[32] Dudai, Y., Karni, A., and Born, J. (2015). The consolidation and transformation of memory. *Neuron*, 88(1):20–32.

[33] Effenberger, F., Jost, J., and Levina, A. (2015). Self-organization in balanced state networks by STDP and homeostatic plasticity. *PLOS Computational Biology*, 11(9):e1004420.

[34] English, D. F., McKenzie, S., Evans, T., Kim, K., Yoon, E., and Buzsáki, G. (2017). Pyramidal cell-interneuron circuit architecture and dynamics in hippocampal networks. *Neuron*, 96(2):505–520.e7.

[35] F Abbott, L. and Gerstner, W. (2004). Homeostasis and learning through spike-timing dependent plasticity.

[36] Fernando, S. and Yamada, K. (2012). Spike-timing-dependent plasticity and short-term plasticity jointly control the excitation of hebbian plasticity without weight constraints in neural networks. *Computational Intelligence and Neuroscience*, 2012:1–15.

[37] Fourcaud, N. and Brunel, N. (2002). Dynamics of the firing probability of noisy integrate-and-fire neurons. *Neural Computation*, 14(9):2057–2110.

[38] Fourcaud-Trocme, N., Hansel, D., van Vreeswijk, C., and Brunel, N. (2003). How spike generation mechanisms determine the neuronal response to fluctuating inputs. *J. Neurosci.*, 23(37):11628–11640.

[39] Fujita, Y. (1968). Activity of dendrites of single purkinje cells and its relationship to so-called inactivation response in rabbit cerebellum. *Journal of Neurophysiology*, 31(2):131–141.

[40] Gerstner, W. (2010). From hebb rules to spike-timing-dependent plasticity: A personal account. *Frontiers in Synaptic Neuroscience*, 2.

[41] Gerstner, W. and Kistler, W. M. (2002). Mathematical formulations of hebbian learning. *Biological Cybernetics*, 87(5-6):404–415.

[42] Gerstner, W., Kistler, W. M., Naud, R., and Paninski, L. (2009). *Neuronal Dynamics*. Cambridge University Press.

[43] Goodhill, G. J. and Barrow, H. G. (1994). The role of weight normalization in competitive learning. *Neural Computation*, 6(2):255–269.

[44] Graupner, M. and Brunel, N. (2012). Calcium-based plasticity model explains sensitivity of synaptic changes to spike pattern, rate, and dendritic location. *Proceedings of the National Academy of Sciences*, 109(10):3991–3996.

[45] Hausser, M. (2000). Diversity and dynamics of dendritic signaling. *Science*, 290(5492):739–744.

[46] Hirase, H., Leinekugel, X., Czurko, A., Csicsvari, J., and Buzsaki, G. (2001). Firing rates of hippocampal neurons are preserved during subsequent sleep episodes and modified by novel awake experience. *Proceedings of the National Academy of Sciences*, 98(16):9386–9390.

[47] Hodgkin, A. L. and Huxley, A. F. (1952). A quantitative description of membrane current and its application to conduction and excitation in nerve. *J. Physiol. (Lond.)*, 117(4):500–544.

[48] Huber, R., Mäki, H., Rosanova, M., Casarotto, S., Canali, P., Casali, A. G., Tononi, G., and Massimini, M. (2012). Human cortical excitability increases with time awake. *Cerebral Cortex*, 23(2):1–7.

[49] Jahnke, S., Timme, M., and Memmesheimer, R.-M. (2015). A unified dynamic model for learning, replay, and sharp-wave/ripples. *Journal of Neuroscience*, 35(49):16236–16258.

[50] Ji, D. and Wilson, M. A. (2006). Coordinated memory replay in the visual cortex and hippocampus during sleep. *Nature Neuroscience*, 10(1):100–107.

[51] Kampa, B. M., Letzkus, J. J., and Stuart, G. J. (2007). Dendritic mechanisms controlling spike-timing-dependent synaptic plasticity. *Trends in Neurosciences*, 30(9):456–463.

[52] Kandel, E. R., Dudai, Y., and Mayford, M. R. (2014). The molecular and systems biology of memory. *Cell*, 157(1):163–186.

[Karpathy] Karpathy, A. Cs231n convolutional neural networks for visual recognition.

[54] Karpicke, J. and RoedigerIII, H. (2007). Repeated retrieval during learning is the key to long-term retention. *Journal of Memory and Language*, 57(2):151–162.

[55] Kempter, R., Gerstner, W., and van Hemmen, J. L. (1999). Hebbian learning and spiking neurons. *Physical Review E*, 59(4):4498–4514.

[56] Killgore, W. D. (2010). Effects of sleep deprivation on cognition. In *Progress in Brain Research*, pages 105–129. Elsevier.

[57] Kirov, S. A., Goddard, C., and Harris, K. M. (2004). Age-dependence in the homeostatic upregulation of hippocampal dendritic spine number during blocked synaptic transmission. *Neuropharmacology*, 47(5):640–648.

[58] Lazar, A. (2009). SORN: a self-organizing recurrent neural network. *Frontiers in Computational Neuroscience*, 3.

[59] Lefort, S., Tomm, C., Sarria, J.-C. F., and Petersen, C. C. (2009). The excitatory neuronal network of the c2 barrel column in mouse primary somatosensory cortex. *Neuron*, 61(2):301–316.

[60] Lissin, D. V., Gomperts, S. N., Carroll, R. C., Christine, C. W., Kalman, D., Kitamura, M., Hardy, S., Nicoll, R. A., Malenka, R. C., and von Zastrow, M. (1998). Activity differentially regulates the surface expression of synaptic AMPA and NMDA glutamate receptors. *Proc. Natl. Acad. Sci. U.S.A.*, 95(12):7097–7102.

[61] Llinas, R., Nicholson, C., Freeman, J. A., and Hillman, D. E. (1968). Dendritic spikes and their inhibition in alligator purkinje cells. *Science*, 160(3832):1132–1135.

[62] Loebel, A. (2009). Multiquantal release underlies the distribution of synaptic efficacies in the neocortex. *Frontiers in Computational Neuroscience*, 3.

[63] Maquet, P. (2001). The role of sleep in learning and memory. *Science*, 294(5544):1048–1052.

[64] Markram, H. (1997). Regulation of synaptic efficacy by coincidence of postsynaptic APs and EPSPs. *Science*, 275(5297):213–215.

[65] Markram, H., Lubke, J., Frotscher, M., Roth, A., and Sakmann, B. (1997). Physiology and anatomy of synaptic connections between thick tufted pyramidal neurones in the developing rat neocortex. *J. Physiol. (Lond.)*, 500 (Pt 2):409–440.

[66] Memmesheimer, R.-M. (2010). Quantitative prediction of intermittent high-frequency oscillations in neural networks with supralinear dendritic interactions. *Proceedings of the National Academy of Sciences*, 107(24):11092–11097.

[67] Miller, K. D. and MacKay, D. J. C. (1994). The role of constraints in hebbian learning. *Neural Computation*, 6(1):100–126.

[68] Mishchenko, Y., Hu, T., Spacek, J., Mendenhall, J., Harris, K. M., and Chklovskii, D. B. (2010). Ultrastructural analysis of hippocampal neuropil from the connectomics perspective. *Neuron*, 67(6):1009–1020.

[69] Mölle, M., Yeshenko, O., Marshall, L., Sara, S. J., and Born, J. (2006). Hippocampal sharp wave-ripples linked to slow oscillations in rat slow-wave sleep. *Journal of Neurophysiology*, 96(1):62–70.

[70] Moser, M.-B., Rowland, D. C., and Moser, E. I. (2015). Place cells, grid cells, and memory. *Cold Spring Harbor Perspectives in Biology*, 7(2):a021808.

[71] Norimoto, H., Makino, K., Gao, M., Shikano, Y., Okamoto, K., Ishikawa, T., Sasaki, T., Hioki, H., Fujisawa, S., and Ikegaya, Y. (2018). Hippocampal ripples down-regulate synapses. *Science*, 359(6383):1524–1527.

[72] O'Brien, R. J., Kamboj, S., Ehlers, M. D., Rosen, K. R., Fischbach, G. D., and Huganir, R. L. (1998). Activity-dependent modulation of synaptic AMPA receptor accumulation. *Neuron*, 21(5):1067–1078.

[73] Oja, E. (1982). Simplified neuron model as a principal component analyzer. *Journal of Mathematical Biology*, 15(3):267–273.

[74] O'Keefe, J. and Dostrovsky, J. (1971). The hippocampus as a spatial map. preliminary evidence from unit activity in the freely-moving rat. *Brain Research*, 34(1):171–175.

[75] O'Keefe, J. and Recce, M. L. (1993). Phase relationship between hippocampal place units and the EEG theta rhythm. *Hippocampus*, 3(3):317–330.

[76] O'Keefe, J. and Speakman, A. (1987). Single unit activity in the rat hippocampus during a spatial memory task. *Experimental Brain Research*, 68(1).

[77] O'Neill, J., Senior, T., and Csicsvari, J. (2006). Place-selective firing of CA1 pyramidal cells during sharp wave/ripple network patterns in exploratory behavior. *Neuron*, 49(1):143–155.

[78] Ostojic, S., Brunel, N., and Hakim, V. (2009). How connectivity, background activity, and synaptic properties shape the cross-correlation between spike trains. *Journal of Neuroscience*, 29(33):10234–10253.

[79] Park, Y., Choi, W., and Paik, S.-B. (2017). Symmetry of learning rate in synaptic plasticity modulates formation of flexible and stable memories. *Scientific Reports*, 7(1).

[80] Pavlides, C. and Winson, J. (1989). Influences of hippocampal place cell firing in the awake state on the activity of these cells during subsequent sleep episodes. *The Journal of Neuroscience*, 9(8):2907–2918.

[81] Perin, R., Berger, T. K., and Markram, H. (2011). A synaptic organizing principle for cortical neuronal groups. *Proceedings of the National Academy of Sciences*, 108(13):5419–5424.

[82] Plesser, H. E. and Gerstner, W. (2000). Noise in integrate-and-fire neurons: From stochastic input to escape rates. *Neural Computation*, 12(2):367–384.

[83] Purves, D. (2001). *Neuroscience.* Sinauer Associates Inc.

[84] Purves, D., Augustine, G. J., Hall, W. C., LaMantia, A., and E.White, L. (2012). *Neuroscience*, volume 5. Sinauer.

[85] qiang Bi, G. and ming Poo, M. (2001). Synaptic modification by correlated activity: Hebb's postulate revisited. *Annual Review of Neuroscience*, 24(1):139–166.

[86] Ramadan, W., Eschenko, O., and Sara, S. J. (2009). Hippocampal sharp wave/ripples during sleep for consolidation of associative memory. *PLoS ONE*, 4(8):e6697.

[87] Rasch, B. and Born, J. (2013). About sleep's role in memory. *Physiological Reviews*, 93(2):681–766.

[88] Richardson, M. J. E. (2004). Effects of synaptic conductance on the voltage distribution and firing rate of spiking neurons. *Physical Review E*, 69(5).

[89] Sadowski, J. H., Jones, M. W., and Mellor, J. R. (2016). Sharp-wave ripples orchestrate the induction of synaptic plasticity during reactivation of place cell firing patterns in the hippocampus. *Cell Reports*, 14(8):1916–1929.

[90] Sayer, R., Friedlander, M., and Redman, S. (1990). The time course and amplitude of EPSPs evoked at synapses between pairs of CA3/CA1 neurons in the hippocampal slice. *The Journal of Neuroscience*, 10(3):826–836.

[91] Skaggs, W. E. and McNaughton, B. L. (1996). Replay of neuronal firing sequences in rat hippocampus during sleep following spatial experience. *Science*, 271(5257):1870–1873.

[92] Song, S., Sjöström, P. J., Reigl, M., Nelson, S., and Chklovskii, D. B. (2005). Highly nonrandom features of synaptic connectivity in local cortical circuits. *PLoS Biology*, 3(3):e68.

[93] Standage, D. and Trappenberg, T. (2007). The trouble with weight-dependent STDP.

[94] Strata, P. and Harvey, R. (1999). Dale's principle. *Brain Research Bulletin*, 50(5-6):349–350.

[95] Sutton, M. A., Ito, H. T., Cressy, P., Kempf, C., Woo, J. C., and Schuman, E. M. (2006). Miniature neurotransmission stabilizes synaptic function via tonic suppression of local dendritic protein synthesis. *Cell*, 125(4):785–799.

[96] Swanson, L. W. (2011). *Brain Architecture*. Oxford University Press.

[97] Tetzlaff, C. (2011). Synaptic scaling in combination with many generic plasticity mechanisms stabilizes circuit connectivity. *Frontiers in Computational Neuroscience*, 5.

[98] Tetzlaff, C., Kolodziejski, C., Timme, M., Tsodyks, M., and Wörgötter, F. (2013). Synaptic scaling enables dynamically distinct short- and long-term memory formation. *BMC Neuroscience*, 14(Suppl 1):P415.

[99] Tetzlaff, C., Okujeni, S., Egert, U., Wörgötter, F., and Butz, M. (2010). Self-organized criticality in developing neuronal networks. *PLoS Computational Biology*, 6(12):e1001013.

[100] Thomson, A. M., Deuchars, J., and West, D. C. (1993). Large, deep layer pyramid-pyramid single axon EPSPs in slices of rat motor cortex display paired pulse and frequency-dependent depression, mediated presynaptically and self-facilitation, mediated postsynaptically. *Journal of Neurophysiology*, 70(6):2354–2369.

[101] Tononi, G. and Cirelli, C. (2003). Sleep and synaptic homeostasis: a hypothesis. *Brain Research Bulletin*, 62(2):143–150.

[102] Tononi, G. and Cirelli, C. (2014). Sleep and the price of plasticity: From synaptic and cellular homeostasis to memory consolidation and integration. *Neuron*, 81(1):12–34.

[103] Tuckwell, H. C. (1988). *Introduction to Theoretical Neurobiology.* Cambridge University Press.

[104] Turrigiano, G. G. (2008). The self-tuning neuron: Synaptic scaling of excitatory synapses. *Cell*, 135(3):422–435.

[105] Turrigiano, G. G., Leslie, K. R., Desai, N. S., Rutherford, L. C., and Nelson, S. B. (1998). Activity-dependent scaling of quantal amplitude in neocortical neurons. *Nature*, 391(6670):892–896.

[106] Turrigiano, G. G. and Nelson, S. B. (2000). Hebb and homeostasis in neuronal plasticity. *Current Opinion in Neurobiology*, 10(3):358–364.

[107] Turrigiano, G. G. and Nelson, S. B. (2004). Homeostatic plasticity in the developing nervous system. *Nature Reviews Neuroscience*, 5(2):97–107.

[108] van Rossum, M. C., Bi, G. Q., and Turrigiano, G. G. (2000). Stable Hebbian learning from spike timing-dependent plasticity. *J. Neurosci.*, 20(23):8812–8821.

[109] Vyazovskiy, V. V., Cirelli, C., Pfister-Genskow, M., Faraguna, U., and Tononi, G. (2008). Molecular and electrophysiological evidence for net synaptic potentiation in wake and depression in sleep. *Nature Neuroscience*, 11(2):200–208.

[110] Wei, Y. and Koulakov, A. A. (2014). Long-term memory stabilized by noise-induced rehearsal. *Journal of Neuroscience*, 34(47):15804–15815.